VOLUME 102 | SUPPLEMENT 1 | MARCH 2022

LI

LABORATORY INVESTIGATION

THE BASIC AND TRANSLATIONAL PATHOLOGY RESEARCH JOURNAL

ABSTRACTS (1187–1248)

PULMONARY, MEDIASTINAL, PLEURAL, AND PERITONEAL PATHOLOGY

2022

USCAP 111TH ANNUAL MEETING

REAL INTELLIGENCE

MARCH 19–24, 2022 LOS ANGELES, CALIFORNIA

Published by SPRINGER NATURE
www.ModernPathology.org

USCAP Creating a Better Pathologist
AN OFFICIAL JOURNAL OF THE UNITED STATES AND CANADIAN ACADEMY OF PATHOLOGY

EDUCATION COMMITTEE

Rhonda K. Yantiss
Chair

Kristin C. Jensen
Chair, CME Subcommittee

Laura C. Collins
Chair, Interactive Microscopy Subcommittee

Yuri Fedoriw
Short Course Coordinator

Ilan Weinreb
Chair, Subcommittee for Unique Live Course Offerings

Carla L. Ellis
Chair, DEI Subcommittee

Adebowale J. Adeniran
Kimberly H. Allison
Sarah M. Dry
William C. Faquin
Karen J. Fritchie
Jennifer B. Gordetsky
Levon Katsakhyan, Pathologist-in-Training
Melinda J. Lerwill
M. Beatriz S. Lopes
Julia R. Naso, Pathologist-in-Training
Liron Pantanowitz
Carlos Parra-Herran
Rajiv M. Patel
Charles "Matt" Quick
David F. Schaeffer
Lynette M. Sholl
Olga K. Weinberg
Maria Westerhoff

ABSTRACT REVIEW BOARD

Benjamin Adam
Oyedele Adeyi
Mariam Priya Alexander
Daniela Allende
Catalina Amador
Vijayalakshmi Ananthanarayanan
Tatjana Antic
Manju Aron
Roberto Barrios
Gregory R. Bean
Govind Bhagat
Luis Zabala Blanco
Michael Bonert
Alain C. Borczuk
Tamar C. Brandler
Eric Jason Burks
Kelly J. Butnor
Sarah M. Calkins
Weibiao Cao
Wenqing (Wendy) Cao
Barbara Ann Centeno
Joanna SY Chan
Kung-Chao Chang
Hao Chen
Wei Chen
Yunn-Yi Chen
Sarah Chiang
Soo-Jin Cho
Shefali Chopra
Nicole A. Cipriani
Cecilia Clement
Claudiu Cotta
Jennifer A. Cotter
Sonika M. Dahiya
Elizabeth G. Demicco
Katie Dennis
Jasreman Dhillon
Anand S. Dighe
Bojana Djordjevic
Michelle R. Downes
Charles G. Eberhart
Andrew G. Evans
Fang Fan
Julie C. Fanburg-Smith
Gelareh Farshid
Michael Feely
Susan A. Fineberg
Dennis J. Firchau
Gregory A. Fishbein
Agnes B. Fogo
Andrew L. Folpe
Danielle Fortuna
Billie Fyfe-Kirschner
Zeina Ghorab
Giovanna A. Giannico
Anthony J. Gill
Tamar A. Giorgadze
Alessio Giubellino
Carolyn Glass
Carmen R. Gomez-Fernandez
Shunyou Gong
Purva Gopal
Abha Goyal
Christopher C. Griffith
Ian S. Hagemann
Gillian Leigh Hale
Suntrea TG Hammer
Malini Harigopal
Kammi J. Henriksen
Jonas J. Heymann
Carlo Vincent Hojilla
Aaron R. Huber
Jabed Iqbal
Shilpa Jain
Vickie Y. Jo
Ivy John
Dan Jones
Ridas Juskevicius
Meghan E. Kapp
Nora Katabi
Francesca Khani
Joseph D. Khoury
Benjamin Kipp
Veronica E. Klepeis
Christian A. Kunder
Stefano La Rosa
Stephen M. Lagana
Keith K. Lai
Goo Lee
Michael Lee
Vasiliki Leventaki
Madelyn Lew
Faqian Li
Ying Li
Chieh-Yu Lin
Mikhail Lisovsky
Lesley C. Lomo
Fang-I Lu
aDeqin Ma
Varsha Manucha
Rachel Angelica Mariani
Brock Aaron Martin
David S. McClintock
Anne M. Mills
Richard N. Mitchell
Hiroshi Miyamoto
Kristen E. Muller
Priya Nagarajan
Navneet Narula
Michiya Nishino
Maura O'Neil
Scott Roland Owens
Burcin Pehlivanoglu
Deniz Peker Barclift
Avani Anil Pendse
Andre Pinto
Susan Prendeville
Carlos N. Prieto Granada
Peter Pytel
Stephen S. Raab
Emilian V. Racila
Stanley J. Radio
Santiago Ramon Y Cajal
Kaaren K Reichard
Jordan P. Reynolds
Lisa M. Rooper
Andrew Eric Rosenberg
Ozlen Saglam
Ankur R. Sangoi
Kurt B. Schaberg
Qiuying (Judy) Shi
Wonwoo Shon
Pratibha S. Shukla
Gabriel Sica
Alexa Siddon
Anthony Sisk
Kalliopi P. Siziopikou
Stephanie Lynn Skala
Maxwell L. Smith
Isaac H. Solomon
Wei Song
Simona Stolnicu
Adrian Suarez
Paul E. Swanson
Benjamin Jack Swanson
Sara Szabo
Gary H. Tozbikian
Gulisa Turashvili
Andrew T. Turk
Efsevia Vakiani
Paul VanderLaan
Hanlin L. Wang
Stephen C. Ward
Kevin M. Waters
Jaclyn C. Watkins
Shi Wei
Hannah Y. Wen
Kwun Wah Wen
Kristy Wolniak
Deyin Xing
Ya Xu
Shaofeng N. Yan
Zhaohai Yang
Yunshin Albert Yeh
Huina Zhang
Xuchen Zhang
Bihong Zhao
Lei Zhao

To cite abstracts in this publication, please use the following format: **Author A, Author B, Author C, et al. Abstract title (abs#). In "File Title."** ***Laboratory Investigation*** **2022; 102 (suppl 1): page#**

1187 Identifying Histological Patterns of Lung Adenocarcinoma in Small Biopsies: Implications, Practical Issues, and Correlation of Findings with Resected Specimens

Abdul Abid[1], Paul Young[1], Ranjana Nawgiri[1], Palawinnage Muthukumarana[1]
[1]*The University of Texas Medical Branch, Galveston, TX*

Disclosures: Abdul Abid: None; Paul Young: None; Ranjana Nawgiri: None; Palawinnage Muthukumarana: None

Background: Lung adenocarcinoma is architecturally heterogenous, has five histologic patterns and classified according to the predominant pattern. The 2015 World Health Organization (WHO) recommends reporting all identifiable patterns of adenocarcinoma in small biopsies to guide therapeutic decisions. Recognizing patterns in small biopsies pose a challenge to the pathologist and studies lack on evaluation of adenocarcinoma pattern on small biopsies.

Design: A retrospective 4-year search of H & E slides from biopsy and subsequent resection specimen, where available, were reviewed and compared. Clinicopathologic and follow up data were collected.

Results: Our database showed 361 biopsies with lung carcinoma; 51 of which were primary lung adenocarcinoma. 26/51 cases had subsequent resections and 69% of these cases were diagnosed at early stage (I and II). Eleven cases (42%) showed concordance in patterns with resection (figure 1) and 9 (35%) showed minor pattern discordance. Of the 6 cases with major pattern discordance; 3 cases of papillary pattern were misinterpreted as lepidic; 2 cases of detached solid (S) pattern were misinterpreted as acinar and 1 as micropapillary (figure 2). Most common cause for overall discordance was small size/fragmentation (12/26 – 46%) followed by obscuring inflammation and scarring. In cases with minor discordance, growth patterns represented ≤20% of the tumor. Subjects without a subsequent resection (n=25) were commonly diagnosed at advanced stage (92% stage III and above); with solid (13/25), acinar (11/25) and micropapillary (9/25) being most common patterns. Follow up data in this cohort showed that 44% have died of disease and one case of adenocarcinoma diagnosed at stage 1 with solid and micropapillary patterns developed intrapulmonary metastasis two years after diagnosis.

Figure 1 - 1187

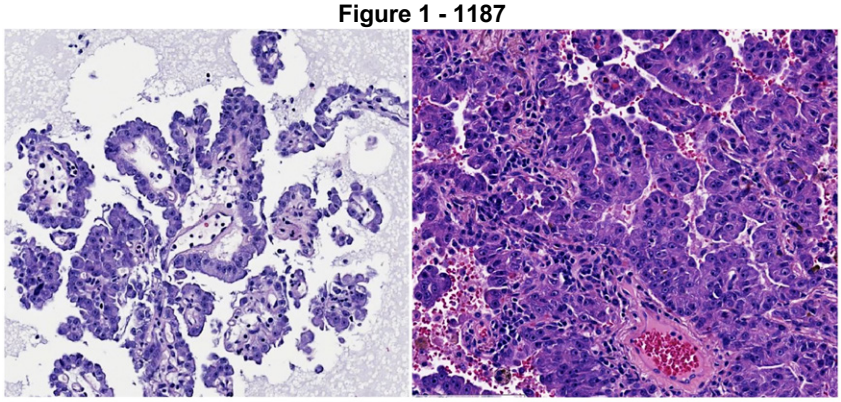

Figure 1: Concordance between biopsy (left) and resection specimen (right) showing papillary patterns

Figure 2 - 1187

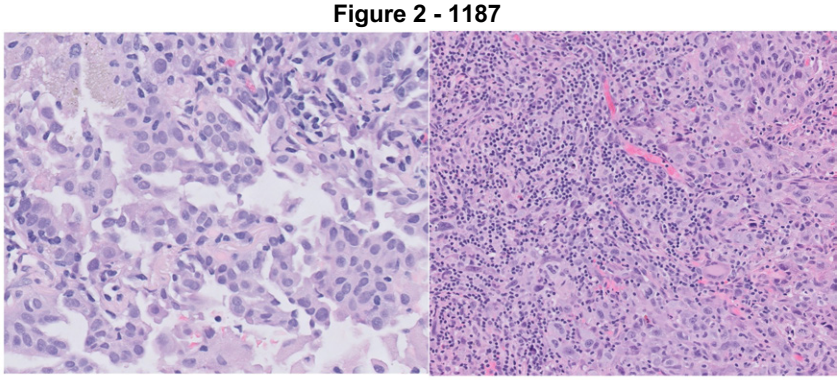

Figure 2: Discordance between biopsy (left) and resection specimen (right) with detached solid pattern interpreted as micropapillary on biopsy

Conclusions: Most biopsies represent the clinically significant predominant patterns of lung adenocarcinoma and are accurately recognized by the pathologists. Few patterns may be underrecognized due to disrupted architecture or small size. Aggressive patterns are known to be of independent prognostic and predictive value and accurate pattern identification on biopsies can guide therapeutic decisions in both resectable and unresectable lung adenocarcinoma. Further studies need to address improving diagnostic accuracy and reproducibility of patterns in small biopsies as pathologists are continuously challenged to provide as much information from small samples for clinical management.

1188 Worst Pattern of Invasion (WPOI) is a Novel Prognostic Factor in Squamous Cell Carcinoma of The Lung

Francesca Ambrosi[1], Federico Chiarucci[2], Costantino Ricci[3], Nazarena Nannini[1], Pietro Bertoglio[4], Piergiorgio Solli[5], Michelangelo Fiorentino[1]

[1]Maggiore Hospital, University of Bologna, Bologna, Italy, [2]Alma Mater Studiorum-University of Bologna, Bologna, Italy, [3]S.Orsola-Malpighi Hospital, University of Bologna, Bologna, Italy, [4]Sant'Orsola-Malpighi Academic Hospital of Bologna, Italy, Bologna, Italy, [5]IRCCS Azienda Ospedaliero-Universitaria di Bologna, Bologna, Italy

Disclosures: Francesca Ambrosi: None; Federico Chiarucci: None; Costantino Ricci: None; Nazarena Nannini: None; Pietro Bertoglio: None; Piergiorgio Solli: None; Michelangelo Fiorentino: None

Background: The worst pattern of invasion (WPOI) is a relevant and validated prognostic factor in oral squamous cell carcinoma (OSCC) mandatory to report according to AJCC. However, WPOI has never been investigated in squamous cell carcinoma of the lung (SCCL), whose morphological characterization and the diagnostic report are still based on conventional histological features.

Design: Forty-six consecutive cases of SCCLs with paired mediastinal lymph nodes were reviewed with hematoxylin and eosin (H&E) and pan-cytokeratin (PAN-CK) stains. The WPOI has been assessed in each tumor as previously described (WPOI-1, well-defined borderline borders; WPOI-2, cords, and less marked borderlines; WPOI-3, groups of cells and no distinct borderlines; WPOI-4, like cord-shaped microtumor nests; WPOI-5, single tumor cells on the edge of the tumor), analyzing its association with other convectional clinical-pathological features [χ^2 tests for dichotomous and categorical data; Student *t*-test (normal distribution) and Mann-Whitney *U*-test (non-normal distribution) for continuous data].

Results: High grade WPOI (WPOI-4 and -5) were found in 39.1% cases (WPOI-4:12 and WPOI-5: 6 patients) and low grade WPOI (WPOI-1, -2 and -3) in 28 cases (WPOI-1:10, WPOI-2:9 and WPOI-3: 9 patients), respectively. WPOI was significantly associated with the status of regional nodal metastasis ($p=0.02$), higher pathological stage ($p=0.03$), and the assessment of lymphovascular invasion ($p<0.01$); besides, aggressive-WPOI were associated with larger nodule diameter ($p=0.01$; Student *t*-test, normal distribution. Interestingly, WPOI-1 and -2 tumors didn't present any regional nodal metastasis in our case series; meanwhile, the 5 pN2 patients (10.8%) only show WPOI-4 (6.5%) and -5 (4.3%). We didn't find any significant association between WPOI and the other conventional clinical-pathological features.

Conclusions: WPOI resulted associated with relevant clinical-pathological features (lymphovascular invasion, pN, and pT stage), and it could represent an innovative diagnostic and strong prognostic biomarker, as well as a therapeutic tool, for patients with SCCL undergone surgical resection; notably, high-grade WPOI (WPOI-4 and -5) identifies cases at high-risk of developing lymph node metastases. Future studies should investigate the association between specific genetic mutations and survival data.

1189 Rare/Novel EGFR Variants in Patients with Non-Small Cell Lung Cancer: An Institutional Experience with Treatment and Outcome

Karen Arispe Angulo[1], Yu-Wei Cheng[2], Maureen Jakubowski[1], Elizabeth Azzato[1]

[1]Cleveland Clinic Foundation, Cleveland, OH, [2]Cleveland Clinic Pathology and Laboratory Medicine, Cleveland, OH

Disclosures: Karen Arispe Angulo: None; Yu-Wei Cheng: None; Maureen Jakubowski: None; Elizabeth Azzato: None

Background: Molecular testing for Non-Small Cell Lung Cancer (NSCLC) is standard practice to guide therapy, including tyrosine kinase inhibitor (TKI) therapy in patients with activating *EGFR* mutations. However, next generation sequencing (NGS) can detect rare and novel variants, for which function, targeted therapy and outcome has not been established. In this study we aim to identify rare *EGFR* variants in our patient population, type of therapy received and clinical outcome.

Design: We performed a 5-year retrospective review of all NSCLC specimens that underwent custom hotspot NGS panel (*EGFR*, *KRAS*, *BRAF*, *ERBB2*, *MET*) at our institution. Specimen types included FFPE and FNA specimens for both primary and metastatic disease. Variants were evaluated using cancer variant databases, literature and guidelines. Medical records were reviewed to collect clinical information.

Results: 3,578 specimens were reviewed (45% FNA, 55% FFPE). *EGFR* variants were detected in 506 (14%) samples, with hotspot variants in exons 18-21 present in the majority of these samples (89%). Of the remaining samples, patients with recurrent variants (>10 instances reported in literature) and those that had previously undergone therapy were not considered. 33 patients with 31 rare *EGFR* variants were identified (aged 54-87 yrs; 13 males). These patients varied in stage at presentation: stage I (n=10), stage II (n=3), stage III (n=6), stage IV (n= 10), unknown (n=3), recurrent disease (n=1). Uncommon variants included missense variants in exons 7, 15, 18-21 and an indel in exon 21. In 18 patients, the rare variant was seen in combination with other driver mutations, including *BRAF* codon 469 (n=1), *EGFR* tyrosine kinase activating mutations (n=11), and *KRAS* codons 12/13 (n=6). 15 patients had a rare *EGFR* mutation as a primary finding; the majority of these patients were advanced stage (n=9 stage III/IV or recurrent, n=2 unknown). Out of the 33 patients with rare *EGFR* variants, *EGFR* TKI therapy was administered in 3 patients with advanced NSCLC. Two patients did not respond to TKI treatment. The third patient had a concurrent L858R mutation, responded to TKI therapy and is alive one year post diagnosis.

Conclusions: Rare or novel *EGFR* alterations can be detected during routine molecular testing for NSCLC. These can be seen in combination with known driver mutations or as a primary finding. Clinical outcomes of patients with such variants treated with *EGFR* TKI therapy may provide insights into function or therapy response.

1190 Unexpected Histologic and Molecular Features in Tumors of Long-Term Survivors (LTS) of Diffuse Pleural Mesothelioma (DPM)

Marina Baine[1], Prasad Adusumilli[1], Francis Bodd[1], Marc Ladanyi[1], Michael Offin[1], William Travis[1], Soo-Ryum Yang[1], Katia Ventura[1], Marjorie Zauderer[1], Jennifer Sauter[1]
[1]Memorial Sloan Kettering Cancer Center, New York, NY

Disclosures: Marina Baine: None; Prasad Adusumilli: None; Francis Bodd: None; Marc Ladanyi: None; Michael Offin: *Speaker*, OncLive, Targeted Oncology, American Society for Radiation Oncology; *Consultant*, PharmaMar, Novartis, Jazz Pharmaceuticals; *Grant or Research Support*, Merck Sharp & Dohme; William Travis: None; Soo-Ryum Yang: None; Katia Ventura: None; Marjorie Zauderer: *Advisory Board Member*, Takeda, GSK, Aldeyra Therapeutics, Novocure, Atara; *Grant or Research Support*, Precog, Epizyme, GSK, Polaris, Sellas Life Sciences, BMS, Takeda, Curis; *Speaker*, Research to Practice, Medical Learning Institute, OncLive; Jennifer Sauter: None

Background: There is increased recognition of prognostically significant histologic features in DPM beyond histologic type; particularly, nuclear grade (Gd), architectural patterns and necrosis in epithelioid (E) DPM. Furthermore, genomically, homozygous *CDKN2A* deletions are associated with poor survival. Pathologic features of DPM in patients with LTS have not yet been described.

Design: DPMs from surgical patients with LTS ($\geq$ 3 years from diagnosis) were retrospectively reviewed. Diagnoses were confirmed by 2021 WHO criteria and immunohistochemistry (IHC) with carcinoma and mesothelial markers (at least 2 each) on all cases. Malignancy was confirmed by invasion or loss of BAP1 expression by IHC. The following were documented: histologic subtype (E or biphasic (B)), lymphovascular invasion (LVI) and presence of necrosis. E DPM were assessed for Gd (2021 WHO 2-tier), architectural patterns (favorable: tubulopapillary (TP) and trabecular (T); unfavorable: micropapillary (MP) and solid (S)), and presence of pleomorphic (Pl) or rhabdoid (Rd) features (both unfavorable). Next generation sequencing (NGS) was performed on 23 DPM.

Results: Archival slides from 76 patients (median age 63 years, 66% male, pathologic stage: I (15%), II (20%), III (50%), IV (15%); 85% completely resected) with DPM and LTS (median 4.35 years) were available. At least one unfavorable feature was seen in 44 (58%) tumors (see Table 1 for details). Although most DPM of LTS were E (72 (95%)), surprisingly, 4 (5%) were B. LVI was seen in 22 (29%). Necrosis was seen in 15 (20%). Of 72 E DPM, 10 (14%) were high Gd. Predominantly unfavorable architectural patterns were seen in 10 E DPM (14%): 6 and 4 with S and MP patterns, respectively. MP architecture was seen, at least focally, in 27 (38%) E DMP. Five tumors showed focal Pl features, and one showed diffuse Rd features, of which 3 and 1 were S-predominant, respectively. Genomically, CDKN2A deletion was detected in 1 (4%) DPM. Additional alterations detected by NGS included: 14 (61%) *BAP1*, 4 (17%) *NF2*, 4 (17%) *SETD2*, and 2 (9%) *TRAF7*. Alterations in *LATS1*, *RB*, *TP53* and *WT1* were detected in 1 DPM each.

Table 1: Prognostically unfavorable histologic and genomic features in diffuse pleural mesothelioma (DPM) of long-term survivors, defined as at least 3 years.

Unfavorable histologic features	Total		
All tumors (N=76)			
Biphasic	4 (5%)		
LVI	22 (29%)		
Necrosis	15 (20%)		
Epithelioid DPM (N=72)			
High nuclear grade (2021 WHO)	10 (14%)		
Architectural pattern	Total	Predominant	Secondary/minor
Solid	22 (31%)	6 (8%)	16 (22%)
Micropapillary	27 (38%)	4 (6%)	23 (32%)
Cytologic features	Total	Diffuse	Focal
Pleomorphic	5 (7%)	0	5 (7%)
Rhabdoid	1 (1%)	1 (1%)	0
DPM with NGS data (N=23)			
CDKN2A deletion	1 (4%)		

Conclusions: Presence of prognostically unfavorable features is surprisingly not uncommon in DPM from patients with LTS, highlighting a need for integration of pathologic features, and molecular and clinical characteristics for more accurate prognostication.

1191 Improving Time-to-Treatment for Advanced Non-Small Cell Lung Cancer Patients in British Columbia through Faster Genetic Testing using the Idylla™ EGFR Testing Platform

Norbert Banyi[1], Curtis Hughesman[2], Diana Ionescu[1], Carmen Ma[2], Kelly McNeil[2], Stephen Yip[3], Barbara Melosky[2], Deepu Alex[2]

[1]The University of British Columbia, BC Cancer, Vancouver, Canada, [2]BC Cancer, Vancouver, Canada, [3]The University of British Columbia, Vancouver, Canada

Disclosures: Norbert Banyi: None; Curtis Hughesman: *Speaker*, AstraZeneca; Diana Ionescu: None; Carmen Ma: None; Kelly McNeil: None; Stephen Yip: *Advisory Board Member*, AstraZeneca, Bayer, Amgen, Roche, EMD Sereno, Novartis; Barbara Melosky: *Advisory Board Member*, Roche, AZ, Merck, BNS, Pfizer, Novartis; Deepu Alex: None

Background: Patients with advanced-stage non-small cell lung cancer (NSCLC) benefit from a short time-to-treatment (TTT) due to disease severity. In British Columbia (BC), patients with NSCLC undergo next-generation sequencing (NGS) for lung cancer genetic biomarkers prior to treatment as outlined by CAP-AMP-IASLC guidelines. NGS gene panels are time-intensive and commonly contribute to increased TTT. This study evaluates the feasibility of adding the Idylla EGFR assay into the molecular testing workflow to improve TTT.

Design: A trial cohort of consecutive advanced NSCLC patients (N = 238) were tested by both, an in-house lab-developed NGS panel and the Idylla EGFR assay. Data was also collected for a control cohort (N = 220) that received only NGS testing. For each patient, the following results were recorded: lab sample-received time, time to NGS and Idylla reports, molecular testing results, time to first-treatment, and final treatment regimen. Differences in the EGFR test results and associated turn-around time (TAT) were compared between NGS and Idylla assays. TTT was defined as the time period from tumor sample receipt in the genetics lab to the patient's first treatment.

Results: A concordance of 97.5% (232/238) was observed between the EGFR results of the Idylla and NGS assays. Discrepant results were observed in three cases; two with rare EGFR mutations found by the NGS assay but not covered by the Idylla test and one where the EGFR mutation detected by Idylla was subthreshold for reporting by the NGS assay. 3 cases with negative Idylla results failed NGS testing. Idylla TAT (N=235) was faster by an average of 12.4 days when compared to NGS ($p < 0.01$). Overall, the average TTT in the trial cohort (N = 114) was 10.1 days faster ($p < 0.05$) than the control cohort (N = 114), a 25% reduction in

TTT. Focusing only on EGFR-positive patients, the average TTT in the trial cohort (N = 33) was 16.8 days faster ($p < 0.05$) than the control cohort (N = 28), a 48% reduction in TTT.

EGFR status/mutation	Idylla EGFR result	NGS EGFR result	Discrepant Results
G719X (Exon 18)	3	3	-
L858R	21	19	NGS FAILS 2
EXON 19 DEL	18	17	SUBTHRESHOLD BY NGS 1
EXON 20 INS	2	2	-
EGFR NEG	194	191	NGS: EXON 20 INS/DUP* 1 NGS: EXON 19 INDEL* 1 NGS FAIL 1 *not detected by Idylla test

Figure 1 - 1191

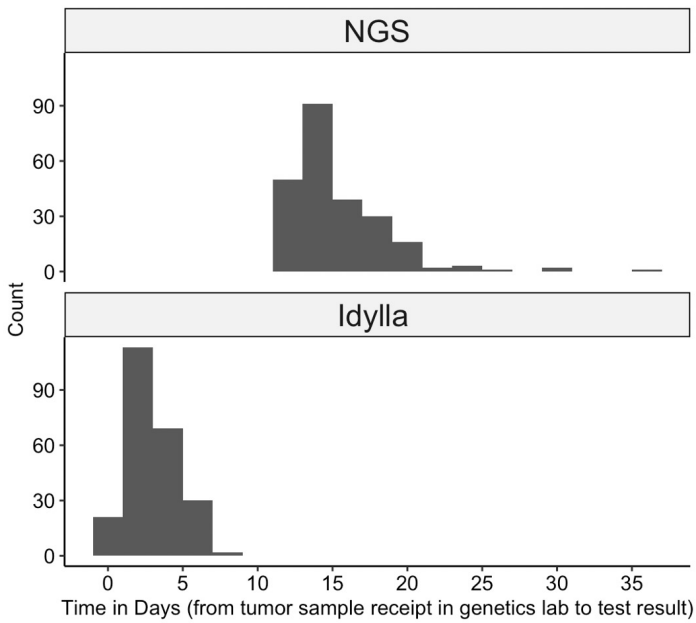

Conclusions: Using the Idylla EGFR test as part of the molecular testing repertoire in advanced-stage NSCLC patients in BC leads to a significant reduction in overall TTT, driven specifically by decreased TTT in EGFR-positive patients.

1192 Grading of Lung Adenocarcinomas: Comparison of Paired Biopsies and Resections

Atreyee Basu[1], Fang Zhou[2], Navneet Narula[3], Andre Moreira[3]
[1]NYU Langone Health, New York City, NY, [2]NYU School of Medicine, New York, NY, [3]NYU Langone Health, New York, NY

Disclosures: Atreyee Basu: None; Fang Zhou: *Stock Ownership*, MRNA, DOCS; Navneet Narula: None; Andre Moreira: *Consultant*, Olympus, Roche

Background: In 2020, the International Association for the Study of Lung Cancer (IASLC) proposed grading criteria for resections of invasive lung adenocarcinoma that independently predicted overall and recurrence-free survival, based on the predominant

pattern and presence of high-grade (HG) patterns. We retrospectively assessed the correlation between biopsies and paired IASLC-graded resections.

Design: IASLC grading criteria were applied to 159 resections:
Grade 1 (G1): lepidic predominant with < 20% HG pattern.
Grade 2 (G2): acinar or papillary predominant with < 20% HG pattern.
Grade 3 (G3, or poorly differentiated): any tumor with ≥20% HG pattern.

The following grading criteria were applied to paired preoperative biopsies:
G1: lepidic predominant with no HG pattern.
G2: acinar or papillary predominant with no HG pattern.
G3: tumor with any amount of HG pattern.

HG pattern was defined as solid, micropapillary, and/or complex glands (cribriform and fused glands).

G1 and G2 were combined into one category (G1-2) while G3 was the second category, and diagnostic test performance characteristics were calculated using resections as the reference group.

Results: On biopsy, there were 101 G1-2 (45 G1+56 G2) and 58 G3 cases. On resection, there were 79 G1-2 (32 G1+47 G2) and 80 G3 cases. Of the 80 G3 resections, 25(31%) were G1-2 on biopsy: 6(8%) were G1 and 19(24%) were G2. Of the 45 G1 biopsies, on resection 26(58%) remained G1, 13(29%) increased to G2, and 6(13%) increased to G3. Of the 56 G2 biopsies, on resection 6(11%) decreased to G1, 31(55%) remained G2, and 19(34%) increased to G3. Of the 58 G3 biopsies, on resection none were G1, 3(5%) decreased to G2, and 55(95%) remained G3.

The accuracy for poorly differentiated grade was 82%. Of the 28 discrepancies, in 25(89%) cases the resection was G3, but no HG pattern was present on biopsy; while 3(11%) discrepancies were due to G3 on biopsy decreasing to G2 on resection (<20% HG pattern). Biopsies showed 75% sensitivity, 96% specificity, 95% positive predictive value (PPV), and 75% negative predictive value for G3.

Table 1 showing "G1-G2" and "G3" grades on Resection (IASLC) vs Biopsy (Modified) specimens

		IASLC GRADE ON RESECTIONS		
		G1-2	**G3**	**Total**
MODIFIED GRADE ON BIOPSIES	G1-2	76	25	101
	G3	3	55	58
	Total	**79**	**80**	**159**

Figure 1 - 1192

Figure 1 showing "G1", "G2" and "G3" grades on Resection (IASLC) vs Biopsy (Modified) specimens

		IASLC GRADE ON RESECTIONS			
		G1	**G2**	**G3**	**Total**
MODIFIED GRADE ON BIOPSIES	**G1**	26	13	6	45
	G2	6	31	19	56
	G3		3	55	58
	Total	**32**	**47**	**80**	**159**

Figure 2 - 1192

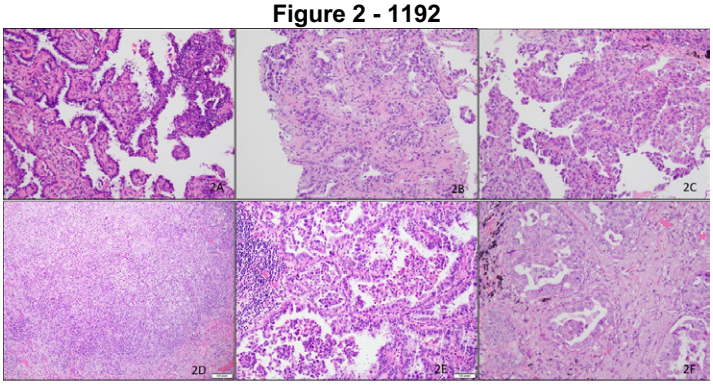

Figure 2: Examples of different patterns of lung adenocarcinoma (2A: Lepidic, H&E at 20X; 2B: Acinar, H&E at 20X; 2C: Papillary, H&E at 20X; 2D: Solid, H&E at 10X; 2E: Micropapillary, H&E at 20X; 2F: Complex glands, H&E at 20X)

Conclusions: It is feasible to grade invasive lung adenocarcinomas on biopsies using a modified method that correlates well with resections graded by the IASLC criteria. G1-2 biopsies tended to underestimate the resection grade, likely due to sampling error.

However, biopsies had 96% specificity and 95% PPV to rule in G3 grade on resection, which has potential clinical relevance in selecting patients for more aggressive therapy.

1193 Point of Care NGS testing in NSCLC

Andrea Beharry[1], Joanne Diep[1], Parneet Cheema[1], Brian Olsen[1], Brandon Sheffield[1]
[1]William Osler Health System, Brampton, Canada

Disclosures: Andrea Beharry: None; Joanne Diep: None; Parneet Cheema: *Speaker*, Thermofisher; *Advisory Board Member*, Amgen, Bristol Myers Squibb, AstraZeneca, Roche, Pfizer, EMD Serono, Novartis, Takeda, Bayer; Brian Olsen: None; Brandon Sheffield: *Consultant*, Abbvie, Biocartis, Jansen; *Grant or Research Support*, Amgen, Astra Zeneca, Eli Lilly, EMD Serono; *Speaker*, Boehringer Ingelheim, Thermo Fisher; *Primary Investigator*, Elevation Oncology; *Advisory Board Member*, Incyte, Merck, Turning Point Therapeutics; *Grant or Research Support*, Novartis, Pfizer, Roche

Background: Next generation sequencing (NGS) is the laboratory cornerstone of precision oncology treatment. This modality allows for the simultaneous interrogation of multiple genetic targets across multiple mutation classes, efficiently utilizing small biopsies. Traditional NGS operations are complicated, requiring specialized equipment and personnel, creating a niche for this service in subspecialized laboratories. In many jurisdictions, the majority of cancer patients are treated in publicly-funded community hospitals, where NGS is not typically utilized and access to testing is via send-out services associated with lengthy turnaround times. Here, we have validated and implemented one of the world's first "point of care" NGS services, localized within an immunohistochemistry (IHC) lab and operated by histotechnologists. Early experience with lung cancer patients is presented.

Design: All NGS studies were performed using the oncomine precision assay (OPA) on the genexus integrated sequencer. All NGS was performed by histotechnologists, simultaneously responsible for IHC, and routine histology services. All NGS results were provided by anatomic pathologists in conjunction with diagnostic information and IHC biomarkers. Retrospective chart review was performed for all patients undergoing sequencing studies and key data, including turnaround time and NGS findings were extracted from the electronic medical record for analysis.

Results: A total of 272 cases of non-small cell lung cancer (NSCLC) were tested using point of care NGS. Median turnaround time was 3 business days (measured as diagnosis to report date, for in-house cases with reflex testing). 39 cases (14.3%) were resulted with NGS findings available simultaneously with a NSCLC diagnosis (0 day turnaround).

Table 1. Turnaround time summary statistics for point-of-care style NGS.

Turnaround time	Business Days
Median	3
Range	0-24
Interquartile range (Q1-Q3)	2-5

Figure 1 - 1193

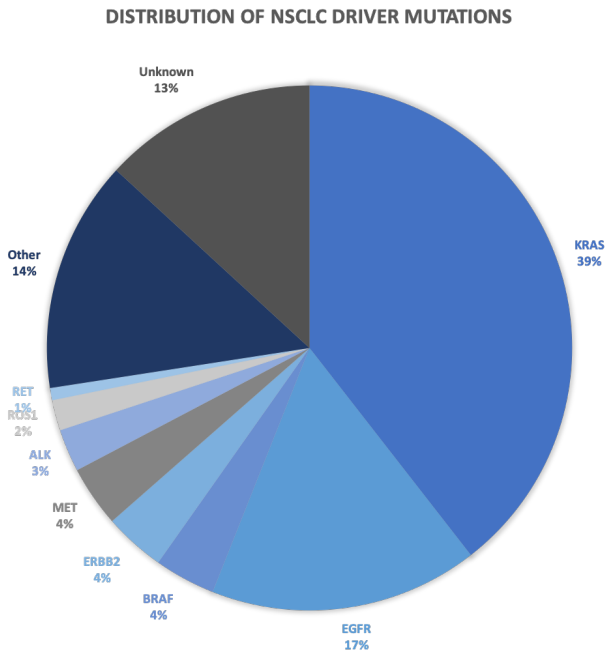

Conclusions: Delayed biomarker results is a widespread barrier to precision medicine practice. Here, we show that comprehensive NGS testing can be performed alongside IHC and run by the same group of laboratory professionals. Having this technology available closer to the front lines of patient care offers an invaluable service to cancer practitioners. The availability of this tool within the histopathology lab also empowers pathologists to utilize this technology in their day-to-day practices. This enables not just predictive biomarker testing, but facilitates the use of NGS as a diagnostic adjunct. More studies are needed to explore the utility of these expanded roles for NGS testing.

1194 Next-Generation Sequencing Analysis of 11 Primary Pediatric Lung Neoplasms: Prevalence of Tumor-Specific Driving Mutations and Copy Number Variations with Low Tumor Mutation Burden and Microsatellite Stability

Jennifer Boland Froemming[1], Benjamin Kipp[1], Shannon Knight[2]
[1]Mayo Clinic, Rochester, MN, [2]Mayo Clinic

Disclosures: Jennifer Boland Froemming: None; Benjamin Kipp: None; Shannon Knight: None

Background: Primary lung tumors are very rare in pediatric patients (≤ 21 years), and the spectrum of neoplasms encountered is quite different from those in adults. There is a relative paucity of genetic data for pediatric lung tumors, and little is known regarding if tumors that also occur in adults (i.e. carcinoid tumors) have similar vs. distinctive genetic profiles.

Design: Diagnostic slides from resected pediatric lung tumors were retrieved from institutional archives (1992-2018), and diagnoses were confirmed. Cases were selected which had adequate material and sufficiently recent formalin-fixed paraffin embedded tissue for advanced molecular analysis. Next-generation sequencing was performed using a solid tumor panel that included assessment of tumor mutation burden, microsatellite stability, somatic sequence variants (514 genes), amplifications (59 genes), fusions (55 genes), and specific transcript variants.

Results: Analyzed tumors (n=11) included 6 carcinoid tumors (2 atypical), and 1 each of paraganglioma, schwannoma, inflammatory myofibroblastic tumor, synovial sarcoma and pleuropulmonary blastoma. All tumors were microsatellite stable and had low tumor mutation burden (range 0-2.4 mut/Mb). Three carcinoid tumors (CTs; 2 typical, 1 atypical) had copy number variations (CNVs) including loss of chromosomes 13, 21, 22, and 15q, and gains of 7 and 8. One typical CT had *ARID1A* c.6747dupA p.E2250fs*28, and 1 atypical CT had a more unusual mutation, *DNMT1* c.445+1G>A. The CTs with CNVs and those with mutations were mutually exclusive. One typical CT had no genetic abnormalities detected. The

pleuropulmonary blastoma showed *DICER1* c.5126A>G p.D1709G. The IMT showed *TOP2A* c.3290T>C p.V1097A (RNA fusion analysis still pending). The paraganglioma demonstrated mutations in *SDHD* c.167delA p.H56fs*30, *VHL* c.598C>T p.R200W, and *RAD51D* c.47T>C p.M16T. The schwannoma had *ATM* c.7865C>G p.A2622G. In addition to the *SS18-SSX1* fusion detected clinically, the synovial sarcoma showed CNVs including losses of chromosome 3, 11q, 22 and X.

Conclusions: Compared to adult lung tumors, primary lung neoplasms in pediatric patients are comparatively genetically simple with low tumor mutation burden and microsatellite stability, and frequent presence of one or more tumor-specific driving mutations and CNVs. Interestingly, while 33% of pediatric CTs showed mutations in chromatin-remodeling genes as reported in adults, half had no mutations but demonstrated CNVs, and one had no detectable genetic abnormalities.

1195 In Search for Putative Precursor Lesions in Invasive Mucinous Adenocarcinoma of the Lung (IMA): Immunohistochemical and Molecular Study

Baris Boyraz[1], Lauren Ritterhouse[2], Treah May Sayo[3], Jaimie Barth[1], Yin (Rex) Hung[1], Angela Shih[1], Mari Mino-Kenudson[2]

[1]Massachusetts General Hospital, Boston, MA, [2]Massachusetts General Hospital, Harvard Medical School, Boston, MA, [3]Massachusetts General Hospital, Lung Center of the Philippines, Boston, MA

Disclosures: Baris Boyraz: None; Lauren Ritterhouse: *Advisory Board Member*, Loxo Oncology, AstraZeneca *Consultant*, Amgen; *Speaker*, Merck; Treah May Sayo: None; Jaimie Barth: None; Yin (Rex) Hung: *Consultant*, Elsevier; Angela Shih: None; Mari Mino-Kenudson: *Consultant*, AstraZeneca, H3 Biomedicine; *Primary Investigator*, Novartis; *Advisory Board Member*, BMS, Sanofi

Background: A precursor lesion for IMA has not been well-established. We have observed well-formed mucinous glands without overt invasion reminiscent of pyloric glands (PGL) in small IMAs. A recent study has also shown increased expression of Muc6, a marker for pyloric glands, associated with better prognosis in IMA. Therefore, we hypothesized that PGL represents a putative precursor lesion for IMA.

Design: IMA or mixed mucinous and non-mucinous adenocarcinoma (mIMA) resected between 2006 to 2017 were searched in our departmental archives. In tumors with available material, several histologic features including growth patterns (PGL, lepidic and invasive) were evaluated on H&E along with mucicarmine/elastic stains. All were evaluated for Muc5AC and Muc6 immunostains and with NGS (104 cancer-related genes).

Results: The study cohort consisted of 21 IMAs and 21 mIMA from 42 patients (29 females; age range: 40-89 [median 68] years). Tumors ranged in size from 0.5-15.0 cm (median 2.1 cm). Histologically, 35 tumors showed PGL in 5-80% (median 20%), 40 showed lepidic pattern in 10-100% (median 50%) and 35 harbored invasive pattern in 5-90% (median 40%) of the areas. *KRAS* mutations were found in 30 tumors. Additional recurrent mutations included *GNAS*, *STK11*, *EGFR*, *TP53*, *ERBB2* (2 tumors each). All expressed Muc5AC in the majority of lesional cells (median 100%). Muc6 expression as seen in 34 was predominantly located in the PGL with loss of Muc6 staining in the invasive and lepidic components (Muc6/Muc5AC%: 0-100%, median 40%). Of 30 *KRAS* mutants, Muc6 expression was extensive (Muc6/Muc5AC% >50%) in 53% of 16 small ($\leq$2cm) tumors, but limited in larger tumors. Of 35 patients with available follow-up (9-168 [median 48] months), 5 developed metastasis/recurrence; their primary tumors ranged 1.8-15.0 cm (median 5.0 cm), 2 had lymphatic invasion with 1 lymph node metastasis and 2 had pleural invasion. The 4 *KRAS* mutants with recurrence showed only limited PGL (5-10%) and Muc6 expression (Muc6/Muc5AC%: 5-10%) in their primary tumors.

Conclusions: PGL was present in most IMA and mIMA, and associated with Muc6 expression, while loss of Muc6 was mostly seen in the invasive and lepidic patterns. Limited Muc6 expression along with large tumor size and lymphatic invasion was associated with worse prognosis. Our findings raise the possibility of PGL being a precursor to (*KRAS*-mutated) IMA. A larger cohort study with additional molecular annotation is underway.

1196 Estrogen Receptors Expression in Female Lung Micropapillary Adenocarcinoma

Carla Caruso[1], Magda Esebua[1]
[1]University of Missouri, Columbia, MO

Disclosures: Carla Caruso: None; Magda Esebua: None

Background: Lung cancer remains the most common malignancy worldwide and is the second most common cancer in females after breast cancer. Approximately 50% of cases are adenocarcinomas. Expression of estrogen receptors (ER) in lung adenocarcinoma has been linked to good prognosis. However, the association between ER expression and lung adenocarcinoma subtypes has not been well studied. In our study, we aim to determine the relationship between female lung adenocarcinoma histologic subtypes and ER expression by immunohistochemistry.

Design: We analyzed surgical specimens of lung adenocarcinoma from 48 women (59±11 years), from our archives obtained from 2002 to 2017. After reviewing the material for adequacy and selection of paraffin blocks for Tissue Microarray Slides preparation, 2 cases were excluded due to tissue loss during processing. The initial diagnosis was confirmed with TTF-1 (EP229), GATA3 (L50-823) and CDX2 (EPR2764Y) immunostains in all cases. Anti-ER antibody SP1 was tested for all patients and two pathologists independently analyzed the intensity of ER nuclear expression and assigned a score according to the breast ER staining protocol (negative, weak, moderate, strong). Also, we evaluated the association between adenocarcinoma subtypes and estimated the proportion of tumoral cells that expressed ER.

Results: All tumors were positive for TTF-1 and negative for CDX2 and GATA3. ER was expressed in 29/46 cases (63%) and absent in 17/46 (37%). ER expression was weak in 21/29 and moderate in 8/29 cases. No tumor had strong ER expression. In the tumors were ER expressed, the proportion of ER positive tumor cells was 11%. All micropapillary carcinomas (8/29) were ER positive (weak, 11% of positive cells). Poorly differentiated carcinomas (5/29) were ER negative. Acinar and lepidic subtypes, as well as mucinous adenocarcinomas displayed variable ER expression.

Conclusions: We identified that micropapillary variant of lung adenocarcinoma, associated with poor prognosis, consistently expressed estrogen receptors. This novel finding, might represent an innovative target to add to standard therapy or for refractory alternative therapy of this type of lung adenocarcinoma.

1197 Lung Carcinoid Tumors: Histology and Ki-67, The Eternal Rivalry

Giovanni Centonze[1], Patrick Maisonneuve[2], Federica Grillo[3], Michele Simbolo[4], Alessandra Fabbri[1], Natalie Prinzi[5], Vincenzo Lagano[1], Giovanna Garzone[1], Martina Filugelli[1], Giovanna Sabella[1], Sara Pusceddu[6], Luisa Bercich[7], Luigi Rolli[8], Luca Roz[1], Aldo Scarpa[4], Carlo Capella[9], Massimo Milione[1]
[1]Fondazione IRCCS Istituto Nazionale Tumori Milano, Milan, Italy, [2]IEO, Milan, Italy, [3]University of Genova, Genova, Italy, [4]University of Verona, Verona, Italy, [5]IRCCS Foundation, Istituto Nazionale dei Tumori, Milan, Italy, [6]Fondazione IRCCS Istituto Nazionale Tumori Milano, [7]University of Brescia at ASST-Spedali Civili, Brescia, Italy, [8]IRCCS Foundation National Cancer Institute, Milan, Italy, [9]Uni-Insubria, Varse, Italy

Disclosures: Giovanni Centonze: None; Patrick Maisonneuve: None; Federica Grillo: None; Michele Simbolo: None; Alessandra Fabbri: None; Natalie Prinzi: None; Vincenzo Lagano: None; Giovanna Garzone: None; Martina Filugelli: None; Giovanna Sabella: None; Sara Pusceddu: None; Luisa Bercich: None; Luigi Rolli: None; Luca Roz: None; Aldo Scarpa: None; Carlo Capella: None; Massimo Milione: None

Background: Lung Carcinoid Tumors, according to the current World Health Organization, are well-differentiated lung neuroendocrine neoplasms (NENs) classified as low grade Typical (TC) and intermediate grade Atypical (AC) carcinoids, depending on the amount of necrosis and mitotic cut-off of 2 mitoses per $2mm^2$. Little is known, however, concerning protein expression and morphological factors able to predict disease aggressiveness and progression. Though Ki67 has proved to be a useful and powerful diagnostic and prognostic factor for gastro-entero-pancreatic NENs, its role in lung NENs is still very much debated

Design: A retrospective series of surgical specimens of more than 370 lung carcinoids (collected from two oncology institutions) was centrally reviewed. Morphology and immunohistochemical (IHC) markers (Ki-67, TTF-1, CD44, OTP, Sstr2a, Ascl1, p53 and Rb1) were studied and correlated with Disease Free Survival (DFS) and Overall Survival (OS).

Results: Carcinoid tumor diagnosis was confirmed in 355 patients: 297 (83.7%) TC and 58 (16.3%) AC. In AC, Ascl1+ tumors were associated with high Ki-67 value (p=0.005), necrosis (p=0.02), air space microscopic infiltration (p<0.001) and absence of Sstr2a (p<0.001). Furthermore, multivariate analysis showed that Ascl1 (Present vs Absent, HR 2.90 (1.26-6.68), p=0.01) was associated with reduced DFS. Regarding the whole population, Ki-67 proliferative index at 3% was the best value in predicting DFS. Tumors with Ki-67≥3% were associated with AC histology (p<0.001), stage III-IV (p=0.004), smoking (p=0.001), vascular invasion (p=0.01), peritumoral lymphocyte infiltrate (p=0.02), air space microscopic infiltration (p<0.001), solid sheet morphologic pattern (p<0.001), OTP absence (p<0.001), and presence of TTF-1 (p<0.001), Ascl1 (p<0.001) and p53 (p<0.001). After adjustment for center, either Ki67 (≥ 3 vs <3, p=0.001) or histology (AC vs TC p<0.001) alone significantly added prognostic information to the OS multivariate model with age, stage and OTP (p<0.001); adding both variables did not provide further prognostic information. Conversely, an improved significance of the prediction model for DFS at multivariate analysis, was seen by adding Ki67 (≥ 3 vs <3, p=0.03) to histology, age, lymph node involvement and OTP (p<0.001).

Conclusions: Ki-67≥3 plays an important role in the clinical outcome of carcinoids, irrespective of their WHO class. Furthermore, ASCl1 staining in AC suggests worst prognosis.

1198 Predicting Tumor Mutational Burden from H&E Slides of Lung Squamous Cell Carcinoma: Pathologists, Non-pathologists, and a Neural Network

Salma Dammak[1], Aaron Ward[2], Sherman Lin[3], Priyadharshini Sivasubramaniam[4], Cady Zeman-Pocrnich[1], Christopher Hartley[4], Matthew Cecchini[1]

[1]London Health Sciences Centre, Western University, London, Canada, [2]Western University, London, Canada, [3]University of Western Ontario, London, Canada, [4]Mayo Clinic, Rochester, MN

Disclosures: Salma Dammak: None; Aaron Ward: None; Sherman Lin: None; Priyadharshini Sivasubramaniam: None; Cady Zeman-Pocrnich: None; Christopher Hartley: None; Matthew Cecchini: *Speaker*, Merck; *Consultant*, Tenomix

Background: The Programmed death-ligand 1 (PD-L1) score is used to guide treatment decisions, but it does not accurately predict response to immunotherapy in all cases. While adding tumor mutational burden (TMB) to PD-L1 improves response prediction, it is costly and typically requires high tumor cellularity. Previous studies have demonstrated that genomic information such as driver mutations, are encoded in the morphologic appearance of cancer cells[1]. However, there are not currently any established means to visually identify cases with high TMB. In this study, we hypothesized that both human observers and a neural network could be trained to recognize cases with high TMB.

Design: We utilized digital slides from the Cancer Genome Atlas LuSC dataset that included 50 patients across 30 centers. We calculated the TMB with a 10 mutations/Mb threshold utilized to separate TMB-High and Low cases. The dataset was split into 30 training and 20 testing slides, each from a unique set of centers.

Four observers were asked to predict the TMB status of test slides and record the features they used twice, once before seeing any labeled examples, and once after reviewing the labelled training set. Two observers are pathologists, and two observers are non-pathologists. In parallel with this, we trained and tested a neural network model (VGG16[2], learning rate = 0.01, batch size = 100, with augmentation) on the same sets as the observers.

Results: All observers and the neural network had sensitivities and specificities higher than chance (table 1). This suggests a relationship between the appearance of a tumor and TMB. Training did not have a consistent effect on the accuracy of the human observers and there was poor interobserver agreement. There is range of morphologies associated with TMB status (figures 1,2). In contrast, the neural network had a greater accuracy than any of the human observers after training on only 30 slides.

Table 1: performance metrics for the classification of the test set (n = 20) by the observers and the neural network

	Classification performance **before** training (observer agreement K=0.16‡)			Classification performance **after** training (observer agreement K=0.04‡)		
	Accuracy	Sensitivity	Specificity	Accuracy	Sensitivity	Specificity
Neural network				70%	86%	62%
Observer A*	40%	46%	29%	65%	62%	71%
Observer B*	65%	62%	71%	35%	38%	29%
Observer C	75%	77%	71%	60%	54%	71%
Observer D	60%	62%	57%	55%	46%	71%

‡Fleiss' Kappa with every subject rated by every observer. Agreement was only measured between human observers. Kappa values were not statistically significant (two-sided, α=0.05)
*Fellowship-trained board-certified pathologists

Figure 1 - 1198

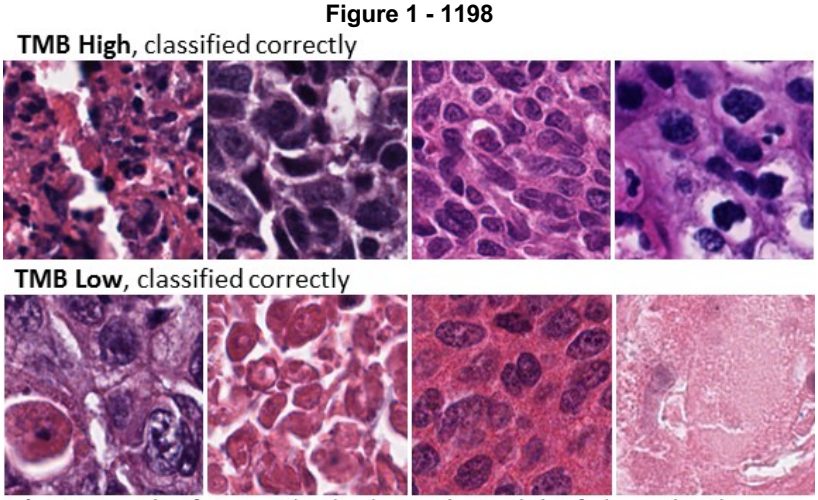

Figure 1: Examples of tissue patches that the neural network classified correctly with more than 90% confidence. Each image is 57 µm x 57 µm, scanned at 0.25 µm/pixel x 0.25 µm/pixel.

Figure 2 - 1198

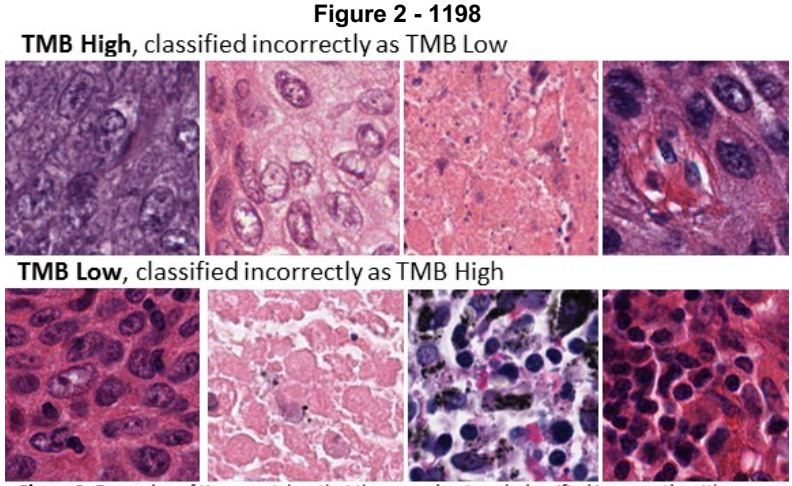

Figure 2: Examples of tissue patches that the neural network classified incorrectly with more than 90% confidence. Each image is 57 µm x 57 µm, scanned at 0.25 µm/pixel x 0.25 µm/pixel.

Conclusions: This study demonstrates that complex genetic features of a tumor are encoded in the morphologic appearance on H&E slides. While it is possible for humans to detect this relationship, the results were mixed, suggesting a need for a machine learning model. This motivates work with expanded data sets to develop reliable means of estimating TMB with neural networks informed by observations by human observers trained on similar datasets.

1. Nat. Med., 2018 Oct;24(10):1559-1567
2. IEEE Trans. Pattern Anal. Mach. Intell., 2016 Oct;38(10):1943-1955

1199 EGFR and ERBB2 Exon 20 Insertion in Advanced Non-Small Cell Lung Cancer: Genomic Profiling and Clinicopathologic Features

Bilge Dundar[1], Ramakrishna Sompallae[2], Natalya Guseva[1], Aaron Bossler[1], Deqin Ma[2]
[1]University of Iowa, Iowa City, IA, [2]University of Iowa Hospitals & Clinics, Iowa City, IA

Disclosures: Bilge Dundar: None; Ramakrishna Sompallae: None; Natalya Guseva: None; Aaron Bossler: None; Deqin Ma: None

Background: Exon (ex)20 in-frame insertions or duplications (ins/dup) in *EGFR* and its analog *ERBB2* are each detected in 1.5% of non-small cell lung cancer (NSCLC). Unlike *EGFR* L858R or ex19 deletions, ex20 ins/dup is associated with de novo resistance to classic EGFR inhibitors, no response to immune checkpoint inhibitors and poor prognosis. FDA recently approved Mobocertinib and Amivantamab which target these ex20 ins/dup. Targeted therapy for patients with this aberration showed sustained response. We identified 16 cases of NSCLC with ex20 ins/dup using next generation sequencing (NGS) assays and correlated the findings with clinical and morphologic information including PD-L1 expression.

Design: NSCLC cases tested at our institution between 2014-2021 were reviewed. The Ion AmpliSeq Cancer Hotspot Panel V2 (ThermoFisher) and a custom-designed 213-gene panel were used for detecting DNA variants and the commercially available FusionPlex CTL panel (ArcherDx) was used for detection of gene fusion. Total nucleic acid extracted from microdissected, formalin-fixed, paraffin-embedded tissue was used to generate NGS libraries and sequencing was performed on Ion Torrent S5 or Illumina NextSeq instrument. Immunohistochemistry (IHC) for PD-L1 was performed using 22C3 or E1L3N clones. Light smoker was defined as a smoking history of 1-20 packs/year.

Results: The variants detected by the 213-gene panel from 250 patients was shown in Fig. 1. *EGFR* (7) or *ERBB2* (9) ex20 ins/dup were identified in 9 males and 7 females, with a mean age of 63; 12 were non/light smokers, and 15 had stage IV disease. Six of 9 cases with available primary tumors had acinar predominant pattern, remainder 1 each had papillary, mucinous, and lepidic pattern. Ex20 ins/dup were heterogenous in-frame 1-4 amino acids spanning A767-V774 (*EGFR*) and Y772-P780 (*ERBB2*), and clustered in the loop following C-helix and α C-helix (Fig. 2). 10 cases (62.5%) had co-existing *TP53* variants. No copy number variants, fusions or microsatellite instability were identified. PD-L1 was positive in 1, low positive in 3, and negative in 11 cases (Table 1).

Table 1. Genomic profiling of *EGFR/ERRB2* exon20 insertion-positive NSCLCs with clinical information

Case	Age	M/F	Stage	Morphology	Exon 20 Ins/Dup	Other Variants	PD-L1 IHC	Treatment	Outcome
1	65	M	IV	AdenoCa,acinar predominant	*EGFR c.2315_2316insGTCCACCC* p.P772_H773insSNP	*TP53* c.814G>T:p.V272L, *PIK3CA c.3140A>G*:p.H1047R	TC:LP IC:N	Chemo XRT	Alive 54 mo
2	59	M	IV	AdenoCa,acinar predominant	*EGFR c.2318_2320delinsTCA* p.H773_V774delinsLM	*TP53 c.740_745del*:p.N247_R248del	TC:N IC:N	Chemo XRT	Hospice 49 mo
3	41	M	IV	AdenoCa vs. atypical carcinoid	*EGFR c.2308_2309insGTT* p.D770delinsGY	none	TC:N IC:N	Chem,XRT Rovalpi-tuzumab	Decd 31 mo
4	77	F	IV	AdenoCa, lepidic predominant	*EGFR c.2310_2311insGGG* p.D770_N771insG	*TP53 c.841G>A*:p.D281N	TPS:N IC:N	Chemo Pembro	Decd 2 mo
5	60	F	IV	AdenoCa, acinar and micropapillary	*EGFR* c.2315_2316insGCACAACCC p.N771_H773dup	*TP53 c.569C>T*:p.P190L	TC:P IC:N	XRT Pembro	Decd 1 mo

6	62	M	IV	Metastatic adenoCa	*EGFR c.2311_2312delAAinsGGCAC* p.N771delinsGT	*TP53 c.659A>G*:p.Y220C	TPS:N IC:N	unknown	Decd 1 mo
7	47	F	IV	AdenoCa, acinar predominant	*EGFR c.2300_2308dup* p.A767_V769dp	*TP53 c.915delG*:p.K305fs *PTENc.367C>T*:p.H123Y *PTEN c.302T>A*: p.I101N	unkn	Chemo Enasitenib	Alive 17mo
8	75	M	IV	Metastatic adenoCa	*ERBB2 c.2313_2324dup* p.Y772_A775dup	none	TC: LP IC: N	XRT Afatinib	Decd 17 mo
9	73	F	IV	Non-small cell lung carcinoma	*ERBB2 c.2313_2324dup* p.Y772_A775dup	none	TC: N IC: N	Chemo XRT Pembro	Alive 50 mo
10	62	M	IV	AdenoCa, papillary predominant	*ERBB2 c.2313_2324dup* p.Y772_A775dup	*TP53 c.661G>T*:p.E221Ter	TC: LP IC: N	Chemo	Decd 30 m
11	47	M	IV	Metastatic AdenoCa	*ERBB2 c.2313_2324dup* p.Y772_A775dup	none	TC:N IC:NA	Afatinib	Decd 1 mo
12	83	F	IV	AdenoCa of uncertain origin	*ERBB2 c.2313_2324dup* p.Y772_A775dup	none	TPS:N IC: NA	unknown	Decd 4 mo
13	44	M	unkn	Metastatic adenoCa	*ERBB2 c.2313_2324dup* p.Y772_A775dup	*TP53 c.652dup*:p.V218Gfs* *RB1 c.446C>G*:p.S149Ter	TPS:N IC:N	Unkn	unkn
14	72	M	IV	Invasive mucinous adenoCa	*ERBB2 c.2313_2324dup* p.Y772_A775dup	*TP53 c.469G>T*:p.V157F *CDKN2A c.307_317del*:p.R103fs	TPS:N IC: N	Chemo XRT Pembro	Alive 54 mo
15	71	F	IV	AdenoCa,acinar predominant	*ERBB2 2c.2331_2339dup* p.G778_P780dup	*TP53 c.659A>C*:pY220S	TPS:N IC:N	Chemo XRT Pembro	Alive 8 mo
16	66	F	IV	Metastatic adenoCa	*ERBB2 c.2325_2326insTCCGTGATGGCT* p.A775_G776insSVMA	*RB1 c.2243A>C*:p.E748A	TC:N IC N	Chemo XRT Transtuzumab Pembro Imprime PGG Anti-TIGIT	Hospice 44 mo

AdenoCa: adenocarcinoma; Chemo, chemotherapy; Decd, deceased; F/M, female/male; IC,

immune cell; LP, low positive; mo, month; N, negative; Pembro, pembrolizumab; P, positive;

TC, tumor cell; TPS, tumor proportion score; unkn, unknown; XRT, radiation.

Figure 1 - 1199

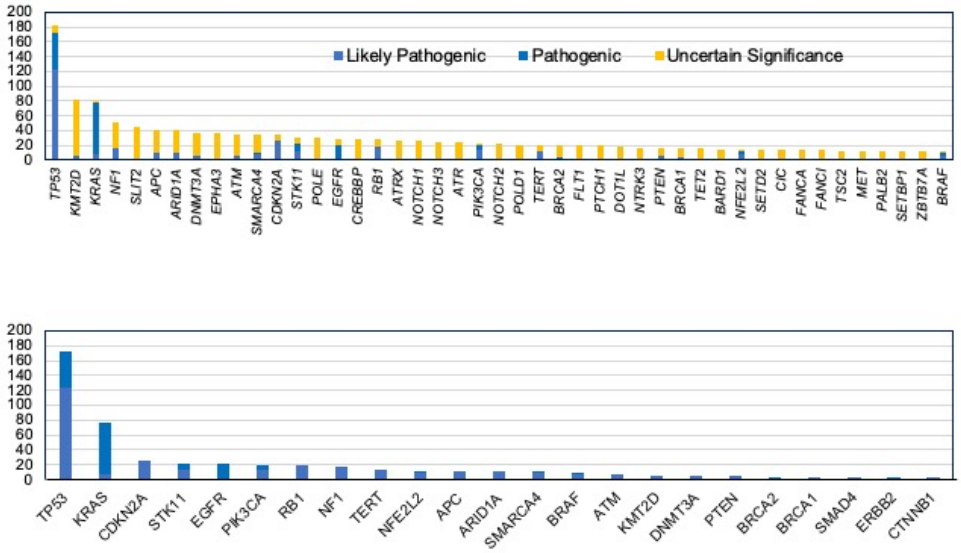

Figure 1. Variants Identified in NSCLCs by the 213-gene NGS panel (250 cases). Top. All variants; Bottom. Pathogenic/likely Pathogenic variants only.

Figure 2 - 1199

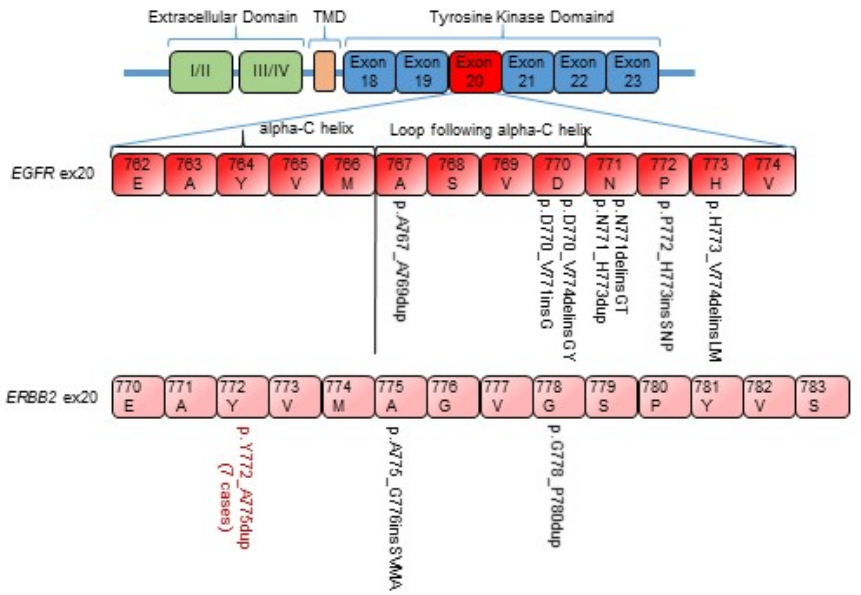

Figure 2. *EGFR/ERBB2* Exon 20 insertion/duplication in non-small cell lung carcinoma. TMD, transmembrane domain.

Conclusions: NSCLCs harboring *EGFR/ERBB2* ex20 ins/dup seemed to be acinar predominant, negative for PD-L1, more frequent in non/light smokers, and mutually exclusive with other driver mutations. Ex20 ins/dup is rare, and the targeted therapy was approved only 6 months ago. The correlation of this variant with histology and response to targeted therapy warrants further investigation.

1200 Early Pulmonary Hypertensive Changes are Often Encountered in COVID-19 Autopsy Lungs

Julie Eclov[1], Stanley Radio[1], Benjamin Swanson[1]
[1]*University of Nebraska Medical Center, Omaha, NE*

Disclosures: Julie Eclov: None; Stanley Radio: None; Benjamin Swanson: *Advisory Board Member*, Cogen Bioscience

Background: The acute autopsy findings associated with COVID-19, due to the novel coronavirus SARS-CoV-2, are well documented. However, the long term sequelae of COVID-19 are still being elucidated. One significant sequela of patients who survive COVID-19 is pulmonary hypertension. Indeed, several groups have reported pathologic pulmonary hypertensive changes in patients who have undergone lung transplantation. The purpose of this study was to determine the frequency of pulmonary hypertensive changes at autopsy as well as identify associated factors.

Design: We retrospectively examined 22 autopsies from patients who died of COVID-19 at our institution. Demographic information collected included age, sex, ethnicity, pre-existing medical conditions, BMI, whether the patient was on a ventilator, as well as treatment. All H&E lung autopsy slides were examined, in addition to MOVAT and VVG stained slides where appropriate. Small arteries (<100 microns in diameter) were evaluated for the presence/absence of medial hypertrophy, intimal thickening, recanalized thrombi, and plexiform lesions according to the Heath and Edwards grade. The COVID-19 autopsy lungs were also evaluated for the presence/absence of diffuse alveolar damage, pneumonia as well as thrombi.

Results: Pathologic findings consistent with pulmonary hypertension were identified in 6 of the 22 COVID-19 lungs identified. Two patients had both medial hypertrophy as well as intimal thickening (Heath and Edwards grade 2), whereas four patients had only medial hypertrophy (Heath and Edwards grade 1). Of the six patients with pulmonary hypertensive changes, 4/6 patients also had pulmonary vascular thrombi, 5/6 patients had previously been on the ventilator, 3/6 patients had pneumonia by pathologic examination, and 4/6 patient had DAD by pathologic examination. None of the six patients had known pulmonary hypertension prior to their terminal hospital admission.

Conclusions: In our retrospective review of COVID-19 autopsy lungs, 27% of lungs demonstrated pathologic features suggestive of pulmonary hypertension. As expected, most patients had early (Grade 1, medial hypertrophy) pulmonary hypertensive changes. Vascular thrombi, history of ventilation, pneumonia and DAD were all commonly associated with pathologic pulmonary hypertension. Movat and/or VVG stains are useful to help identify these pathologic changes. We hypothesize there will be an increase in pulmonary hypertension in long-term survivors of COVID-19.

1201 Comprehensive Next-Generation Sequencing Reliably Distinguishes Primary Squamous Cell Carcinoma of the Lung from Metastatic Lung Tumors of Head & Neck Origin

Mahmoud Elsayad[1], Christopher Febres-Aldana[1], Ronald Ghossein[1], William Travis[1], Natasha Rekhtman[1], Jason Chang[1]
[1]*Memorial Sloan Kettering Cancer Center, New York, NY*

Disclosures: Mahmoud Elsayad: None; Christopher Febres-Aldana: None; Ronald Ghossein: None; William Travis: None; Natasha Rekhtman: None; Jason Chang: None

Background: The differential diagnosis of squamous cell carcinoma (SCC) in the lung in patients with a history of head & neck squamous cell carcinoma (HNSCC) is a common clinical problem with profound implications for proper staging and management. The origin of the lung tumors often remains ambiguous in cases that are unrelated to Human papillomavirus (HPV), even after clinical and radiologic correlation and histologic comparison of the two tumors. We investigate the usefulness of targeted comprehensive next-generation sequencing (NGS) in separating primary lung squamous cell carcinoma (LSCC) from metastatic HNSCC.

Design: The specimens included 38 samples from 18 patients with non-HPV-related HNSCC and subsequent SCCs in the lung, previously characterized by a broad NGS panel comprising 410-505 cancer-related genes. Lung tumors were considered metastatic if paired genomic profiles by NGS shared two or more mutations. Separate primaries were designated for cases without overlapping
mutations. Tumor relatedness predicted by clinical and histopathological findings was examined.

Results: Out of 18 lung tumors, comparative genomic profiling revealed that 6 cases (33%) were primary LSCC while 12 (67%) tumors were metastatic HNSCC. Solitary lung mass was the main mode of presentation in primary LSCC (5/6, 83%); however, 42% (5/12) of metastatic HNSCC in this cohort was also solitary (P=0.15). NGS results resolved 11 cases (61%) with inconclusive

or equivocal prospective histologic comparison of lung tumors and HNSCC. Keratinization status was often discordant between metastatic HNSCC and its primary (5/12; 42%), while histologic features appeared to be similar in two pairs of LSCC and HNSCC primaries (2/6; 33%). NGS unambiguously resolved clonal relationships in all patients, including a patient with 4 morphologically similar but clonally unrelated tumors (Figure 1). HNSCCs and LSCCs showed similar distribution of SCC-associated genes, number of mutations, and tumor mutational burden. TERT promoter (35%) and NOTCH1 (28%) mutations were observed in HNSCCs only.

Figure 1 – 1201

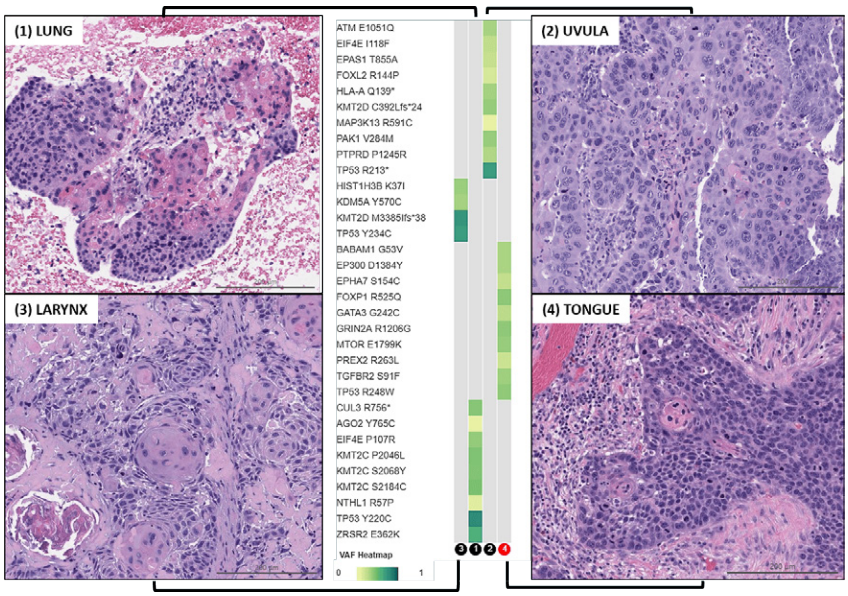

Conclusions: Parallel comprehensive NGS of the tumor pairs represented a reliable method to distinguish primary LSCC from metastatic non-HPV-related HNSCC. Establishing clonal relationships by molecular methods is a useful adjunct when tumor relationships are not clear on clinical, radiographic, or even histopathologic grounds.

1202 Differences in Ki67 Proliferation Index Between Peripheral and Central Small Carcinomas of the Lung

Rachel Fanaroff[1], Allen Burke[2], Kristen Stashek[2], Allison Herring[3]
[1]University of Maryland, Baltimore, MD, [2]University of Maryland School of Medicine, Baltimore, MD, [3]University of Maryland Medical Center, Baltimore, MD

Disclosures: Rachel Fanaroff: None; Allen Burke: None; Kristen Stashek: None; Allison Herring: None

Background: Traditionally, small cell carcinomas of the lung (SCC) were thought to occur predominantly in a central location, however recent studies have shown that a subset of SCCs occur peripherally, and these tumors may behave in a less aggressive manner. While endocrine marker expression has been compared in peripheral versus central SCC, differences in Ki67 proliferation rate have not been adequately assessed. We retrospectively compared Ki67 proliferation rates in peripheral versus central SCC in an institutional series.

Design: 90 cases of SCC were identified using a CERNER database search. A radiologist specializing in thoracic radiology reviewed imaging associated with each case to determine a peripheral versus central location. Ki67 immunohistochemical (IHC) staining (clone 30-9) was performed on all cases. Cases were excluded if insufficient tissue for Ki67 staining or if localization of tumor (central/peripheral) was indeterminate by imaging. Scanscope Aperio software was used to quantify the proliferation index. In cases in which the tissue was crushed or otherwise unable to be quantified morphometrically, quantification was performed by visual inspection of glass slides. Endocrine markers (CD56, synaptophysin, chromogranin) and TTF1 were compared when available.

Results: Cases included 45 TBNA, 12 transbronchial biopsies, 9 core biopsies, 14 endobronchial biopsies, 9 resections, and 1 lymph node biopsy. Immunostains for endocrine markers (synaptophysin, chromogranin, CD56) and TTF-were reviewed in 31 cases. 44 cases were central (mean age 63.7 y, range 48-84; M:F = 13/31), and 47 were peripheral (mean age = 68.0 y, range = 52-85; M:F = 16/31). Mean Ki67 was 84.1 ± 2.7 for central and 77.5 ± 2.5 for peripheral tumors (p=.02). There was no difference in Ki67 values for lymph node samples (78.7 ± 3.1 v. 81.8 ± 2.3 for primary sampling). There was no significant difference in the rate of any endocrine marker staining in central v. peripheral tumors (91% v. 89%, respectively) and there was a statistically insignificant decrease in peripheral TTF-1 positivity (73% v. 62%, respectively).

Conclusions: When strict radiologic criteria are used, we found that more SCC are located peripherally versus centrally. The Ki67 proliferation rate is somewhat lower in peripheral tumors, which may explain their reportedly lesser aggressiveness. Further study is warranted, including survival data, to better define these differences.

1203 Do Additional Histologic Features Improve Pattern-Based Grading of Resected Adenocarcinomas of the Lung?

Rachel Fanaroff[1], Kristen Stashek[2], Allen Burke[2]
[1]University of Maryland, Baltimore, MD, [2]University of Maryland School of Medicine, Baltimore, MD

Disclosures: Rachel Fanaroff: None; Kristen Stashek: None; Allen Burke: None

Background: The International Association for the Study of Lung Cancer (IASLC) recently proposed a three-tiered histologic grading scheme for invasive non-mucinous lung adenocarcinoma. Because of a strong correlation between pattern and other histologic features, only pattern was recommended in the grading system. The aim of this study was to confirm the utility of the IASLC/WHO grading system in an institutional dataset and to compare it to a modification adding other histologic features.

Design: We performed a retrospective review of node-negative, T1-2, non-mucinous lung adenocarcinoma resections from 2004-2018. These were assigned a pattern-based grade using the IASLC criteria and staged using CAP protocol version 4.2.0.0. Mitotic count, presence of spread through airspaces, and nucleolar grade were evaluated by review of H&E-stained slides. Kaplan Meier survival curves were generated with end-point of tumor recurrence using T stage and WHO pattern grade. WHO grade was modified three ways and analyzed separately by upstaging G1 and G2 each by one grade if mitotic figures > 1/10 hpf; if nucleolar grade 2 or higher (prominent eosinophilic nucleoli), and in the presence of STAS, respectively.

Results: 211 cases were identified, 113 female, (65 ± 10 y), and 83 male, (67 ± 8 y) with an average follow-up interval of 49 months. There were 26 stage 1a, 102 1b, 61 1c, 8 2a and 6 2b tumors. 62% of patients were recurrence-free during the time of follow-up. There was no significant difference in time to recurrence by T stage. Recurrence rate increased with IASLC/WHO grade (p=.005). Upgrading with mitotic figures resulted in a p value of .003; modified by upgrading with STAS and nucleolar grade result in p values each of .002. No patient with G1 tumor by nucleolar upgrade developed recurrence.

Figure 1 - 1203

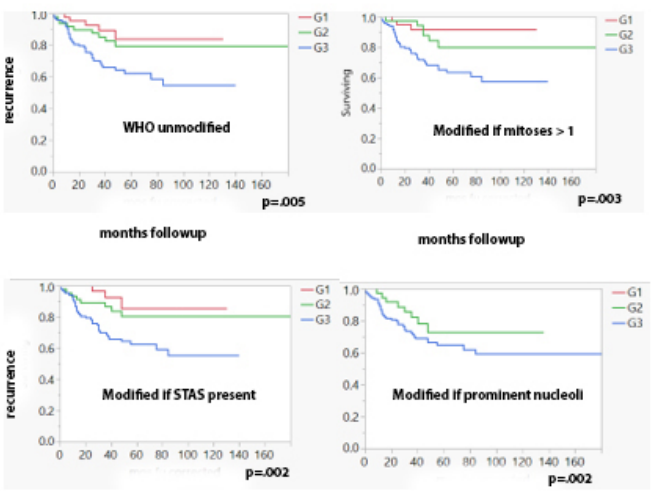

Conclusions: Grading of lung cancers by WHO system greatly improves prognostication over T-stage alone. There is a marginal increase in efficacy adding additional histologic variables. In our patient set, no G1 tumor with bland nucleoli developed recurrence.

1204 NUT Carcinoma: A Clinicopathologic and Comprehensive Immunohistochemical Analysis of 54 Cases

Ayesha Farooq[1], Ying-Chun Lo[1]
[1]Mayo Clinic, Rochester, MN

Disclosures: Ayesha Farooq: None; Ying-Chun Lo: None

Background: NUT carcinoma is an aggressive carcinoma defined by translocations involving *NUTM1* gene and is characterized by primitive round cells with areas of abrupt keratinization. It is morphologically challenging as it overlaps with poorly differentiated squamous cell carcinoma, small cell carcinoma, SMARCA4-deficient tumor, and other small round blue cell tumors. We comprehensively studied the immunohistochemical(IHC) features of a large cohort.

Design: Archives were searched for NUT carcinoma. 54 cases were identified (8 in-house and 46 external consult cases) from 2012-2021. Inclusion criteria are either NUT+ IHC (39), *NUTM1* rearrangement by FISH (3) or both (12) at diagnosis. Pathology reports and available slides were reviewed. We stained in-house cases for NUT, AE1/AE3, Cam5.2, OSCAR keratin, CK7, CK20, p40, p63, DSG3, CK5/6, TTF-1 (SPT24 and 8G7G3), synaptophysin, chromogranin, CD56, INSM1, S100, desmin, Ki-67 and PD-L1 in cases where these stains were not previously performed.

Results: Patients age ranged from 2 to 83 (median 48) years. No gender tendency (28 M, 52%). Primary sites included 35(65%) thoracic/mediastinal, 13(24%) sinonasal/head & neck and 6(11%) others (2 colorectal, 2 terminal ileum/right colon/appendiceal, 1 pancreas, 1 pelvic soft tissue). Keratin stains were variable positive: AE1/AE3 84% (36/43), Cam5.2 88% (21/24), Oscar keratin 73% (19/26), CK7 62% (16/26) and CK20 19% (4/21), indicating their unreliability. Among squamous markers, DSG3 was positive in 100% (9/9), p63 in 86% (19/22), p40 in 62% (21/34), and CK5/6 in 68% (21/31) cases, suggesting p40 is insensitive for NUT carcinoma diagnosis. TTF-1 was mostly negative with focally positive in 28% (9/32) cases. Neuroendocrine markers were focal/weak positive in few cases: synaptophysin 11% (4/37), chromogranin 0% (0/31) and CD56 15% (4/26), except INSM1 70% (7/10). S100 3% (1/33), desmin 6% (2/31), CD45 8% (2/25) were rarely positive, helping differential diagnosis. However, CD34 15% (3/20) and CD99 21% (3/14) could present pitfalls. BRG1 and INI1 were retained in all (22, 28) cases. Ki-67 proliferative index was high (range 20-90%, median 70%). PD-L1 was negative in all (8) tested cases.

Conclusions: We provided a comprehensive immunoprofile to raise differential diagnosis awareness and pitfall recognition. Individual keratin is not sensitive enough and would require multiple ones. Some beloved markers might be misleading: p40 is insensitive compared to p63 and DSG3, INSM1 has a high % of being focally positive.

1205 Retinoblastoma (Rb) Protein in Small Cell Lung Carcinoma: Combined Genomic and Immunohistochemical Analysis with a Description of a Rare Rb-Proficient Subset

Christopher Febres-Aldana[1], Marina Baine[1], Jason Chang[1], Ryan Ptashkin[1], Erika Gedvilaite[1], Katia Ventura[1], Francis Bodd[1], Jacklynn Egger[1], William Travis[1], Wei-Chu Lai[1], Joseph Chan[1], Triparna Sen[1], Charles Rudin[1], Natasha Rekhtman[1]
[1]Memorial Sloan Kettering Cancer Center, New York, NY

Disclosures: Christopher Febres-Aldana: None; Marina Baine: None; Jason Chang: None; Ryan Ptashkin: None; Erika Gedvilaite: None; Katia Ventura: None; Francis Bodd: None; Jacklynn Egger: None; William Travis: None; Wei-Chu Lai: None; Joseph Chan: None; Triparna Sen: None; Charles Rudin: None; Natasha Rekhtman: None

Background: *RB1* mutations and loss of Rb protein expression represent a consistent but not entirely invariable hallmark of small cell lung cancer (SCLC). The prevalence and characteristics of SCLC that lack *RB1* alterations and retain Rb expression (Rb-proficient SCLC) are not well established. Here we performed a comprehensive analysis of a large series of SCLC with combined next-generation sequencing (NGS) and Rb immunohistochemistry (IHC) to elucidate the characteristics of this poorly defined subset.

Design: Clinical samples of 208 SCLC were analyzed by targeted NGS for 341-505 cancer genes, covering all exons of *RB1,* and for Rb expression by IHC (clone:13A10). Detailed genomic and clinicopathologic analysis of Rb-proficient SCLC was performed in comparison to Rb-deficient cases.

Results: Of 208 SCLC, 14 cases (6.7%) were Rb-proficient, whereas the rest (n=194, 93.3%) were Rb-deficient. Rb-proficient SCLC had the following patient characteristics: median age of 69, 57% male, and 100% smoker (43 mean pack-years), which was comparable to that of Rb-deficient SCLC. The histologic features of SCLC were confirmed for all Rb-proficient cases; a mean Ki67 labeling index was 82%. Notably, Rb-proficient SCLCs were significantly enriched in combined histology: non-SCLC (NSCLC) components were present in 8/14 (57%) of Rb-proficient SCLC vs 23/194 (12%) of Rb-deficient SCLC (P<0.001). Genomically, compared to Rb-deficient SCLC, Rb-proficient tumors had a striking enrichment in *CDKN2A* mutations/loss (36% vs 2%; P<0.001), *CCND1* or *CCND2* amplifications (36% vs 0%; P<0.001), *FGFR1* amplification (36% vs 4%, P<0.001), and *KEAP1* mutations/loss (36% vs 3%; P<0.001), respectively. There were no differences in the rate of *TP53* mutations (100% vs 96%) or the overall tumor mutation burden (10 vs 8 mt/Mb), respectively.

Conclusions: This is the largest study to-date to concurrently analyze *RB1* by NGS and IHC in SCLC, identifying a 6.7% rate of Rb-proficient cases. This subset is characterized by several highly distinctive features, including strong association with NSCLC histologic components, NSCLC-type genomic alterations, and functional inactivation of Rb via D-type cyclin activation and *CDKN2A* (p16) inactivation. These data suggest a distinct derivation of Rb-proficient SCLC from NSCLC-related progenitors. The potential utility of CDK4/6 inhibitors in this unique subset of SCLC warrants clinical investigation.

1206 Histologic, Immunohistochemical and Molecular Stratification of Thymic Neuroendocrine Neoplasms

Daffolyn Rachael Fels Elliott[1], Audrey Jajosky[2], Chaehwa Kim[1], Steven Hrycaj[1], Kristine Konopka[3], Carol Farver[4], Jeffrey Myers[3], Aaron Udager[5], Tao Huang[1]

[1]University of Michigan, Ann Arbor, MI, [2]University of Rochester Medical Center, Rochester, NY, [3]Michigan Medicine, Ann Arbor, MI, [4]Cleveland Clinic, Cleveland, OH, [5]University of Michigan Medical School, Ann Arbor, MI

Disclosures: Daffolyn Rachael Fels Elliott: None; Audrey Jajosky: None; Chaehwa Kim: None; Steven Hrycaj: None; Kristine Konopka: None; Carol Farver: None; Jeffrey Myers: None; Aaron Udager: None; Tao Huang: None

Background: Thymic neuroendocrine tumors (NETs) behave more aggressively in comparison to their lung counterparts. Integrating the WHO category of G3 well-differentiated NET (WD-NET) from gastroenteropancreatic neuroendocrine neoplasms (GEP NENs) has been proposed to address the variability in clinical behavior and therapeutic regimens. We stratified thymic NENs by morphology, Ki67 index and molecular subgroups, with temporal and spatial comparison for a subset of patients with metastases.

Design: A database search identified 15 patients with thymic NEN (median age 51y; 60% male) and 32 samples including primary (12 pts), local recurrence (2 pts), lymph nodes (6 pts) and distant metastases (7 pts). Tumors were reclassified by morphology, mitoses and immunostains for Ki67, p53 and Rb using WHO criteria for GEP NEN. Targeted amplicon-based next-generation DNA sequencing (DNAseq) was performed using the Oncomine Comprehensive Assay Plus (501 genes) and Ion Torrent NGS System.

Results: 18/32 (56%) samples were reclassified into a different histologic grade using WHO GEP NEN classification (Table): all (12) large cell neuroendocrine carcinoma (LCNEC) reclassified as G2/G3 WD-NET; 2/13 atypical carcinoid (AC) as G3 WD-NET; 4/6 typical carcinoid (TC) as G2 WD-NET. All G3 WD-NETs showed retained Rb and wild-type p53. One small cell carcinoma showed loss of Rb and aberrant p53 expression. Sequencing for 9 patients with G2/G3 WD-NETs (2 TC, 4AC, 7 LCNEC; 5 primary, 1 recur, 2 LN, 5 mets) identified 3 tumor subclasses characterized by 1) RAS/MAPK pathway mutations (*HRAS*, *NRAS*) with low copy number variants (46.5 mean CNVs, 2 G3 WD-NETs); 2) MEN1 and/or mTOR pathway mutations (*MEN1*, *TSC1*) with high CNVs (106.5, 2 G2 WD-NETs); and 3) other/no prioritized mutations (e.g., *SMARCB1*) with intermediate CNVs (76.8, 5 G2/G3 WD-NETs). Recurrently amplified genes included *AKT3* (mTOR pathway), *MAP2K7* (RAS/MAPK pathway), *DAXX*, *CHD4* and *ENO1;* and deletions included *ADAMTS2/12, A1CF, KDR* and *FGF4*. Metastases showed increased genomic instability in comparison to primary tumors (86.5 vs 43.5 mean CNVs).

Patient	Site	Mitoses (per 2 square mm)	Ki67 hotspot	2021 WHO Thoracic Diagnosis	2019 WHO GEP Diagnosis	Mutations	Total CNVs
1	Primary	<1	3.3%	TC	G2 NET	PENDING	
	Local recurrence	<1	14.8%	TC	G2 NET	None	72
	LN	3	19.7%	AC	G2 NET	PENDING	
2	Primary (low Ki67)			LCNEC	G3 NET	SMARCB1 p.R374Q (14%)	30
	Primary (high Ki67)	15	44.6%	LCNEC	G3 NET	PENDING	
3	Metastasis (adrenal)	16	13.2%	LCNEC	G2 NET	PENDING	
4	Primary	12	36.6%	LCNEC	G3 NET	HRAS p.K117R (44%), FAT1 p.E124K (42%)	28
	LN #1	27	42.8%	LCNEC	G3 NET	HRAS p.K117R (37%), FAT1 p.E124K (36%)	30
	LN #2	12	45%	LCNEC	G3 NET	PENDING	
	Metastasis (breasts, L seq'd)	11 (L), 7 (R)	36% (L), 25.4% (R)	AC	G3 NET	HRAS p.K117R (38%), FAT1 p.E124K (31%)	66
5	Primary (2 nodules)	22, 25	42.8%, 32.3%	LCNEC	G3 NET	PENDING	
6	Primary	6	15.8%	AC (with comedo necrosis)	G2 NET	None	70
	LN #1	6	12.6%	AC (with comedo necrosis)	G2 NET	None	63
	LN #2	3	11.4%	AC (with comedo necrosis)	G2 NET	PENDING	
	Metastasis (pancreas)	5	8.6%	AC	G2 NET	PENDING	
7	Primary (low Ki67)			LCNEC	G3 NET	PENDING	
	Primary (high Ki67)	17	24.5%	LCNEC	G3 NET	NRAS p.Q61R (47%)	19
	LN #1	14	23%	LCNEC	G3 NET	PENDING	
	LN #2	5	14.6%	AC	G2 NET	PENDING	
8	Primary	<1	2.7%	TC	G1 NET	PENDING	
9	Primary	1	7.5%	TC	G2 NET	PENDING	
10	LN	20	35%	LCNEC	G3 NET	PENDING	
	Metastasis (L breast)	20	54.5%	LCNEC	G3 NET	None	40
11	Primary	6	17.2%	AC	G2 NET	PENDING	
	Metastasis (retroperitoneum)	1	6.9%	TC	G2 NET	MEN1 p.L103fs (92%)	89
	Metastasis (liver)	<1	1.7%	TC	G1 NET	PENDING	
12	Local recurrence	4	6.9%	AC	G2 NET	PENDING	
	Metastasis (phrenic nerve)		4.3%	AC	G2 NET	MEN1 p.E200* (50%), MEN1 p.T202_W203del (46%), TSC1 p.Y790* (49%)	124
13	Primary	6	8.2%	AC	G2 NET	PENDING	
	LN		4.3%	AC	G2 NET	PENDING	
	Metastasis (epidural)	4	28%	AC	G3 NET	PENDING	
14	Primary	15	8.6%	LCNEC	G2 NET	None	42
	Metastasis (abdominal wall)	28	39%	LCNEC	G3 NET	None	134
15	Primary	115	64.8%	Small cell carcinoma	Small cell carcinoma	PENDING	

AC: atypical carcinoid, CNV: copy number variation, GEP: gastroenteropancreatic, LCNEC: large cell neuroendocrine carcinoma, LN: lymph node, NEC: neuroendocrine carcinoma, NEN: neuroendocrine neoplasm, NET: neuroendocrine tumor, TC: typical carcinoid

Conclusions: In our cohort, all LCNEC were reclassified as G2/G3 WD-NET by morphology and Ki67 index using WHO GEP NEN criteria. G3 WD-NET appears along a molecular spectrum with G2 WD-NET, and biologically distinct from high grade NEC in the thymus. Thymic NENs may be stratified into at least 3 molecular subgroups, including a subset of G3 WD-NET with RAS/MAPK pathway mutations, with potential therapeutic implications.

1207 Tissue Age Affects the Proportion Score in the 22c3 Immunohistochemistry Companion Diagnostic Test

Patricia Gaule[1], Aileen Fernandez[2], David Rimm[2]
[1]Yale University, New Haven, CT, [2]Yale School of Medicine, New Haven, CT

Disclosures: Patricia Gaule: None; Aileen Fernandez: None; David Rimm: *Consultant*, Astra Zeneca, Cell Signaling Technology, Cepheid, Danaher, Merck, NanoString, PAIGE.AI, Roche, Ventana; *Grant or Research Support*, Amgen, Cepheid, Konica/Minolta, Navigate Biopharma, NextCure

Background: Companion diagnostic 22c3 is the approved IHC test for treatment with Keytruda and Libtayo in multiple cancer types. Studies have described the interchangeability of 22c3 with other approved diagnostics (SP263, 28-8 and LDT assay E1L3N). 22c3 and 28-8 tests target the extracellular domain (ECD) of PD-L1 which is known to contain N-glycosylation sites. Degradation of glycosyl residues is an artefact of FFPE tissue aging. Here we present previously positive PD-L1 (TPS >1) samples that express significantly lower PD-L1 when assayed years later by 22c3 but not by intracellular (ICD) PD-L1 E1L3N. We hypothesize that degradation of the epitope containing both protein and sugar components is unstable over time and may lead to false negative results.

Design: 10 whole tissue sections of NSCLC from 2018 were selected for varying PD-L1 levels. TPS scores were read by a pathologist and compared to the previous clinical diagnoses. Assay drift was ruled out as a source of error by semi-quantitative intensity analysis on historical controls. Deglycosylation experiments were performed on both cell lines with varying PD-L1 levels and a 180-patient TMA. Fresh cut serial sections of samples for each case were stained on DAKO Link48 for 22c3 according to the protocol on label. In parallel, a previously described LDT using E1L3N was performed on the Leica BondRX.

Results: 6/7 archival positive samples showed significant reduction in positive staining with 22c3 compared to original diagnostic sample. Only 1/7 seven stained with E1L3N showed a discrepant result to the original.

In a TMA cohort, a significant difference in signal intensity was noted when staining with 22c3 compared to E1L3N. This loss of signal was not noted in a freshly prepared TMA indicating a time dependent degradation of staining. Quantitative assessment of both TMAs showed significant loss of signal after a deglycoslation procedure when stained with 22c3 (not seen when stained with E1L3N).

Figure 1 - 1207

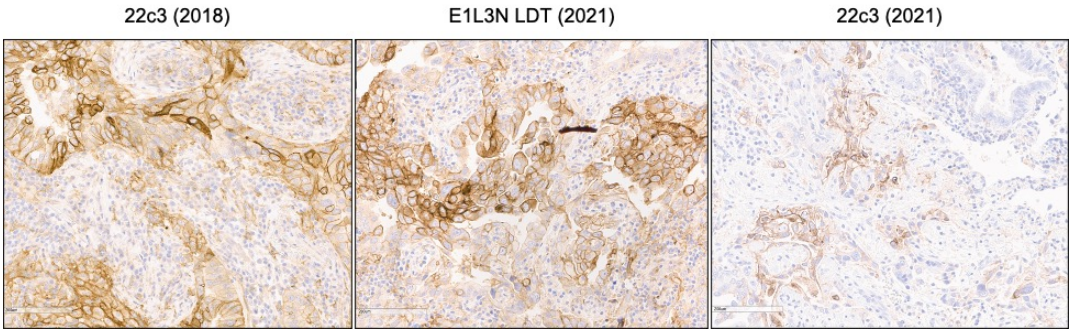

Figure 2 - 1207

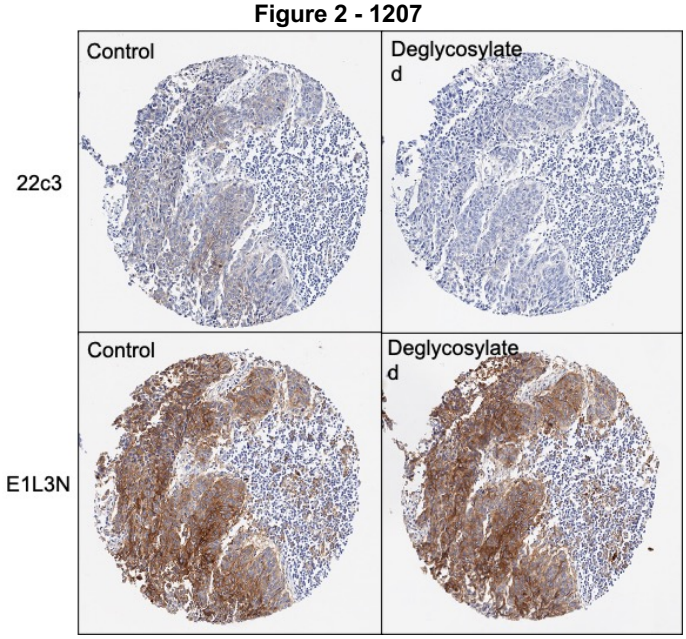

Conclusions: We show time dependent loss of signal using the 22c3 assay with an ECD epitope compared to the E1L3N assay with an ICD epitope. We can reproduce this signal loss by experimental degradation of glycosyl residues in FFPE tissue. This data suggests that when older tissues are used in the 22c3 companion diagnostic test, there may be significantly reduced positive staining. This could lead to false negative tests and suggests that the 22c3 assay should only be used on fresh (<1 year old) tissue.

1208 Histopathologic Pulmonary Involvement of COVID-19: A Comparative Study of SARS-CoV-2 Variants in Mouse Models

Jerome Givi[1], Md. Shahrier Amin[2], Fredrick Damron[3], Katherine Lee[3], Ting Wong[3]
[1]West Virginia University School of Medicine, Morgantown, WV, [2]West Virginia University Health Sciences Center, Morgantown, WV, [3]West Virginia University, Morgantown, WV

Disclosures: Jerome Givi: None; Md. Shahrier Amin: None; Fredrick Damron: None; Katherine Lee: None; Ting Wong: None

Background: A thorough understanding of the inflammatory reaction to SARS-CoV-2 variants, specifically the Delta and Alpha variants, can provide crucial insight into future treatment of individuals infected with these strains. Mice are an effective model for predicting the pathologic processes of these viruses in humans.

Design: K18-hACE2 transgenic mice were raised either under normal conditions (control) or infected with either the Alpha (strain B.1.1.7) or Delta (B.1.617.2) variant of SARS-CoV-2, via intranasal challenge with 1000 PFU virus. Mice were then euthanized at days 2 and 6 post-challenge. Lung sections were used for pathological evaluation of H&E stained slides scanned using the Dynamyx software. Blood vessel cross sections were examined and the average number of marginating inflammatory cells per millimeter of vessel were quantified. Additionally, the percentage of total tissue area that was inflamed was calculated.

Results: Our data indicates that the Delta variant elicits a strong lymphocytic immune response in the lungs. At two days post-challenge, Inflammation and margination of inflammatory cells could be appreciated in Delta infected mice, but not in Alpha infected mice. The inflammatory infiltrate was composed predominantly of lymphocytes and occasional histiocytes at 2 days.

By day 6, marked perivascular inflammation and margination was appreciated, more prominently in Delta (36 lymphocytes per mm. of endothelium) than Alpha infected mice (22 lymphocytes per mm. endothelium) (p=0.022). At this time point, Alpha infected mice showed 4% involvement of pulmonary area by inflammation, compared to 20% for Delta infected mice (p=0.014).

Conclusions: This study quantifies the lymphocytic immune response in the lungs to the Alpha and Delta variants of SARS-CoV-2 in mouse models. Both variants showed a lymphocyte predominant inflammatory response. However, the response was much more robust and severe in Delta infected mice compared to Alpha. The results support why the Delta variant is more virulent and fatal compared to Alpha. Ongoing longer term studies and effects in other organs are ongoing and will help to provide further insight into pathogenesis of long COVID-19.

1209 Comparison of Biphasic Mesothelioma and Epithelioid Mesothelioma with Reactive Stroma and Utility of BAP1 and MTAP Expression in Identifying a True Sarcomatoid Component

Naomi Hardy[1], Erica Glass[1], Allen Burke[2]
[1]University of Maryland Medical Center, Baltimore, MD, [2]University of Maryland School of Medicine, Baltimore, MD

Disclosures: Naomi Hardy: None; Erica Glass: None; Allen Burke: None

Background: Biphasic malignant mesothelioma has a poorer prognosis than epithelioid malignant mesothelioma. There is a subset of cases of epithelioid mesothelioma with reactive stroma that have atypia occasionally mimicking that seen in the sarcomatoid component of a biphasic mesothelioma. We investigated whether these cases with reactive stroma had poorer clinical outcome than classic epithelioid mesothelioma, and if IHC for BAP1 and MTAP, both frequently lost in the epithelioid component of mesotheliomas, could be utilized to differentiate a true sarcomatoid component from reactive stroma.

Design: A retrospective review was performed on patients diagnosed with biphasic or epithelioid with reactive stroma pleural mesothelioma at an academic hospital from 2015-2020. BAP1 and MTAP were ordered on available cell blocks from a subset of these patients with staining assessed by a thoracic pathologist.

Results: 53 total cases were identified (16 cases of biphasic malignant mesothelioma, 13 cases of epithelioid mesothelioma with reactive stroma, and 24 cases of classic epithelioid mesothelioma). Survival curve analysis showed a statistically significant difference between each epithelioid mesothelioma type and biphasic malignant mesothelioma (p=0.009, Figure 1). None of the cases of epithelioid malignant mesothelioma showed BAP1 or MTAP loss in the reactive stroma compared to loss seen in the sarcomatoid component of biphasic mesothelioma cases, although difference of expression did not reach significance in this limited dataset (p=0.2, Table 1). BAP1 loss in the epithelioid component of all cases was 71%, similar to that described by Kinoshita et al. and differed in the spindle cell component, which showed loss of expression in 25% of cases. MTAP loss was 46% in the epithelioid component, similar to that described previously, and differed from the spindle cell component that showed loss in 8% of cases.

	Patient No.	BAP1 LOSS in epithelioid component	BAP1 LOSS in spindle cell component	MTAP LOSS in epithelioid component	MTAP LOSS in spindle cell component
Biphasic MM (n=8)	1	+	+/-	-	-
	2	+	+	-	+/-
	3	+	+	+	+
	4	+	-	+	-
	5	+	+	-	-
	6	-	-	-	-
	7	+	-	+/-	+/-
	8	+	-	+	-
Epithelioid MM with Reactive Stroma (n=6)	9	-	-	+	-
	10	+	-	+	-
	11	+	+/-	-	-
	12	-	-	-	-
	13	-	-	+	-
	14	+	-	-	-

MM=Malignant Mesothelioma

Figure 1 - 1209

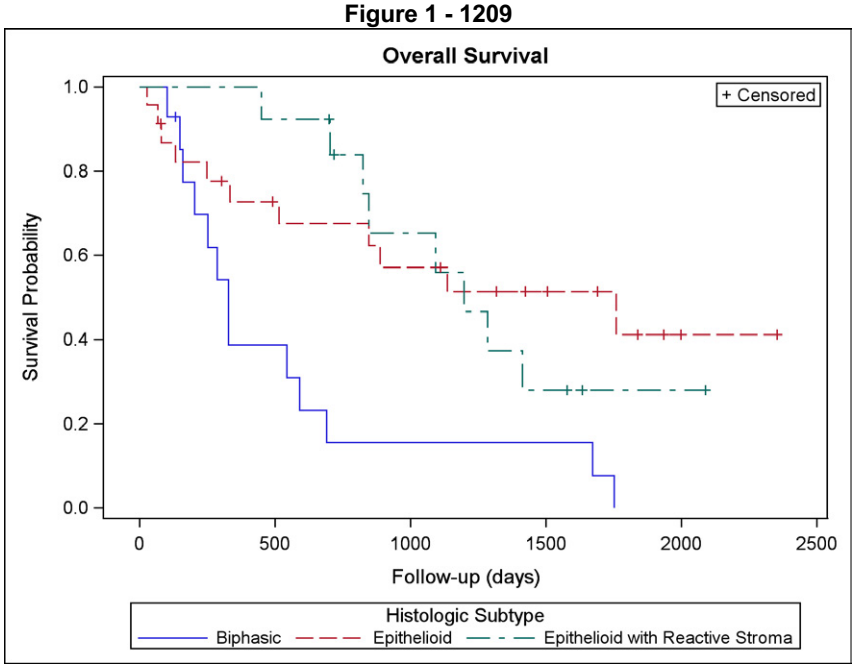

Conclusions: Biphasics have a poorer clinical outcome than epithelioid mesothelioma with reactive stroma and BAP1 and MTAP may be useful in differentiating reactive stroma from a sarcomatoid component of a biphasic mesothelioma; however, additional studies with a larger patient cohort are necessary. As demonstrated previously, BAP1 and MTAP loss are seen at a high rate in malignant mesothelioma.

1210 Clinicopathologic and Molecular Features of Driver-Positive Pulmonary Neuroendocrine Carcinomas

Yin (Rex) Hung[1], Marina Kem[1], Martin Taylor, Mari Mino-Kenudson[2]
[1]Massachusetts General Hospital, Boston, MA, [2]Massachusetts General Hospital, Harvard Medical School, Boston, MA

Disclosures: Yin (Rex) Hung: *Consultant*, Elsevier; Marina Kem: None; Martin Taylor: *Consultant*, ROME Therapeutics; Mari Mino-Kenudson: *Consultant*, AstraZeneca, H3 Biomedicine; *Primary Investigator*, Novartis; *Advisory Board Member*, BMS, Sanofi

Background: Pulmonary high-grade neuroendocrine carcinoma (HGNEC) includes large cell neuroendocrine carcinoma (LCNEC) and small cell carcinoma (SCLC). As oncogenic driver mutations are uncommon in these tumors (particularly SCLC), data on clinicopathologic and molecular features of these driver-positive pulmonary HGNEC remain limited.

Design: We searched our institutional surgical pathology files in 2013-2021 for pulmonary HGNEC with oncogenic driver mutations (*EGFR*, *KRAS*, *ALK*, *ROS1*, *RET*, *MET* exon skipping, *BRAF*, *NTRK*1/2/3) detected by targeted DNA-based next-generation sequencing (NGS) performed at our institution; we reviewed their clinicopathologic, immunohistochemical, and molecular features.

Results: This cohort included 33 patients: 19 (58%) with *EGFR* mutations (exon 19 indel [14], L858R [5]); 11 (33%) with *KRAS* mutations (G12V/C/D [7], G13C/D [2], Q61H/L [2]), 2 (6%) with *KIF5B-RET* fusion, and 1 (3%) with *SQSTM1-NTRK3* fusion. No other driver alterations were identified. Of 19 *EGFR*-mutant HGNEC patients (13F, 6M; age 40-83 [median 64] yr; 18 never/light smokers; all stage IV), 6 presented *de novo*; 13 had lung adenocarcinomas 4-69 (median 22) months prior. *EGFR*-mutant HGNEC displayed prototypical SCLC, combined SCLC-adenocarcinoma, and those with intermediate features between SCLC and LCNEC in 11, 5, and 3 cases, respectively; and displayed aberrant p53 and loss of Rb expression in 10 of 13 and 11 of 12 cases, respectively. All 11 *KRAS*-mutant HGNEC patients (6F, 5M; age 42-74 [median 66] yr; 2 never/light smokers; 7 stage IV, 4 stage I) presented *de novo*, with classic LCNEC histology in 8, those with intermediate features between SCLC and LCNEC in 2, and combined SCLC-adenocarcinoma in 1 case. The *RET*- or *NTRK3*-rearranged tumors presented *de novo* as LCNEC (2 stage IV, 1 stage I). In addition to the driver mutations, targeted NGS detected mutations in *TP53* and/or *RB1* in 89% of *EGFR*-mutant and 64% of *KRAS*-mutant HGNEC, along with mutations in *PIK3CA*, *PTEN*, *AKT1*, *TSC1*, *MAP2K1*, *CDKN2A*,

and *STK11* in a subset of tumors. The stage IV patients in the entire cohort had a median overall survival of 14.7 months, with no significant difference between *EGFR*-mutant and *KRAS*-mutant cases.

Conclusions: Driver-positive pulmonary HGNEC comprises distinct subgroups: *EGFR*-mutant arising *de novo* or transformed and enriched for never smokers and SCLC-histology, *KRAS*-mutant *de novo* in smokers with LCNEC-histology, and those with other alterations. Prototypical SCLC is seen only in *EGFR*-mutant tumors in this cohort.

1211 Ki67 Analysis of Pulmonary Small Cell Lung Carcinoma in Patients with Clinical Recurrence

Philip Hurst[1], Joanne Yi[1], Marie Passow[1], Marie-Christine Aubry[1], Joseph Maleszewski[1], Anja Roden[1], Jennifer Boland Froemming[1], Ying-Chun Lo[1], Melanie Bois[1]
[1]Mayo Clinic, Rochester, MN

Disclosures: Philip Hurst: None; Joanne Yi: None; Marie Passow: None; Marie-Christine Aubry: None; Joseph Maleszewski: *Consultant*, Edwards Scientific; Anja Roden: None; Jennifer Boland Froemming: None; Ying-Chun Lo: *Advisory Board Member*, Takeda Pharmaceutical Company Limited; Melanie Bois: None

Background: Recent molecular data suggests that small cell lung carcinomas (SCLC) may be heterogenous with respect to driver mutations and disease progression. Limited studies have shown that a high Ki67 labelling index (LI) in SCLC correlates with favorable treatment response. However, up to 70% of patients will relapse following therapy. We sought to understand the proliferative characteristics of tumors that are inherently treatment-resistant and associated with clinical recurrence.

Design: Cases of SCLC with recurrence were identified from institutional surgical pathology archives (2001-2018). Relevant clinical information was abstracted from the medical record. Ki67 staining (MIB-1; Dako) was performed on the index (baseline) cases in established SCLC patients with clinical recurrence, and those with available formalin-fixed paraffin-embedded tissue. Digital image analysis was performed using Aperio ImageScope Software (Leica Biosystems). A minimum of 250 cells were analyzed. Ki67 LI were evaluated as a categorial variable, with ≥60% designated as “high” LI.

Results: 20 patients were included in the study (median age 70; IQR 57-73; 11 women). 95% were deceased at the time of data abstraction (median months to death 24.6, IQR 18.7-36). 25% of patients underwent surgical resection prior to adjuvant therapy. Radiation and chemotherapy were given in 80% and 95% of patients respectively. Median time to clinical recurrence was 11 months from diagnosis (IQR 8.2-16.5), with 80% having limited disease at presentation. Ki67 automated LI revealed a median percent positive nuclei of 65% (IQR 55-73; range 24-84). Patients with high (≥60%; n=12) Ki67 LI had a decreased time to recurrence (10.7 vs 16.9 months; p=0.048). Overall survival was not significantly affected by Ki67 LI, although a trend was present (high vs low, 24.7 vs 43.1 months; p=0.16).

Conclusions: Among patients with clinical relapse of SCLC, those with high baseline Ki67 LI experience a decreased time to recurrence. Overall survival does not appear to be significantly affected by Ki67LI in this cohort. Analysis of the recurrent tumor Ki67 LI is ongoing. Interestingly, a wide range of Ki67 LI was present, underscoring the heterogenous nature of SCLC and providing a framework for future studies.

1212 Paired Box 9 Expression Defines a Distinct Clinicopathological Subset of Lung Adenocarcinoma

Monami Kishi[1], Takuo Hayashi[2], Kei Sano[1], Satsuki Kishikawa[1], Noriko Sasahara[2], Tsuyoshi Saito[1], Kazuya Takamochi[1], Kenji Suzuki[1], Takashi Yao[3]
[1]Juntendo University, School of Medicine, Tokyo, Japan, [2]Juntendo University Graduate School of Medicine, Tokyo, Japan, [3]Juntendo University, Tokyo, Japan

Disclosures: Monami Kishi: None; Takuo Hayashi: None; Kei Sano: None; Satsuki Kishikawa: None; Noriko Sasahara: None; Tsuyoshi Saito: None; Kazuya Takamochi: None; Kenji Suzuki: None; Takashi Yao: None

Background: Thyroid transcription factor 1 (TTF-1) is essential for the development and differentiation of the lung. As approximately 70% of lung adenocarcinoma (LAD) cases express TTF-1, it is widely used as the most specific marker for LAD in pathological examination. Paired box 9 (PAX9), a transcription factor of the PAX family, is also likely involved in lung development. However, clinicopathological significance of *PAX9* in LADs remain largely unknown.

Design: Transcriptome expression of LAD was analyzed in 71 LADs using cap analysis gene expression (CAGE) sequencing data, which provide genome-wide expression levels of the transcription start sites of different isoforms. Immunohistochemical examination for PAX9 and TTF-1 was performed in 1085 invasive LADs using whole sections from formalin and embedded in paraffin (FFPE) blocks. For immunohistochemical analyses of PAX9 expression in adenocarcinomas from various organs including 947 lung, 941 breast, 991 colorectum, 1011 prostate gland, and 271 thyroid gland, these tumors were assembled into tissue microarrays (TMAs), using 2.0-mm cores sampled from one or two different representative areas of each FFPE tissue block. Expression of PAX9 and TTF-1 was considered positive in each adenocarcinoma if 1% or more tumor cells were stained.

Results: High expression of *PAX9* was preferentially detected in LADs without TTF-1 expression in the CAGE dataset. Immunohistochemically, PAX9 was expressed in the nuclei of bronchial and bronchiole epithelium, and bronchial glands, in contrast to nuclear TTF-1 expression in type II pneumocytes in lung tissues. Nuclear PAX9 expression was observed in 339 LADs (31%). Among these, 307 LADs co-expressed TTF-1, and significant correlation between the immunohistochemical expression of TTF-1 and PAX9 was not observed. PAX9-positive LADs were significantly associated with male sex ($p = 0.004$), heavy smoker ($p < 0.0001$), non-lepidic subtype ($p < 0.0001$), *EGFR* wild-type tumors ($p < 0.0001$), and PD-L1 expression ($p < 0.0001$). Patients with PAX9-positive tumors exhibited significantly unfavorable overall survival ($p < 0.0001$). Furthermore, PAX9 was more frequently expressed in LADs (14%) than breast (3%), colorectal (0%), prostate (1%), and thyroid (6%) adenocarcinomas in the TMAs.

Conclusions: Subsets of LADs that expressed PAX9 may have originated from bronchial and bronchiole epithelium, or bronchial glands. Furthermore, PAX9 can be a novel diagnostic and prognostic marker in LADs.

1213 MUC1 and MUC4 Expression in Bronchiolar Adenoma

Satsuki Kishikawa[1], Takuo Hayashi[2], Kazuya Takamochi[1], Shiori Takekawa[3], Noriko Sasahara[2], Takashi Handa[2], Tsuyoshi Saito[1], Kenji Suzuki[1], Takashi Yao[3]
[1]Juntendo University, School of Medicine, Tokyo, Japan, [2]Juntendo University Graduate School of Medicine, Tokyo, Japan, [3]Juntendo University, Tokyo, Japan

Disclosures: Satsuki Kishikawa: None; Takuo Hayashi: None; Kazuya Takamochi: None; Shiori Takekawa: None; Noriko Sasahara: None; Takashi Handa: None; Tsuyoshi Saito: None; Kenji Suzuki: None; Takashi Yao: None

Background: Bronchiolar adenoma (BA), a benign peripheral lung tumor comprising bilayered bronchiolar-type epithelium containing a continuous basal cell layer, has recently been categorized as an adenoma variant as per the 2021 World Health Organization (WHO) classification. One of the hallmarks of BA is abundant mucin; however, its expression in BA is not fully understood.

Design: Twenty cases of BA were classified as proximal and distal types based on the WHO classification, and the clinicopathological, immunohistochemical, and molecular features of 20 BAs were assessed. Retrospective review of frozen sections was possible in 18 out of the 20 BA cases. Expression of mucins (MUC1, MUC2, MUC4, MUC5AC, and MUC6) was evaluated using immunohistochemistry. Next-generation sequencing was performed in 18 BAs using the Ion-Torrent Personal Genome Machine Platform and the Ion AmpliSeq Cancer Hotspot Panel v2. *EGFR, KRAS,* and *BRAF* mutations were assessed with Sanger sequencing in the remaining two cases.

Results: Fourteen (70%) of the patients were male, and 18 (90%) were over 60 years old. Fourteen were smokers (70%). All BAs were located in the lower lobes. Only seven cases (35%) were correctly diagnosed using frozen section. The remainder were diagnosed as adenocarcinoma and atypical proliferation with inflammation (n=9 and n=2, respectively). Among the 20 BAs, proximal type with papillary structure, proximal type with flat structure, and distal type was identified in three (15%), seven (35%) and 10 (50%) cases, respectively. The expression of MUC1, MUC4, MUC5AC, and MUC6 was assessed via immunohistochemistry in 20 (100%), 20 (100%), 9 (45%), and 5 (25%) cases, respectively. No tumors expressed MUC2. Furthermore, luminal cells were positive for MUC4 in all cases. The most frequently mutated gene was *BRAF*V600E (35%), followed by *KRAS* mutations (30%) and *EGFR* exon 20 insertion or unusual exon 19 deletion (15%), which were mutually exclusive. All cases with *KRAS* mutations had smoking history. In contrast, all cases with *EGFR* mutations had never smoked.

Conclusions: Our data revealed that BA preferentially occurs in the lower lobe of male elderly smokers. Furthermore, BA recurrently harbored *BRAF* and *KRAS* mutations, and MUC1 and MUC4 were commonly expressed in both proximal and distal type BAs. BAs exhibit distinct features of genetic alteration and mucin expression that may indicate the cellular origin of this rare neoplasm.

1214 RICTOR Amplification Is Associated with Rictor Membrane Staining and Does Not Correlate with PD-L1 Expression in Lung Squamous Cell Carcinoma

Ildiko Krencz[1], Anna Sebestyen[1], Daniel Sztankovics[1], Titanilla Dankó[1], Elmar Lutz[2], Andras Khoor[2]
[1]Semmelweis University, Budapest, Hungary, [2]Mayo Clinic, Jacksonville, FL

Disclosures: Ildiko Krencz: None; Anna Sebestyen: None; Daniel Sztankovics: None; Titanilla Dankó: None; Elmar Lutz: None; Andras Khoor: None

Background: RICTOR gene, which encodes mTORC2 scaffold protein Rictor, can be amplified in various malignancies including squamous cell carcinoma (SCC) of the lung. When RICTOR is amplified, the amplification likely plays an important role in tumorigenesis through hyperactivation of mTORC2. The amplification also offers a targetable genetic alteration, which might be especially important for PD-L1 negative SCC patients who are not eligible for immune checkpoint inhibitor therapy.

Design: The purpose of this study was to compare RICTOR amplification with Rictor and PD-L1 expression in SCC of the lung. Fifty cases of lung SCC were analyzed using fluorescence in situ hybridization (FISH) to detect RICTOR gene amplification and immunohistochemistry (IHC) to assess Rictor and PD-L1 expression. A RICTOR copy number of 4 or more and a RICTOR/Con5 ratio of 2 or more were considered positive for RICTOR amplification. Both Rictor and PD-L1 expression were assessed by using Tumor Proportion Score (TPS) and were classified into TPS < 1%, TPS 1 to 49%, and TPS ≥ 50% categories. A TPS ≥ 1% was considered positive.

Results: RICTOR amplification was observed in 18% of the cases. IHC was positive for Rictor and PD-L1 in 72% and 44% of the cases, respectively. For Rictor, two characteristic staining patterns were observed: (1) membrane staining (16%) and (2) cytoplasmic staining (56%). Rictor membrane staining predicted RICTOR amplification as detected by FISH with a sensitivity of 67% and a specificity of 95%. RICTOR amplification was detected in 17% of PD-L1 positive and 19% of PD-L1 negative cases; there was no correlation between RICTOR amplification and PD-L1 expression.

Conclusions: (1) Correlation between RICTOR amplification and Rictor membrane staining suggests that the latter can potentially be used as a surrogate marker to identify RICTOR-amplified lung SCCs. (2) Our findings also indicate that a significant proportion of PD-L1 negative lung SCCs harbor RICTOR amplification. Analysis of PD-L1 negative tumors using RICTOR FISH or Rictor IHC can help select patients who may benefit from mTORC2 inhibitor therapy.

1215 Considering Uncertainty Improves Deep Learning-based Lung Cancer Subtyping

Yongeun Lee[1], Tae-Yeong Kwak[2], Sun Woo Kim[1], Hyeyoon Chang[1]
[1]Deep Bio Inc., Seoul, South Korea, [2]Deep Bio Inc., Guro-gu, South Korea

Disclosures: Yongeun Lee: *Employee*, Deep Bio Inc.; Tae-Yeong Kwak: *Employee*, Deep Bio Inc.; Sun Woo Kim: *Stock Ownership*, DeepBio; Hyeyoon Chang: *Employee*, Deep Bio Inc.

Background: The histological subtype of lung cancer is a very important factor in predicting a patient's prognosis or determining the treatment course. The previously published deep learning-based lung cancer subtyping models divided the entire slide image into patch image units, classified each patch into subtypes, and aggregated them to slide level diagnose. This method has limitations in subtyping performance due to errors in areas where judgment is ambiguous. In this study, we tried to increase the subtyping performance in a way that considers uncertainty.

Design: We used the TCGA dataset for training and validation. Non-small cell lung cancers (NSCLCs) account for 85% of all lung cancer. Adenocarcinoma (LUAD) and squamous cell carcinoma (LUSC), which account for the majority of tumors in NSCLCs, were selected as the target. The training data set consisted of 1364 LUAD slides, 1265 LUSC slides, and 591 benign slides.

The whole diagnostic process was as follows. After extracting patches from the entire slide area excluding the background, patches determined to be uncertain by the deep learning model were filtered out. Then, the final diagnosis was made on the slide by subtyping the selected patches. (Figure 1)

Also, to analyze the effect of filtering out the ambiguous patches on diagnosis, the performance of the subtyping using the entire patch and using the filtered patches were compared.

Results: When comparing the performance of subtyping using the entire patch and the filtered patches, the sensitivity of LUSC and LUAD improved from 0.7777 to 0.9047 and from 0.8122 to 0.8860, respectively. The specificity also improved from 0.8240 to 0.8921 and from 0.7928 to 0.9132 for LUSC and LUAD respectively. Also, even on the slide level, 7 out of 20 slides that were misdiagnosed as LUAD when analyzed using the entire patch could be correctly diagnosed through patch filtering. An example of filtered patches on the LUSC slide is attached to Figure 2. The upper line of Figure 2 is a patch that is judged to be suitable for diagnosis with the characteristics of LUSC, and the lower line is rejected patches because it is judged to be uncertain for diagnosis.

Figure 1 - 1215

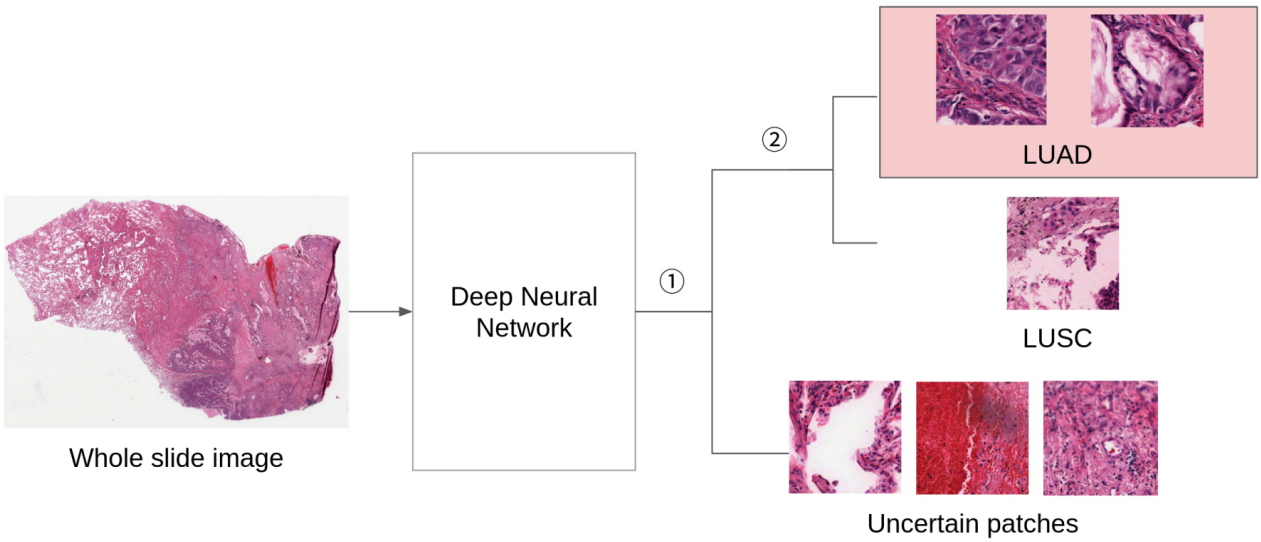

Figure 2 - 1215

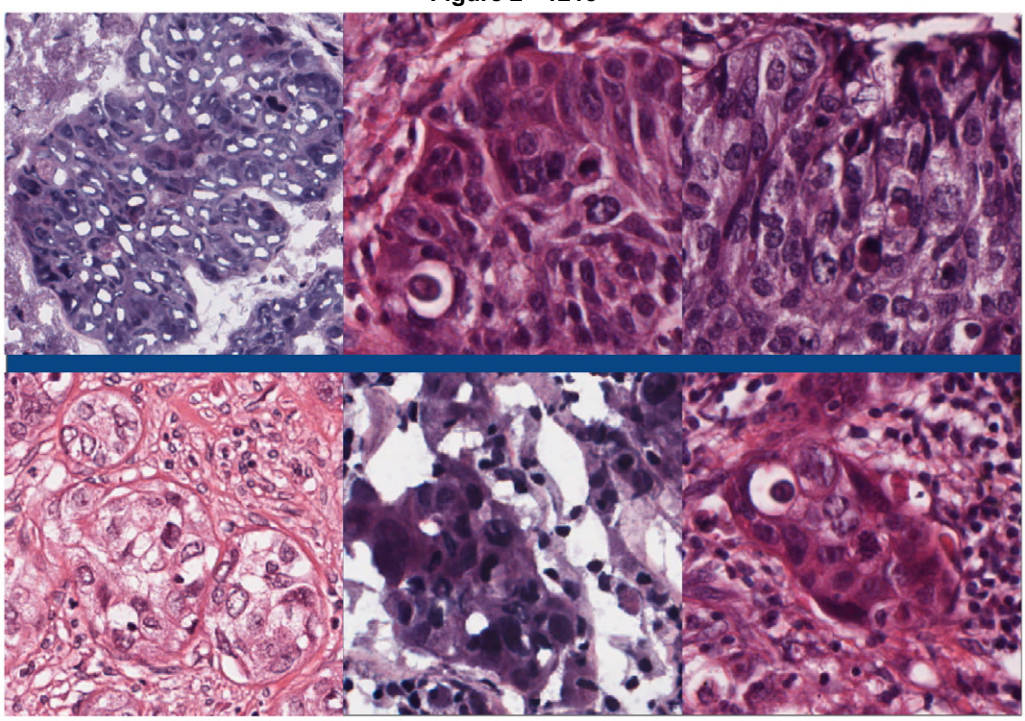

Conclusions: Our model outperformed the existing deep learning models for lung cancer subtyping and was able to cope with particularly difficult problems better.

1216 Gene Expression Profiles in Late-Stage EGFR-Sensitive NSCLC are Associated with Early vs Intermediate vs Late Resistance to Osimertinib

Xiaomo Li[1], Matthew Gayhart[2], Sungyong You[1], Ren Sun[1], Chintda Santiskulvong[1], Yizhou Wang[1], Eric Vail[1], Saleh Heneidi[1], Elias Makhoul[1], Jean Lopategui[3]

[1]Cedars-Sinai Medical Center, Los Angeles, CA, [2]Massachusetts General Hospital, Harvard Medical School, Boston, MA, [3]Cedars-Sinai Medical Center, West Hollywood, CA

Disclosures: Xiaomo Li: None; Matthew Gayhart: None; Sungyong You: None; Ren Sun: None; Chintda Santiskulvong: None; Yizhou Wang: None; Eric Vail: *Speaker*, Bayer, Eli Lilly, Illumina, Thermo Fisher; *Consultant*, PierianDx; *Employee*, LungLifeAI; Saleh Heneidi: None; Elias Makhoul: None; Jean Lopategui: None

Background: Osimertinib, a third generation EGFR tyrosine kinase inhibitor (TKI), is FDA approved for first-line monotherapy for late-stage NSCLC patients based on the results of the FLAURA trial. However, the duration of the response (DR) in the Osimertinib treated patient cohort ranged from 0 to 23.8 months. By analyzing the transcriptome of NSCLC using RNA-sequencing (RNA-seq), we aimed to identify gene expression signatures predictive of early, intermediate, or late relapse. The goal is to identify which patients will have long DR to Osimertinib and which patients may benefit from alternate therapies by early identification of activated or inhibited pathway regulators.

Design: Twenty late-stage NSCLC patients (19 stage IV, 1 Stage III) with EGFR-sensitizing mutations and Osimertinib only treatment were selected retrospectively. Normal lung samples (n=4) were used for control. Initial tissue diagnostic samples were obtained, RNA was extracted, and whole transcriptome RNA-seq was performed. Patients were divided into early (less than 10 months, n=5), intermediate (10-17 months, n=7), and late (more than 17 months, n=8) relapse. Unsupervised principal component analysis (PCA) was performed to assess sample distribution. Differential expression (DE) analysis to identify DE genes (DEGs) with a false discovery rate (FDR) < 0. The DEGs were used as input for pathway enrichment analysis.

Results: On PCA, a distinct separation existed between normal lung and early and late relapsed NSCLC. In comparing between early relapse vs late relapse, 136 DEGs (90 up- and 46 downregulated) were identified (all p-value<0.05). Fifty-nine DEGs (29 up- and 20 downregulated) were identified by comparing intermediate and late relapse. RTKN2, TMEM100, TTC32 were more than 8-fold higher in the early-relapse group compared with late-relapse, while APP1, HMGV2, ST6GALNAC1 were significantly downregulated. Up-regulated DEGs in early relapse NSCLC were significantly enriched in vasculature development and cell proliferation.

Figure 1 - 1216

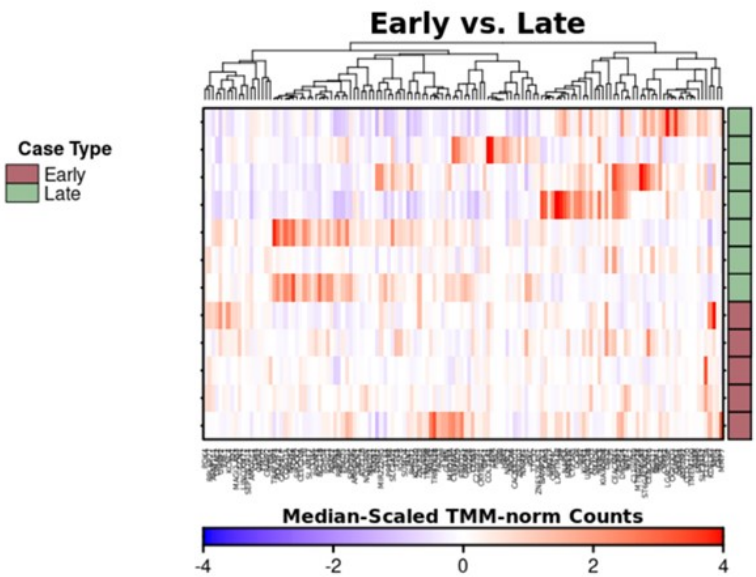

Figure1. Heat map showing gene expression profile difference between Early and Late relapse group

Conclusions: The distribution of the DEGs between early and late relapse showed significant differences that may explain why some late-stage NSCLC patients with EGFR sensitizing mutations have a short DR on Osimertinib, while other patients have a

multi-year DR. The uncovered up and downregulated pathways may provide insight into targeted therapies in future studies to improve DR in early relapse patients.

1217 Potential Clinical Values and Mechanisms of BIRC5 Expression in Lung Squamous Cell Carcinoma

Guo-Sheng Li[1], Rong-Quan He[1], Lin-Yi Li[1], Da-Peng Yu[1], Cheng-Xin Li[1], Wei-Ying He[1], Lin-Jie Yang[1], Zhou Hua-fu[1], Jin-Liang Kong[1], Gang Chen[1]
[1]The First Affiliated Hospital of Guangxi Medical University, Nanning, China

Disclosures: Guo-Sheng Li: None; Rong-Quan He: None; Lin-Yi Li: None; Da-Peng Yu: None; Cheng-Xin Li: None; Wei-Ying He: None; Lin-Jie Yang: None; Zhou Hua-fu: None; Jin-Liang Kong: None; Gang Chen: None

Background: The clinical value and mechanisms of BIRC5 in lung squamous cell carcinoma (LUSC) remains obscure. Exploring aspects is conducive to improving clinical management and understanding of LUSC.

Design: One in-house tissues microarrays (n = 379), one in-house microarray matrix (n = 6), and 95 raw datasets (n = 4,719) samples from public databases were included in this study. The t-test and standardized mean difference were utilized to explore BIRC5 expression in LUSC at both protein and mRNA levels. *Wilcoxon* test was used to evaluate correlation of BIRC5 levels and clinical parameters of LUSC patients. Kaplan-Meier curve was used to detect prognosis significance of *BIRC5* expression in LUSC. Receiver operating characteristic curves were for assessing the ability of BIRC5 expression to distinguish LUSC from non-LUSC. Underlying molecular mechanisms of BIRC5 expression in LUSC were studied with gene ontology, disease ontology, and signal pathways. To explore mechanisms of differential *BIRC5* expression, the transcription factors may regulate *BIRC5* expression were screened and selected via correlation analysis and ChIP-Seq data.

Results: Both protein (Figure 1) and mRNA (Figures 2A) expression of BIRC5 are increased in LUSC (standardized mean difference > 0, Figure 2B). Upregulated *BIRC5* expression is relevant to favorable prognosis of LUSC patients at clinical stages I and II (p < 0.05, Figures 2C). BIRC5 expression makes it feasible to distinguish LUSC from non-LUSC (area under the curve ≥ 0.9, Figures 2D). BIRC5 may affect occurrence and development of LUSC via cell cycle signal pathway (Figures 2E). High expression of transcription factors *E2F1* and *EZH2* may contribute to the observed increased expression of *BIRC5* in LUSC, with the fact that expression of both of them is positively relevant to *BIRC5* expression and that ChIP-seq binding peaks located at the upstream of the transcription start site of *BIRC5*.

Figure 1 - 1217

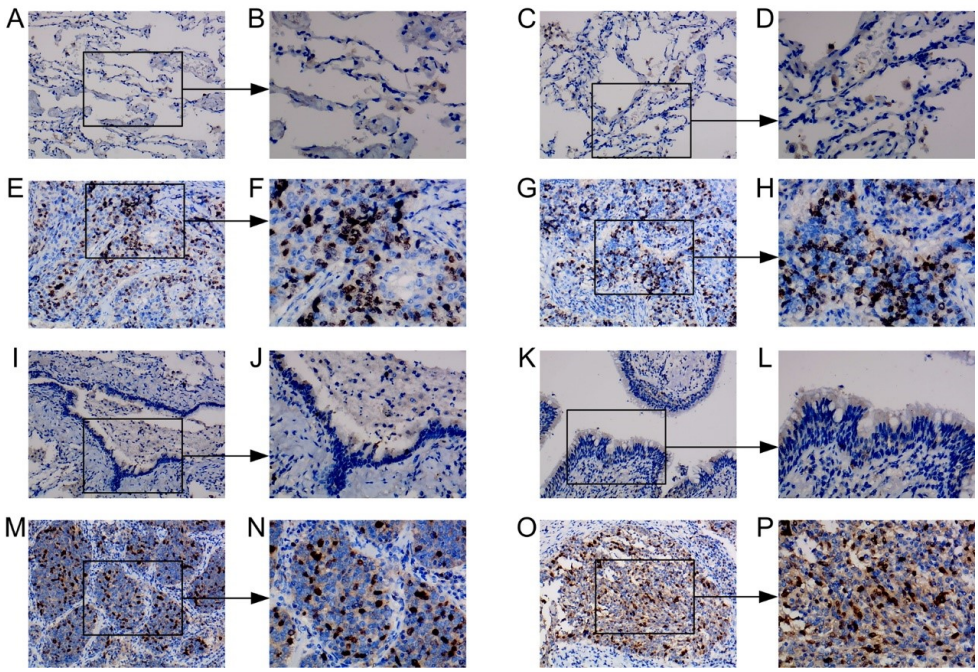

Figure 2 - 1217

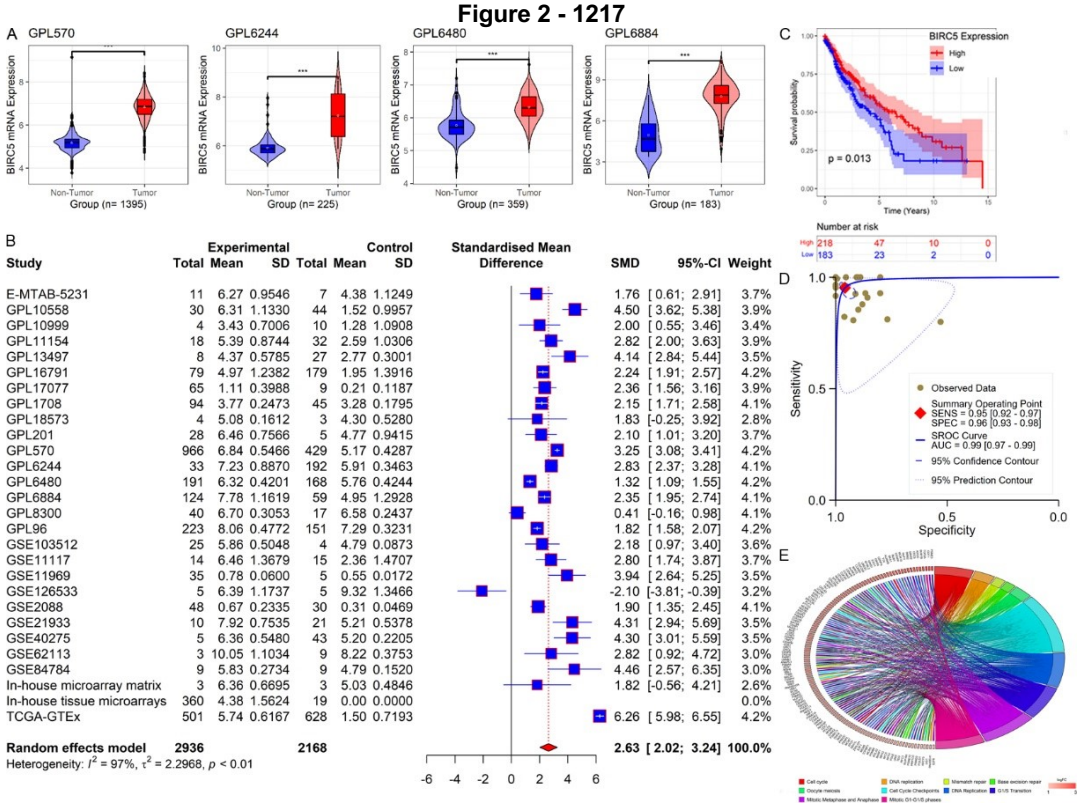

Conclusions: Upregulated BIRC5 expression shows clinical value in LUSC, providing useful insights for understanding the molecular mechanism of LUSC pathogenesis.

1218 Reproducibility of Nuclear Grade in Epithelioid Malignant Mesothelioma

Hui-Hua Li[1], Brittany Cody[2], Darya Buehler[3], Carter Norton[3], Rakesh Sarda[4], Paul Weisman[3], Aliya Husain[5], Jefree Schulte[3]

[1]University of Wisconsin School of Medicine and Public Health, Madison, WI, [2]UChicago Medicine, Chicago, IL, [3]University of Wisconsin-Madison, Madison, WI, [4]University of Wisconsin Hospital and Clinics, Madison, WI, [5]University of Chicago, Chicago, IL

Disclosures: Hui-Hua Li: None; Brittany Cody: None; Darya Buehler: None; Carter Norton: None; Rakesh Sarda: None; Paul Weisman: None; Aliya Husain: None; Jefree Schulte: None

Background: Nuclear grading has been shown to be a strong prognostic tool in epithelioid malignant mesothelioma (EMM). Assigning a nuclear grade (NG) to EMM utilizes a three-tier (NG1, NG2, or NG3) system based on the sum of nuclear atypia (NA) and mitotic count (MC) scores. More recently, a two-tier system of high (NG 2 with necrosis and nuclear grade 3) and low grade (NG 1 or NG 2 without necrosis) has been recommended by international consensus and NG reporting is now part of synoptic reporting in pleural EMM. However, most work on NG has been done by pathologists with expertise in thoracic pathology, and the reproducibility of NG, especially among non-expert pathologists, has not been determined. This study seeks to determine the reproductivity of NG in EMM.

Design: Sixty cases of EMM were retrieved from the pathology archives. Diagnosis, NG, and presence or absence of necrosis were determined by two expert thoracic pathologists. Published articles on NG were provided to three pathologists without specific expertise in diagnosis of MM. After independent review of NG literature, each of the pathologists provided a NA score, MC score, NG, and determined presence or absence of necrosis. The NG and presence or absence of necrosis was used to generate a two-tier low- or high-grade score. Kappa statistic was generated to determine reproducibility (κ = 0.21 to 0.40 = fair, κ = 0.41 to 0.60 = moderate, κ = 0.61 to 0.80 = substantial, and κ ≥ 0.81 = excellent agreement).

Results: Based on expert review, 34 NG 1, 14 NG2, and 12 NG3 EMM were included; 10 with necrosis, 50 without. NA scoring showed fair agreement (κ = 0.37) and MC score showed substantial agreement (κ = 0.63). The agreement of the three-tier NG was moderate (κ = 0.49). There was substantial agreement in determining the presence or absence of necrosis (κ = 0.74). Combining the three-tier NG with necrosis status improved reproducibility, as two-tiered grading showed excellent agreement (K = 0.82).

Conclusions: This study demonstrates that the three-tier NG scoring system, when employed by non-expert pathologists yields only moderate agreement. While MC score reproducibility was substantial, overall agreement of NG is likely lessened by the fair agreement observed in assignment of NA. Reproducibility is higher when utilizing the two-tier system. This data suggests that NG can by employed successfully by non-thoracic pathologists, but some training may be beneficial in determination of NA.

1219 Digital Quantification of Tumor Cellularity as a Novel Prognostic Feature in Lung Adenocarcinoma

Sherman Lin[1], Joshua Samsoondar[2], Samantha Keow[1], Binit Pokharel[1], Djarren Tan[1], Jacobo Martinez-Acevedo[1], Michelle Pham[1], Nina Wu[1], Tanya Misra[1], Victor Lam[1], Irene Sansano[3], Matthew Cecchini[4]
[1]University of Western Ontario, London, Canada, [2]Western University, London, Canada, [3]Hospital Universitari Vall d'Hebron, Barcelona, Spain, [4]London Health Sciences Centre, Western University, London, Canada

Disclosures: Sherman Lin: None; Joshua Samsoondar: None; Samantha Keow: None; Binit Pokharel: None; Djarren Tan: None; Jacobo Martinez-Acevedo: None; Michelle Pham: None; Nina Wu: None; Tanya Misra: None; Victor Lam: None; Irene Sansano: *Speaker*, Roche, Pfizer, AstraZeneca, Boehringer Ingelheim; Matthew Cecchini: *Speaker*, Merck; *Consultant*, Tenomix

Background: Lung cancer is currently staged based on the size of the tumors and involvement of other structures. This staging may be a surrogate measure for the number of cells present in the tumor. The recently updated grading system of lung adenocarcinoma assesses the presence of high risk architectural patterns, which tend to have more complex cellular growth. Counting individual tumor cells is impractical for a pathologist using a conventional analog light microscope. Image analysis tools applied to digital slides can be utilized to automate the quantification of lung adenocarcinoma. In this study, we test the hypothesis that tumor cellularity can be used as a novel prognostic tool in lung cancer that integrates quantification of high risk architectural patterns.

Design: Digital slides (n=102) from the Cancer Genome Atlas (TCGA) lung adenocarcinoma (LUAD) dataset were obtained and analyzed in QuPath. Representative areas of tumour were annotated and reviewed by a thoracic pathologist, the annotations were used as training data for a random trees based object classifier that utilized detected cell features to identify and quantify tumor cells across entire slides. This was normalized with the surface area of the tumor present on the slide to provide a measure of tumor density. The overall total cellularity was calculated by combining the size of the grossly measured tumor with the tumor density. Major histologic patterns in representative panels were determined by a thoracic pathologist and were compared with the tumor density of the tile. The overall and progression free survival was compared between groups of high and low tumor cellularity.

Results: High-grade histologic patterns had a significantly greater tumor density compared with other patterns of lung adenocarcinoma. A trend between survival and cellularity was identified and a cut-off of 5.5 x 10^10 cells was found to predict outcome in cases. Cases with a low cellularity had an improved progression free survival (HR 0.21; 95% CI 0.096-0.47) and overall survival (HR 0.25; 95% CI 0.088-0.7) compared with cases that had higher cellularity.

Figure 1 - 1219

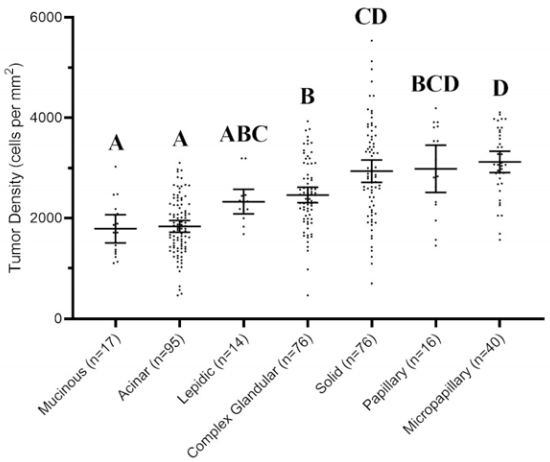

Figure 1: Tumor density varies across architectural patterns of lung adenocarcinoma. Data points represent individual density measurements in representative 1.26 x 1.26 mm tiles with means and standard deviation shown. Letters indicate statistical difference between groups by one-way ANOVA followed by Tukey's post-hoc test ($p < 0.05$).

Figure 2 - 1219

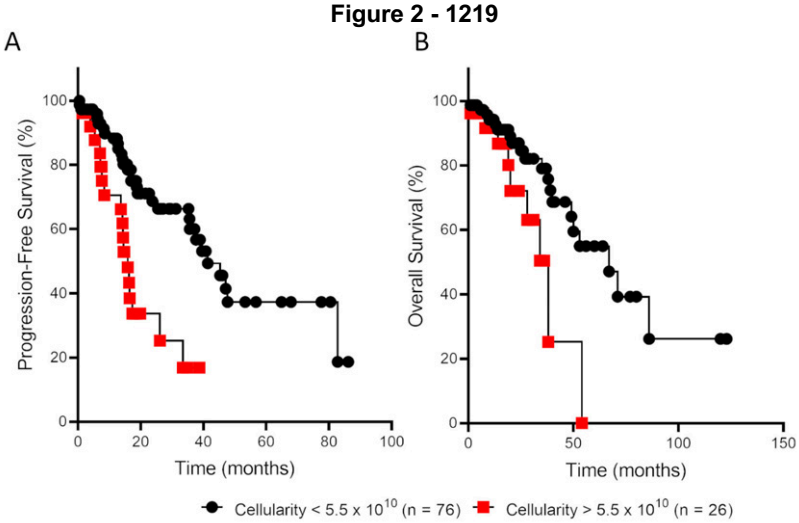

Figure 2: (A) Progression free survival and (B) overall survival analysis of tumors with low overall cellularity compared with tumors with high overall cellularity.

Conclusions: Tumor cellularity represents a novel prognostic tool in lung cancer that takes into account both the size and composition of the tumor. Use of advanced image analysis tools allows for the automation of this task in a simplified and efficient manner. Future work will seek to validate these findings in additional larger datasets to refine the classification of tumors by cellularity.

1220 Histologic Diagnosis of Combined Pulmonary Fibrosis and Emphysema (CPFE)

Meghan Lindstrom[1], Liberty Bonestroo[1], Emilian Racila[1]
[1]University of Minnesota Medical Center, Minneapolis, MN

Disclosures: Meghan Lindstrom: None; Liberty Bonestroo: None; Emilian Racila: None

Background: Combined pulmonary fibrosis and emphysema (CPFE) is a unique entity, clinically characterized as coexistence of emphysema and interstitial fibrosis, and radiologically associated with upper lobe predominant emphysema and lower lobe predominant fibrosis. Important differences exist between CPFE and usual interstitial pneumonia (UIP) regarding prognosis, response to antifibrotic therapy and risk of complications such as lung cancer development. Although important progress has been

recorded over the last fifteen years in recognizing CPFE as a clinically separate ILD entity, there are no standardized criteria for histologic diagnosis and often CPFE patients are misdiagnosed as UIP. The aim of this study is to better define the histology of CPFE and its major differentiation features from UIP.

Design: Twenty-four CPFE patients and 117 UIP patients diagnosed between 2011-2021 who received lung transplantation at our institution were sequentially included in this study. The pathologic material from the available explants (two central and two peripheral samples per lobe, collected from each lung lobe) was histologically evaluated with emphasis on presence of emphysema, presence of small airway disease and its morphologic characteristics, distribution and severity of interstitial fibrosis and frequency of fibroblastic foci.

Results: Among CPFE patients, 21 were male and 3 female, compared to 79 male and 38 female UIP patients. No major age difference at lung transplantation was found between males and females (60.5 years vs. 61.6 years). Seven male patients and two female patients died after transplant. CPFE is characterized by presence of small airway disease, with peri-airway fibrosis and bronchiolar metaplasia being the most frequent and consistent findings in CPFE and absent or limited in UIP. Interstitial fibrosis in CPFE patients did not show the characteristic spatial distribution with subpleural accentuation and disparity between upper and lower lobes seen in UIP. Finally, fibroblastic foci are infrequently observed in CPFE and located predominantly adjacent to airways, compared to the interstitial interface of the characteristically progressive fibrosis from periphery to center seen in UIP.

Conclusions: There are major morphologic differences between CPFE and UIP that facilitate recognition of each entity and accurate pathologic diagnosis. A score is currently being developed to help pathologists objectively assess patients with clinical diagnosis of idiopathic pulmonary fibrosis.

1221 Histopathological Features in Mesothelioma Following Neoadjuvant Therapy and Their Correlation with Outcome

Ying-Chun Lo[1], Aakash Desai[1], Sarah Jenkins[1], Grant Spears[1], Tobias Peikert[1], Aaron Mansfield[1], Anja Roden[1]
[1]Mayo Clinic, Rochester, MN

Disclosures: Ying-Chun Lo: *Advisory Board Member*, Takeda Pharmaceutical Company Limited; Aakash Desai: None; Sarah Jenkins: None; Grant Spears: None; Tobias Peikert: None; Aaron Mansfield: *Advisory Board Member*, Janssen, AbbVie, Astra Zeneca, Genentech; *Grant or Research Support*, nference, Novartis; Anja Roden: None

Background: Mesothelioma is an aggressive tumor; predictive markers for individual patient management are needed. Histopathologic features post neoadjuvant therapy are not well characterized. We aimed to systematically describe histopathologic findings of mesotheliomas post neoadjuvant therapy and to correlate them with outcome of patients.

Design: Institutional database was searched for resection specimens of mesothelioma. Slides were re-reviewed by one (N=26) or two (N=15) thoracic pathologists independently; histopathological features were recorded, including nuclear grade (2021 WHO classification), tumor regression grade (TRG, scores 1-5; score 1-no viable tumor, score 5-no treatment response), and features commonly described in tumor beds of other neoplasms. Medical records were reviewed.

Results: Forty-one patients with pleural (N=35, 85.4%), peritoneal (N=3, 7.3%), or both (N=3) mesothelioma (median age 64 years, range 33-76; 34 males, 82.9%) underwent neoadjuvant therapy [chemotherapy (CT) (N=32, 78.0%), CT+immunotherapy (N=4, 9.8%), or radiation (N=5, 12.2%)]. Mesotheliomas were of epithelioid (N=38, 92.7%) or biphasic (N=3, 7.3%) subtype. Among the 15 specimens assessed by two pathologists, interobserver agreements were 86.7% (subtype), 69.2% (nuclear grade), 73.3% (TRG), and 86.7% (presence of necrosis). In epithelioid mesotheliomas, nuclear grade (evaluated in N=13) was 1 (N=6, 46.2%), 2 (N=6), or 3 (N=1, 7.7%). Among all specimens, TRG 1-5 were seen in 0, 1 (2.4%), 11 (26.8%), 19 (46.3%), and 10 (24.4%) cases, respectively. Median % of viable tumor cells was 80% (range, 5-100%). Potential features of tumor bed included collagen fibrosis (N=38, 92.7%), necrosis (N=11, 26.8%), hemorrhage (N=3, 7.3%), foamy histiocytes (N=10, 24.4%), calcification (N=1, 2.4%), cholesterol clefts (N=1, 2.4%), and granulomatous inflammation (N=2, 4.9%). During follow-up (N=41, median 15.4 months, range 1.4-63.1) 22 patients had a recurrence or metastasis, and 28 patients died. Biphasic morphology was associated with worse disease-free survival (hazard ratio 4.76, p=0.04). Nuclear grade, TRG, % viable tumor, or % necrosis were not associated with outcome. Treatment-specific associations were prohibited by low number of cases.

Conclusions: In mesothelioma, typical histopathological features of treatment effect are not commonly observed. Correlation with RECIST by imaging studies and a control group of patients with treatment-naïve mesothelioma will be performed.

1222 Clinical and Histopathologic Characteristics of Recurrent Sarcoidosis in Post-transplant Lungs: 25 Years of Experience

Liang Lu[1], Alexander Wein[2], Christopher Jones[1], Adam Anderson[1], Jon Ritter[3], Chieh-Yu Lin[3]
[1]Washington University in St. Louis, St. Louis, MO, [2]Barnes-Jewish Hospital/Washington University, St. Louis, MO, [3]Washington University School of Medicine, St. Louis, MO

Disclosures: Liang Lu: None; Alexander Wein: None; Christopher Jones: None; Adam Anderson: None; Jon Ritter: None; Chieh-Yu Lin: *Consultant*, Natera

Background: Lung transplantation is the treatment for end-stage pulmonary sarcoidosis. While recurrent sarcoidosis in allografts has been described in several case reports, the incidence and clinicopathologic characteristics remain unclear. In this study, we characterize the clinical and histopathologic features of recurrent sarcoidosis diagnosed in post-transplant lung surveillance transbronchial biopsies (TBBx).

Design: With IRB approval, we conducted a single-center, retrospective study to identify pulmonary sarcoidosis patients who received a lung transplant from 1995 to 2020. Patients with recurrent sarcoidosis were identified by histopathological evidence of granulomatous inflammation in post-transplant TBBx, and clinical data was collected. The TBBx were reviewed for specimen adequacy, presence of acute and chronic rejection, and type and histological features of the granulomatous inflammation.

Results: We identified 36 lung-transplant patients with pulmonary sarcoidosis. Among them, 18 patients (50%) experienced recurrent sarcoidosis post-transplant. There were 7 females and 11 males with mean age at recurrence of 51.6 years. The average time interval from transplant to recurrence was 243 days (22-984 days). There were 33 surveillance TTBx that contained granulomatous inflammation. All TBBx contained more than 4 pieces of alveolated lung tissue with no evidence of clinically significant acute cellular rejection (ISHLT grade A2 and above), chronic rejection or antibody mediated rejection. On average, 3.6 well-formed granulomas were identified per TBBx (range 1 to > 20). Multinucleated giant cells were identified in 11 TBBx (33.3%), with one case containing asteroid bodies. While most of the granulomas were “naked granulomas," five cases (15.2%) showed prominent lymphoid cuffing at the periphery. Two cases showed evidence of fibrosis. One of the cases included focal necrosis; however, no infectious organisms were identified by special stains; clinical correlation suggested this case represented recurrent sarcoidosis.

Conclusions: This is the first case series to systemically characterize the incidence and clinicopathologic features of recurrent sarcoidosis in post-lung transplant patients. Biopsies of recurrent sarcoidosis usually show multiple well-formed granulomas. Giant cells can be seen in one third of the cases, while lymphoid cuffing, fibrosis, asteroid bodies and caseating granulomas are uncommon findings. Pathologists need to be aware of recurrent sarcoidosis after lung transplant.

1223 Mucin Distribution in Bronchiolar Adenoma Reveals Organoid Differentiation Simulating the Normal Lung

Hisanori Matoba, Shinshu University, Matsumoto, Japan

Disclosures: Hisanori Matoba: None

Background: Bronchiolar adenoma is a lung neoplasm exhibiting various degrees of proximal and distal bronchiolar differentiation. Previous reports have identified mucin types produced in bronchiolar adenoma. Based on these reports, immunohistochemistry (IHC) for MUC5AC in bronchiolar adenoma is focally positive, while bronchiolar adenoma tissues are largely negative for MUC6 and MUC2, and one study reported MUC5B production in bronchiolar adenoma. Nonetheless, distribution of these mucins, especially MUC5AC and MUC5B, in bronchiolar adenoma is not yet completely clear.

Design: In this study, we evaluated regional distribution of MUC5AC and MUC5B in bronchiolar adenoma and compared that with distribution seen in normal respiratory tract using immunohistochemistry. Airways included in 7 bronchiolar adenoma cases were classified as 1) bronchi (>2 mm in diameter), 2) proximal bronchioles (1–2 mm in diameter), and 3) distal bronchioles (<1 mm in diameter), based on airway diameter and morphology. MUC5AC and MUC5B positivity in each of these segments of respiratory tract and submucosal glands was evaluated, and percentage of positive cells was calculated as an average of all evaluated airways and submucosal glands. (n = 5 for submucosal glands and bronchi; n = 8 for proximal bronchioles; n = 18 for distal bronchioles.) Positivity for MUC5AC, MUC5B, MUC2, MUC6, HIK1083, β-tubulin, and TTF-1 in luminal cells and positivity for p40 in basal cells of 7 bronchiolar adenoma cases were also evaluated in the entire lesion and percentage of positive cells in each case was calculated.

Results: In normal respiratory tract, MUC5AC was mainly distributed in large bronchi, while MUC5B was distributed in bronchi, bronchioles, and submucosal glands. In bronchiolar adenoma, MUC5AC was primarily distributed in luminal cells of large airspaces, and MUC5B was distributed in luminal cells of small airspaces and mucinous glands, in addition to large airspaces, regardless of distal or proximal differentiation. In particular, MUC5B was distributed in non-mucinous club and ciliated cells in both the normal respiratory tract and bronchiolar adenoma.

Conclusions: The distribution patterns of MUC5AC and MUC5B in bronchiolar adenoma resemble those seen in normal airways, especially MUC5B distribution in non-mucinous club and ciliated cells in peripheral airways. We interpret these findings as indicating organoid differentiation of bronchiolar adenoma simulating the normal lung. Because MUC5B is expressed in some invasive mucinous adenocarcinoma cases, MUC5B expression itself cannot be a useful marker to distinguish invasive mucinous adenocarcinoma from bronchiolar adenoma. However, here we found that bronchiolar adenoma cells primarily express MUC5B in addition to small amounts of MUC5AC, and those tissues show organoid differentiation simulating the normal lung, being different from invasive mucinous adenocarcinoma which shows organoid differentiation simulating gastric pyloric mucosa and MUC5AC and MUC6 positivity.

1224 Clinicopathological Characteristics and Response to Targeted Therapy in Patients with ALK-rearranged Non-small-cell Lung Carcinoma harboring TP53 Mutations

Harshita Mehrotra[1], Shannon Rodgers[2], Laura Favazza[2], Dhananjay Chitale[2]
[1]Henry Ford Health System, Detroit, MI, [2]Henry Ford Hospital, Detroit, MI

Disclosures: Harshita Mehrotra: None; Shannon Rodgers: None; Laura Favazza: None; Dhananjay Chitale: None

Background: Anaplastic lymphoma kinase (*ALK*) rearrangements are reported in 3-7% of patients with non-small cell lung carcinoma (NSCLC), where *ALK* tyrosine kinase inhibitors (*ALK*-TKIs) have shown to improve progression free survival (PFS) and overall survival (OS). However, most develop resistance post-treatments due to primary and progressive acquired resistance mechanisms. Recent studies have shown that concurrent mutations such as *TP53* can affect the prognosis by generating inherent resistance and inferior treatment response. We sought to evaluate the clinicopathological characteristics of patients with *ALK*-rearranged NSCLC and correlate targeted therapy response in patients with/without concurrent *TP53* mutations.

Design: All NSCLC cases tested for *ALK* rearrangements over 5.5 years were reviewed. Genomic DNA and RNA were extracted using standard tissue extraction protocols. Fluorescent in situ hybridization (FISH) was performed using a DNA probe cocktail specific for 2p23 chromosome breakpoint. RNA sequencing was performed using Archer Solid Tumor FusionPlex panel that included primers flanking exons 19 through 22 of *ALK* gene. Targeted DNA NGS panel included *TP53* gene covering exons 2, 4-8, 10. All cases fulfilled the NGS and FISH assay acceptability criteria.

Results: 23 patients were positive for *ALK* gene rearrangement, and 7 had concurrent *TP53* mutations. Patient characteristics are given in table 1. 5/16 patients with *ALK* rearranged NSCLC without *TP53* mutations developed resistance to first line *ALK*-TKIs. Median PFS on *ALK*-TKIs and OS were 12 months (range 1 to 65) and 19 months (range 1 to 87) respectively. 4/7 patients with *ALK*-rearranged NSCLC with *TP53* mutations developed resistance to first line *ALK*-TKIs. Median PFS on *ALK*-TKIs and OS was 6 months (range 1 to 38) and 42 months (range 1 to 110) respectively (Figure 1). 15 patients (65%) were alive with disease at the time of review. One tumor underwent small-cell change (patient 11), one squamous change (patient 21), and two acquired progressive mutations in the *ALK* gene (patients 17 and 18).

S.No	Age at diagnosis (years)	Sex	Ethnicity	Smoker	Stage at Diagnosis	TP53 mutation	PDL1 (22C3) TPS	Targeted therapy	PDL1 inhibitors	Primary Resection	Chemotherapy	Radiotherapy	Progression on ALK-TKI yes=1; no=0	Survival status	Progression Free Survival (PFS) on ALK-TKI (months)	Overall Survival from time of diagnosis (months)
1	58	M	Caucasian	No	IIB	No NGS data	N/A	No	No	No	Yes	No	Yes	Alive	33	36
2	63	F	African American	No	IVa	Negative	N/A	Crizotinib	No	No	Yes	Yes	Yes	Died	15	33
3	84	F	Hispanic	No	IVa	Negative	N/A	Alectinib	No	No	Yes	Yes	No	Alive	40	54
4	45	F	African American	No	IVc	Negative	<1%	Alectinib	No	No	Yes	No	No	Alive	41	42
5	78	F	Middle Eastern	No	IIIa	Negative	40%	Alectinib	No	No	Yes	Yes	No	Died	5	10
6	52	F	Caucasian	No	IVa	Negative	N/A	Crizotinib	No	No	No	No	Yes	Alive	33	74
7	58	F	Caucasian	Yes	IVa	Negative	60%	Alectinib	No	No	Yes	No	No	Died	2	4
8	70	M	African American	Yes	IVb	Negative	97%	No	No	No	No	No	No	Died	1	1
9	56	F	Caucasian	No	IVb	Negative	55%	Alectinib	No	No	Yes	Yes	No	Alive	14	18
10	65	F	Caucasian	No	IVb	Negative	N/A	Alectinib	Keytruda	No	Yes	Yes	No	Died	2	61
11	69	F	Caucasian	Yes	IVc	Negative	N/A	Crizotinib	No	No	Yes	Yes	Yes	Alive	65	87
12	78	F	African American	No	IVa	Negative	Indeterminate	Alectinib	No	No	No	No	No	Alive	12	14
13	64	M	Caucasian	Yes	IVa	Negative	TPS < 1	Brigatinib	No	No	No	No	No	Alive	10	12
14	29	M	Middle Eastern	No	IIIa	Negative	N/A	No	No	Yes	Yes	No	Yes	Alive	13	21
15	56	M	African American	No	IVc	Negative	TPS 30%	Alectinib	No	No	No	No	No	Alive	4	5
16	62	M	Asian	No	IVa	Negative	TPS 90%	Brigatinib	No	Yes	No	No	No	Alive	2	3
17	43	F	Caucasian	No	IVb	Positive	N/A	Crizotinib	No	No	Yes	Yes	Yes	Died	6	30
18	44	M	African American	No	IVb	Positive	<1%	Crizotinib	Keytruda	No	Yes	Yes	Yes	Alive	1	102
19	51	M	African American	No	IIIb	Positive	98%	Alectinib	Keytruda	No	Yes	Yes	Yes	Died	3	41
20	57	M	Caucasian	Yes	IVb	Positive	80%	Alectinib	Keytruda	No	No	Yes	Yes	Alive	36	42
21	69	M	Caucasian	Yes	IB	Positive	N/A	Alectinib	No	Yes	Yes	Yes	Yes	Died	38	63
22	39	M	Caucasian	Yes	IVc	Positive	TPS 55%	Lorlatinib	No	No	No	No	No	Alive	1	1
23	61	F	Caucasian	Yes	IA	Positive	20%	Alectinib	No	Yes	No	yes	No	Alive	23	110

Figure 1 - 1224

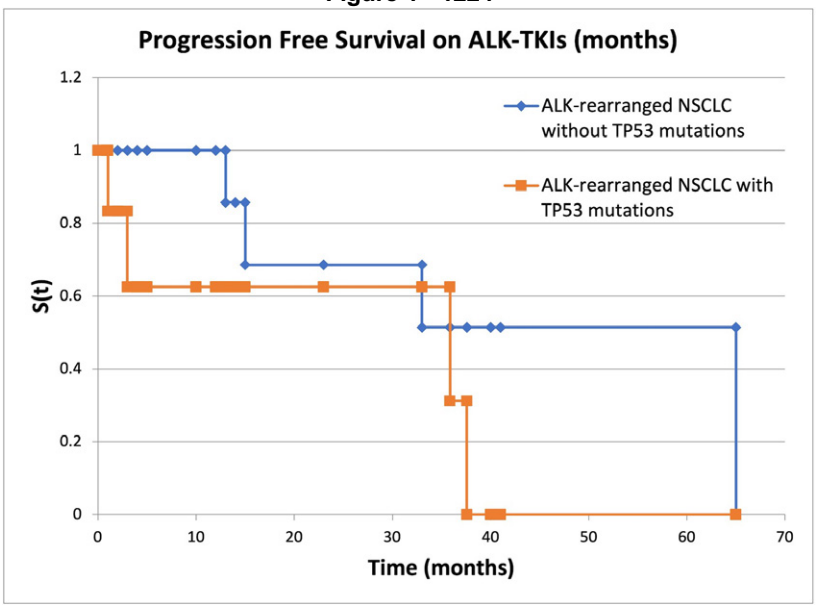

Conclusions: In our cohort, *ALK*-rearrangements were predominantly observed in adenocarcinoma in non-smokers in younger age group. Patients with concurrent *TP53* mutations had worse PFS with 57% patients manifesting resistance to first line TKIs. Testing for *TP53* in patients with *ALK*-rearranged NSCLC and repeating mutational analysis in case of disease progression on *ALK*-TKIs may be beneficial in planning treatment options and improving survival.

1225 Molecular Profiling Is Superior to Morphology to Determine Relatedness of Multiple Lung Squamous Cell Carcinomas

Marie-Pier Montminy[1], David Hwang[2], Bruce Johnson[3], Lynette Sholl[4], Steven Mentzer[1]
[1]Brigham and Women's Hospital, Boston, MA, [2]Brigham and Women's Hospital, MA, [3]Dana-Farber Cancer Institute, Boston, MA, [4]Harvard Medical School, Boston, MA

Disclosures: Marie-Pier Montminy: None; David Hwang: None; Bruce Johnson: *Consultant*, Novartis, Boston Pharmaceuticals, Checkpoint Therapeutics, Daiichi Sankyo, Foundation Medicine, G1 Therapeutics, Genentech, GlaxoSmithKline, GlaxoSmithKline, Hengrui, Janssen Scientific Affairs, Lilly, Jazz Pharmaceuticals; *Grant or Research Support*, Novartis, Cannon Medical Systems; *Employee*, Dana-Farber Cancer Institute; Lynette Sholl: *Consultant*, Genentech, Lilly; *Grant or Research Support*, Genentech; Steven Mentzer: None

Background: Patients with two synchronous or metachronous squamous cell carcinomas of the lung (LUSC) can be diagnosed with two independent primary tumors (IPT) or intrapulmonary metastases (IPM), but the accuracy of this distinction based on clinical and pathologic grounds remains untested.

Design: 1255 patients had lung resection or biopsy for squamous cell carcinoma at our institution between 2015-2021; 36 patients with suspected or confirmed squamous carcinoma metastases to the lung from other sites were excluded from the analyses. Of the 1219 remaining patients, we found 50 (4%) that had more than one sampled tumor. Of these 50 patients, 11 pairs had panel next generation sequencing performed on both tumors, all of which had explicit comments in the clinical record regarding relatedness on pathologic grounds. Tumors were classified as molecularly related based on shared versus independent somatic alterations including single nucleotide variants, copy changes, and structural variants. The molecular classification was compared with the original pathologic and clinical impression of tumor relatedness.

Results: Five patients were initially diagnosed with IPT, five with IPM and one was uncertain. Based on molecular classification, 10 of 11 pairs represented independent primary tumors. Only one pair of tumors was molecularly related, in a patient with contralateral tumors presenting 44 months apart. Four (36%) out of 11 were correctly diagnosed by morphology and all were IPT cases. Consequently, 6 (55%) patients were misclassified. Molecular classification downstaged 5 patients (45%) and upstaged 1 patient (9%). In one case, the pathologist could not commit to tumor relatedness based on morphologic features; molecularly, these were IPT.

Pt	Site	Interval (month)	Highest stage by morphology	molecular	Stage correlation
1	RUL RLL	0	T4	T2b	0
2	LLL LUL	57	T4	T1a	0
3	LUL RUL	15	M1a	T1a	0
4	RLL LUL	9	M1a	T1a	0
5	LUL LUL	0	T2a	T2a	1
6	RLL LLL	44	T1b	M1a	0
7	RLL LLL	24	T1b	T1b	1
8	RUL LLL	2	Uncertain	T1b	NA
9	LUL RLL	9	T1a	T1a	1
10	RLL RUL	0	T3	T3	1
11	RUL RLL	0	T4	T1c	0

Conclusions: Multifocal LUSC appears to be relatively uncommon, and when detected typically represents independent primaries based on molecular classification. Our data demonstrate the limitations of synchronous or metachronous LUSC classification based on tumor morphology alone. Our limited experience suggests that sequencing better establishes the relationships of multiple LUSCs and that histologic evaluation as applied in clinical practice is often inaccurate.

1226 Pulmonary Pathology in Post-Acute COVID-19 Syndrome Treated with Bilateral Orthotopic Lung Transplantation

Samira Mortazavi[1], Alberto Marchevsky[2], Mariza De Peralta-Venturina[1]
[1]Cedars-Sinai Medical Center, Los Angeles, CA, [2]Cedars-Sinai Medical Center, West Hollywood, CA

Disclosures: Samira Mortazavi: None; Alberto Marchevsky: None; Mariza De Peralta-Venturina: None

Background: Lung transplantation has been performed as a life-saving treatment in a small number of post-acute COVID- 19 patients who develop severe pulmonary insufficiency. We report a detailed clinicopathologic analysis of 7 such patients that underwent bilateral orthotopic lung transplantation at our institution.

Design: The time interval between initial diagnosis of Covid-19 infection and lung transplantation, other clinical findings, and imaging features of the 7 patients were reviewed. The pathologic findings in the 14 explants were assessed and histologic abnormalities were classified into parenchymal, airway and vascular changes. The extent (1+-to 4+ based on # of slides with the abnormality) and severity (mild, moderate, marked) of histologic abnormalities were recorded.

Results: Patients ranged in age from 34 to 55 years old and were transplanted at 10.4 to 24 weeks after initial diagnosis of Covid-19 (median 16 weeks). Six of these patients had been previously treated with ECMO for 82-145 days. Other clinical and imaging features are summarized in Table 1. All 14 explants showed diffuse marked interstitial fibrosis with a nonspecific interstitial pneumonia (NSIP) pattern. Other pathologic changes included extensive alveolar hemosiderosis (n=7 patients); prominent peribronchial metaplasia (n=7); focal multinucleated giant cells in either the parenchyma, vascular wall or peribronchiolar location (n=6); focal thrombosis involving medium to large vessels (n=4) and lung cysts associated with delicate calcifications and multinucleated giant cells (n=1). No diffuse alveolar damage changes (DAD) or vasculitis were identified.

	Case 1	Case 2	Case 3	Case 4	Case 5	Case 6	Case 7
Clinical Findings							
Age	35	40	34	51	52	55	37
Sex	F	M	F	M	M	M	M
Race	Caucasian	Hispanic	Hispanic	Hispanic	Black	Hispanic	Hispanic
BMI	22.96	26.59	28.11	28.5	24.12	22.36	26.73
Comorbidities	pregnant 36 wks	Ramsay Hunt syndrome, hypertension	None	chronic deep venous thrombosis	drug/alcohol use	hypertension	obesity, fatty liver
Vaccination status	unknown	unknown	unknown	unknown	unvaccinated	unknown	unvaccinated
Covid treatment received	convalescent plasma, Remdesivir	steroid, Remdesivir	steroid	steroid Remdesivir, tocilluzimab	steroid, Remdesivir	steroid, Remdesivir, tociluzimab	steroid, Remdesivir, tociluzimab
Chest CT prior to transpliant	consolidation, ground glass opacity (GGO), dilated main PC	RLL consolidation	diffuse GGO and reticulonodular densities	diffuse GGO with few subpleural cysts	extensive consolidation both lungs	Increase diffuse peribronchovascular fibrosis; enlarged main PA	extensive bilateral pulmonary fibrosis; superimposed cavitary disease bilateral
Days on VV ECMO prior to transpliant	119 days	82 days	87 days	145 days	104 days	122 days	not applicable
Time from initial positive Covid test to lung transpliant	18.7 wks	14.3 wks	15.8 wks	24 wks	13.3 wks	20.4 wks	10.4 wks
Covid related complications prior to transpliant	stroke, thrombosis, left forearm compartment syndrome	bacteremia	multiple infections	multiple brain hemorrhages	bilateral pneumothorax and pneumomediastinum ; left subsegmental PE	stroke, Candida sepsis; large RV mass ? Endocarditis	none
Complications during transpliant surgery	extensive coagulopathy	Intraoperative bleeding	none	Intraoperative bleeding	Intraoperative bleeding	Intraoperative bleeding	none
Clinical follow up (days after transpliant)	Alive (158 days)	Alive (149 days)	Alive (67 days)	Alive (71 days)	Alive (54 days)	Dead (13 days)	Alive (10 days)
Pathologic Findings							
Interstitial fibrosis	4+ marked	4+ marked	4+ marked	4+ marked	4+ marked	4+ marked	4+ marked
NSIP-pattern of fibrosis	3+	3+	3+	3+	3+	3+	3+
Interstitial inflammation	2+ mild	4+ marked	minimal	minimal	minimal	moderate	moderate
Alveolar hemosiderosis	3+ mild	3+ mild	4+ marked	4+ marked	1+	3+ mild	3+ mild
Acute inflammation	0	2+	0	0	0	1+	cavitary abscess
Organizing pneumonia	0	2+	1+	0	1+	0	2+
Foreign material possible aspiration pneumonia	0	1+	0	0	1+	0	0
Focal alveolar fibrin	1+	1+	2+	2+	0	2+	0
Microscopic honeycombing	1+	0	0	1+	0	1+	0
Multinucleated giant cells	1+ peribronchial	2+ within vascular wall	2+ peribronchial	1+ associated with subpleural cyst	2+ intra-alveolar	0	3+ associated with calcification and cystic change
Acute bronchiolitis	0	3+	0	0	1+ with intrabronchial foreign material	4+ marked	0
Peribronchial metaplasia	3+	3+	4+ moderate	4+	3+ mild	4+ marked	0
Mucoid impaction	4+	0	0	0	0	1+	0
Bronchiolization of alveoli	0	0	2+	0	3+	1+	0
Obliterative bronchiolitis	1+	0	1+	0	1+	0	0
Thrombosis, large to medium vessels	1+	0	0	0	2+	3+	1+
Obliterative thrombosis, small vessels	1+	0	1+	0	0	1+	0
Vasculitis	0	0	0	0	0	0	0
Chronic pleuritis with dense adhesions	present	present	present	0	present	present	present

Figure 1 - 1226

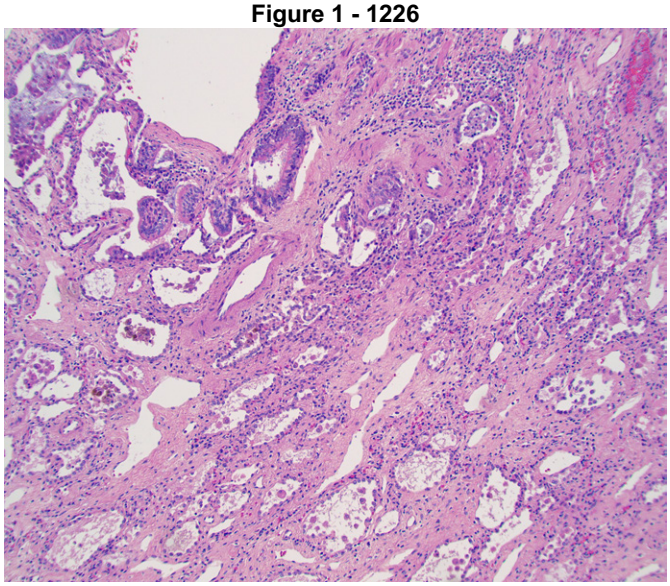

Figure 2 - 1226

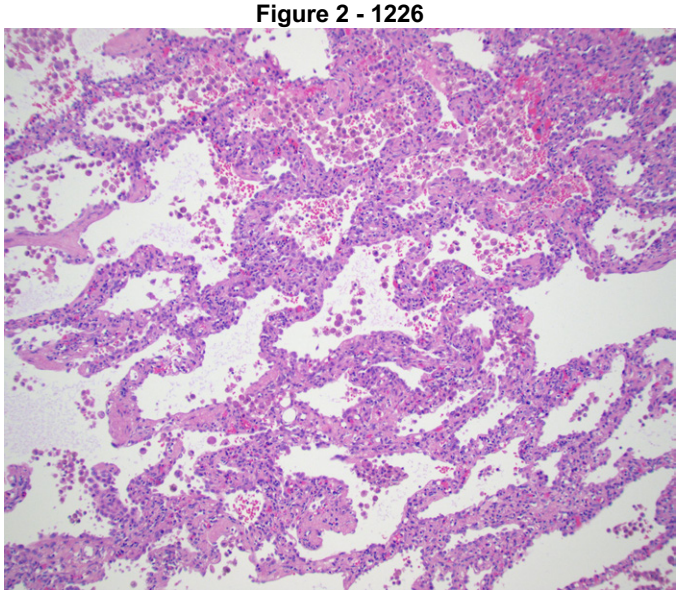

Conclusions: Lung explants from patients with post-acute COVID-19 syndrome show severe NSIP pattern of fibrosis and other pathologic changes that do not resemble the extensive fibrotic changes resulting from organizing phase of DAD or the extensive vascular changes seen in patients dying during the acute or subacute phases of COVID-19 infection. Further studies with lung biopsies are needed to understand the mechanism of fibrosis in post-acute COVID-19 syndrome and identify individuals who are likely to develop severe pulmonary fibrosis requiring lung transplantation.

1227 Concurrent STK11 and TP53 Mutations Correlate with a Unique Morphological Phenotype and Clinical Stage in Lung Adenocarcinomas

Selvaraj Muthusamy[1], Patrick Memari[2], Elizabeth Barrie[2], Vernell Williamson[3], Andrea Ferreira-Gonzalez[3], Raghavendra Pillappa[4], Valentina Robila[5]

[1]VCU School of Medicine, Richmond, VA, [2]VCU Health, Richmond, VA, [3]Virginia Commonwealth University, Richmond, VA, [4]VCU Health System, Richmond, VA, [5]Virginia Commonwealth University Health System, Richmond, VA

Disclosures: Selvaraj Muthusamy: None; Patrick Memari: None; Elizabeth Barrie: None; Vernell Williamson: None; Andrea Ferreira-Gonzalez: None; Raghavendra Pillappa: None; Valentina Robila: None

Background: Development of selective inhibitors targeting oncogenic driver mutations and immune checkpoint inhibitors have changed the treatment approach and prognosis of lung adenocarcinomas. Clinical and morphological features associated with common targetable driver mutations involving *EGFR, KRAS, ALK* and *ROS1* have been investigated. However, there is a relative paucity of literature describing the histologic correlates and clinical behavior of cancers harboring relatively less frequent driver mutations.

Design: We performed a retrospective study to correlate gain of function mutations involving *PIK3CA, STK11,* and *BRAF* with histological patterns, PD-L1 expression, and tumor stage. A total of 157 lung adenocarcinoma with results from an NGS assay targeting 161 genes were analyzed and 30 cases harboring *PIK3CA, STK11,* and *BRAF* mutations were selected. The corresponding slides of surgical resections (20 cases) and biopsies (10 cases) were reviewed for histological patterns, with emphasis on poorly differentiated morphologies, including solid and complex glandular architecture, and PD-L1 (TPS) tested with the 22c3 (Dako) antibody. The tumor stage was determined using the surgical outcome or review of clinical and radiological data.

Results: In our cohort, the aggregate frequency of *PIK3CA, STK11, BRAF* mutations is approximately 19%. Nineteen cases with *STK11* mutations were identified, often co-existing with mutations in *KRAS* or *TP53* (Table 1). In cases with *STK11* mutations, the presence of *KRAS* and *TP53* mutations were mutually exclusive. Of these, cases with concurrent *TP53* mutations had a significantly higher association with poorly differentiated morphologic patterns compared with cases harboring concurrent *KRAS* mutations or mutations in *STK11* alone ($p<0.05$). In addition, cases with *STK11* and *TP53* mutations demonstrated more advanced tumor stage (66%) and higher PD-L1 expression, while the remaining cases were predominantly low stage and negative for PD-L1. *PIK3CA* mutations were associated with either *EGFR* or *TP53* mutations, and well differentiated morphological patterns. *BRAF* mutations, some encountered along with *KRAS*, correlated with low stage, favorable morphology, and PD-L1 expression in 43% cases.

Mutations	No. Cases	Poorly differentiated morphology	Low stage (pT1 or pT2)	High stage (at least pT3)	PD-L1 negative (<1%)	PD-L1 positive (≥1%)
STK11; KRAS	8	1 (12%)*	6 (75%)	2 (25%)	8 (100%)	0
STK11; TP53	9	7 (78%)	3 (33%)	6 (66%)	4 (45%)	5 (55%)
STK11	2	0	2 (100%)	0	2 (100)	0
PIK3CA; EGFR; TP53	1	0	1 (100%)	0	0	1 (100%)**
PIK3CA; EGFR	1	0	0	1 (100%)	1 (100%)	0
PIK3CA; TP53	2	0	1 (50%)	1 (50%)	1 (50%)	1 (50%)
BRAF; KRAS; TP53	1	1 (100%)	1 (100%)	0	0	1 (100%)**
BRAF; KRAS	1	0	0	1 (100%)	1 (100%)	0
BRAF	5	0	4 (80%)	1 (20%)	3 (60%)	2 (40%)

*Only minor poorly differentiated solid component; ** PD-L1 >50%

Conclusions: Despite the small sample size, the current cohort indicates that tumors harboring mutations involving *STK11* and *TP53* are associated with unfavorable morphology and high TNM stage. In addition, these tumors may benefit from treatment with immunotherapy.

1228 Role of Activating KRAS Mutations in the Pathogenesis of Type 1 and Type 3 CPAMs

Nya Nelson[1], Feng Xu[1], Prashant Chandrasekaran[1], David Frank[1], Marilyn Li[1], William Peranteau[1], Jenny Pogoriler[1]
[1]The Children's Hospital of Philadelphia, Philadelphia, PA

Disclosures: Nya Nelson: None; Feng Xu: None; Prashant Chandrasekaran: None; David Frank: None; Marilyn Li: None; William Peranteau: None; Jenny Pogoriler: None

Background: Congenital pulmonary airway malformations (CPAMs) have been hypothesized to arise secondary to bronchial atresia during development. The data is most compelling for type 2 CPAMs but is less well established for other types, and rare CPAMs are reported in mosaic genetic disorders. We and others have shown in small series that a subset of type 1 CPAMs harbor *KRAS* mutations in mucinous and non-mucinous tissue. To further evaluate the role of these mutations in pathogenesis, we correlated *KRAS* sequencing results with histologic features in a large cohort.

Design: Morphologic features were evaluated blinded to mutation status. Regions of interest were enriched via macrodissection of FFPE, DNA was extracted, and exon 2 of *KRAS* was amplified. PCR products were Sanger sequenced and analyzed using Mutation Surveyor (SoftGenetics,PA). BaseScope mutation-specific in situ hybridization was performed.

Results: We present the largest series of type 1 and type 3 CPAMs ever characterized. We identified activating *KRAS* mutations (including 2 mutations previously unpublished in CPAMs) in non-mucinous tissue in 81/89 total cases (91%). These included all cases with mucinous foci (62) and 19/27 cases without mucinous foci. Of the 8 WT cases, 2 were in patients with mosaic genetic disorders in other genes (previously published). Mutation distribution was confirmed by in situ hybridization. In the case tested (Fig 1), mutant *KRAS* expression was identified in mucinous (Fig 2 yellow arrows) and non-mucinous (black arrows) epithelial cells. We also found that specific *KRAS* mutations strongly correlated with morphology (Table 1, p <0.0001). Finally, in contrast to type 1 and type 3 lesions, all type 2 CPAMs and all intrapulmonary bronchogenic cysts had WT *KRAS* exon 2 sequences.

Distribution of KRAS exon 2 mutation by cyst morphology (*not previously reported in CPAMs)

CPAM morphology	WT *KRAS*	*KRAS* p.G12D	*KRAS* p.G12V	*KRAS* p.G12R	*KRAS* p.G12C*	*KRAS* p.G10dup*
Type 1 (n= 58)	1 (2%)	48 (83%)	8 (14%)	0	1 (2%)	0
Type 3 (n=13)	6 (46%)	0	5 (38%)	0	1 (8%)	1 (8%)
Mixed type 1/3 (n= 18)	1 (6%)	5 (28%)	8 (44%)	4(22%)	0	0
Type 2 (n=18)	18 (100%)	0	0	0	0	0
Intrapulmonary bronchogenic cyst (n=10)	10 (100%)	0	0	0	0	0

Figure 1 - 1228

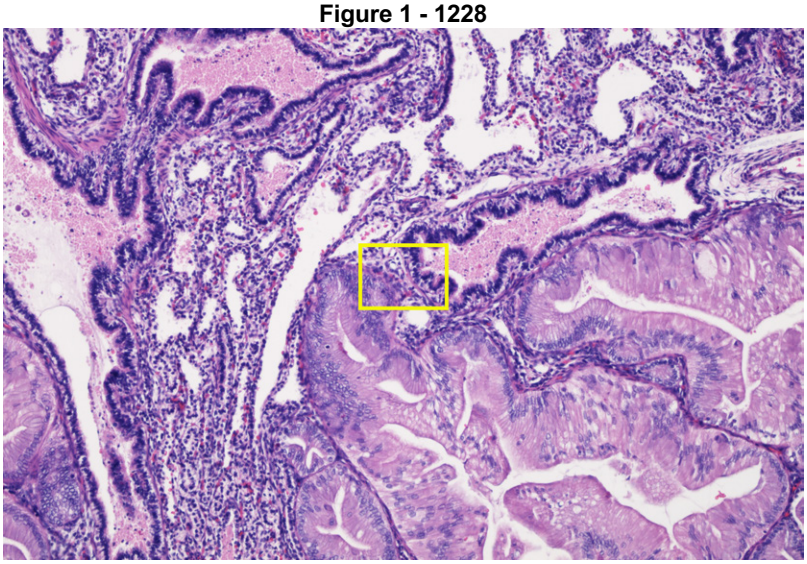

Figure 2 - 1228

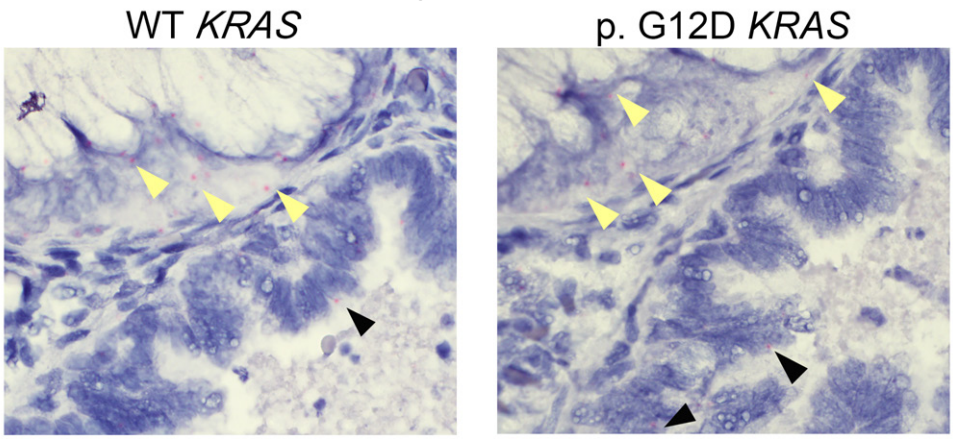

Conclusions: Type 1 and 3 CPAMs are overwhelmingly associated with activating *KRAS* mutations. Type 1 morphology is strongly associated with the highly activating p.G12D mutation. In conjunction with published mouse data showing cystic lung disease with embryonic expression of *KRAS* p.G12D, these findings support the hypothesis that most type 1 and type 3 CPAMs arise secondary to somatic *KRAS* mutations occurring early in development: they therefore represent a limited form of mosaicism. Rarely, other driver mutations may be identified. Importantly, these findings suggest that asymptomatic cases and those without mucinous clusters should be completely resected. In contrast to type 1 and type 3 lesions, *KRAS* mutations were not detected in type 2 CPAMs or bronchogenic cysts, suggesting a distinct pathogenesis in keeping with the described bronchial atresia sequence.

1229 Histopathologic and Molecular Findings from Cryobiopsy Transbronchial Tissues for Interstitial Lung Disease

Chinelo Onyenekwu[1], Yuri Sheinin[1]
[1]Medical College of Wisconsin, Milwaukee, WI

Disclosures: Chinelo Onyenekwu: None; Yuri Sheinin: None

Background: Interstitial lung disease (ILD) represents a heterogeneous class of diseases affecting the lung parenchyma, characterized by varying histopathologic presentations. Transbronchial biopsy using a cryoprobe, otherwise known as cryobiopsy is a technique that is gaining popularity for the definitive diagnosis of ILD through histologic examination due to its acclaimed provision of larger quantity and better-preserved tissue than traditional transbronchial biopsy. We examined cryobiopsy tissues over

a thirteen-month period to determine the definitive diagnoses that comprise ILD based on clinic-radiologic impression. We compared the findings on microscopic examination to results of genomic test for idiopathic pulmonary fibrosis/usual interstitial pneumonitis (IPF/UIP).

Design: This was a retrospective review of cryobiopsy specimens sent for pathology examination for ILD. Data on histologic findings were retrieved from the laboratory information system. Clinical information including radiologic findings, and results of molecular test for IPF (Envisia) where available, were extracted from the patients' charts onto a Microsoft excel sheet. The final pathological diagnoses were categorized as specific ILD entities: hypersensitivity pneumonitis (HP), non-specific interstitial pneumonitis (NSIP) or connective tissue disease associated interstitial lung disease (CTD-ILD); other (comprised of non-ILD entities); and mixed picture (in cases of overlapping features warranting differential diagnoses that cut across ILD and Non-ILD entities). The molecular test results were compared to the pathological diagnoses.

Results: Fifty patients were reviewed. Two biopsies (4.0%) did not allow adequate evaluation of interstitial fibrosis. Non-ILD diagnoses constituted 42.0% of the cases (21/50); 11 cases (22.0%) showed a mixed picture (figure 1), of the 17 exclusive ILD diagnoses, HP was responsible for nearly 60.0% (10/17) while 5 cases (29.4%) had a final pathology diagnosis of UIP.

3 of 15 (20.0%) cases of ILD had genomic testing were positive for UIP and all three had UIP as a diagnostic consideration on histological examination (figure 2).

Figure 1 - 1229

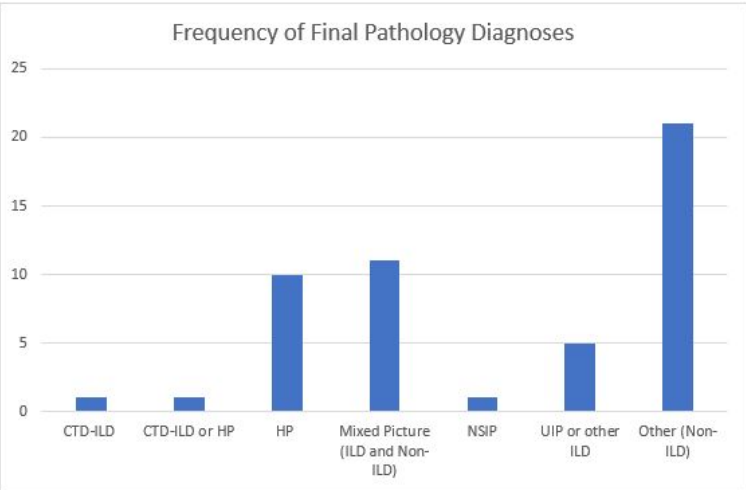

Figure 1: Distribution of Final Pathology Diagnoses of Cases Examined for Interstitial Lung Disease. ILD: Interstitial lung disease; CTD-ILD: Connective tissue associated interstitial lung disease; HP: Hypersensitivity pneumonitis; NSIP: Nonspecific interstitial pneumonitis, UIP: Usual interstitial pneumonitis

Figure 2 - 1229

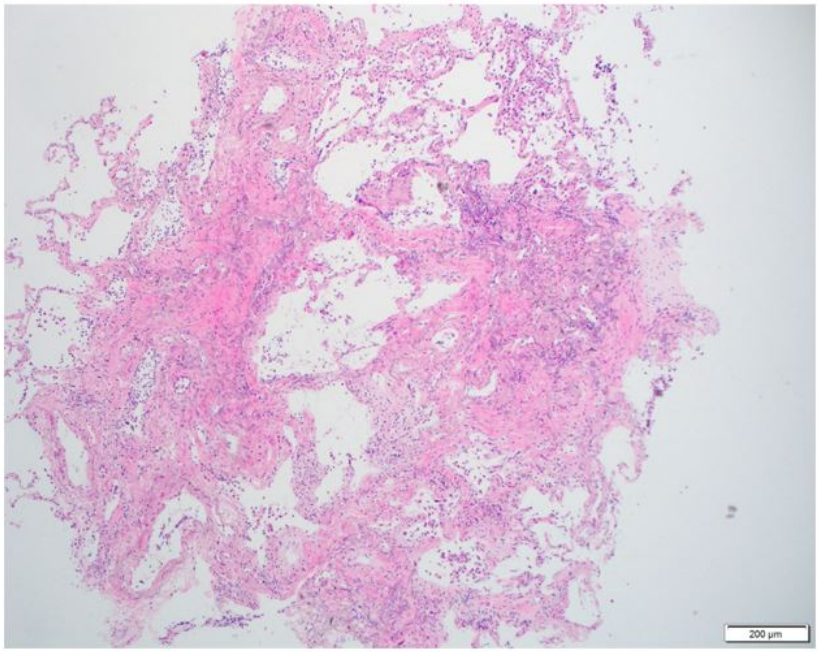

Figure 2: Hematoxylin & Eosin stain (magnification x40) of a representative case considered for UIP on histopathologic examination and positive for UIP by Envisia genomic test.

Conclusions: Cryobiopsy provides sufficient tissue for definitive diagnosis of parenchymal lung diseases in most cases. Non-ILD entities constitute nearly half of our specimens evaluated for ILD. Less than one-third of our patients undergo genomic testing for definitive UIP diagnosis. Envisia genomic test has a high negative predictive value for UIP.

1230 Evidence for Continuity of Interstitial Spaces Within and Outside the Human Lung

Jeffrey Ordner[1], Luis Chiriboga[2], Briana Zeck[1], Mariam Majd[3], Fang Zhou[4], Andre Moreira[1], Jane Ko[1], Rami Imam[5], Rebecca Wells[6], Neil Theise[7], Navneet Narula[1]

[1]NYU Langone Health, New York, NY, [2]New York University, New York, NY, [3]Galloway, NJ, [4]NYU School of Medicine, New York, NY, [5]New York University Langone Health, New York, NY, [6]Perelman School of Medicine at the University of Pennsylvania, Philadelphia, PA, [7]NYU Grossman School of Medicine, New York, NY

Disclosures: Jeffrey Ordner: None; Luis Chiriboga: None; Briana Zeck: None; Mariam Majd: None; Fang Zhou: *Stock Ownership*, MRNA, DOCS; Andre Moreira: *Consultant*, Olympus, Roche; Jane Ko: None; Rami Imam: None; Rebecca Wells: None; Neil Theise: None; Navneet Narula: None

Background: Interstitial spaces (IS) within collagenous tissue are filled by hyaluronic acid (HA) and intermittently lined by CD34+/vimentin+ interstitial lining cells (ILC). In human tissues (skin/subcutaneous fascia, colon/mesenteric fascia, vascular adventitia, perineurium), IS have been shown to be continuous across organ boundaries (Cenaj et al. 2020, Comm Bio). Methods for showing continuity included HA staining and assessment of tattoo pigment. We now use HA and anthracotic pigment particles (APP) to assess the continuity of IS in the human lung.

Design: Formalin fixed paraffin embedded tissue from lobectomy specimens from male/female patients (n=9) were examined. The IS of the different anatomic compartments of the human lung (around bronchovascular bundles including bronchi and bronchioles, within alveolar walls, and in interlobular septa and visceral pleura) were examined by chromogenic multiplex staining with hyaluronic acid binding protein (HABP; brown) and immunohistochemistry (IHC) for vimentin and CD34 (magenta and teal, respectively; overlap: navy blue) (Discovery Ultra, Ventana).

Extracellular APP (n=40) in IS of each compartment (n=5) in lungs from 9 patients were examined. CD68 and vimentin IHC were utilized to exclude pigment within macrophages and ILC. APP diameters were measured digitally (Olympus CellSens software). Statistical analysis for difference in mean APP size between compartments was performed (R statistics).

Results: Continuity of IS of all lung compartments (Fig 1) and also of perivascular adventitia and perineurium was confirmed by HABP staining. Extracellular APP were identified within interstitial spaces of each lung compartment. Statistical analyses were two tailed; p-values are displayed in Table 1. The smallest APP were found within IS of alveolar septa, with increasingly larger aggregates in directly continuous IS compartments (Fig 2). Intracellular APP were most prominently seen in macrophages and less so in ILC.

Table 1. Anthracotic particle size differences between lung anatomic compartments.

Dependent variable	Mean	Standard Deviation	Independent variable		p-value
Bronchus and vessels at hilum	2.810	0.980	Alveolar wall		1.56×10^{-123}
			Interlobular septum		1.00×10^{-4}
			Bronchiole and vessel in secondary lobule		7.14×10^{-8}
			Visceral pleura		3.70×10^{-66}
Alveolar wall	0.966	0.265	Interlobular septum		3.19×10^{-143}
			Bronchiole and vessel in secondary lobule		1.45×10^{-149}
			Visceral pleura		7.25×10^{-63}
Interlobular septum	2.583	0.757	Bronchiole and vessel in secondary lobule		3.17×10^{-2}
			Visceral pleura		2.39×10^{-64}
Bronchiole and vessel in secondary lobule	2.468	0.677	Visceral pleura		1.79×10^{-58}
Visceral pleura	1.628	0.591			

Figure 1 - 1230

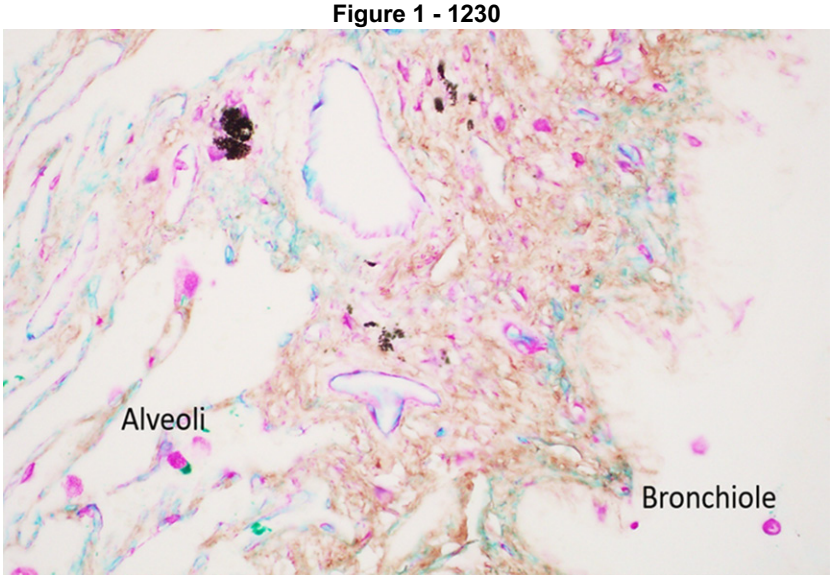

Figure 2 - 1230

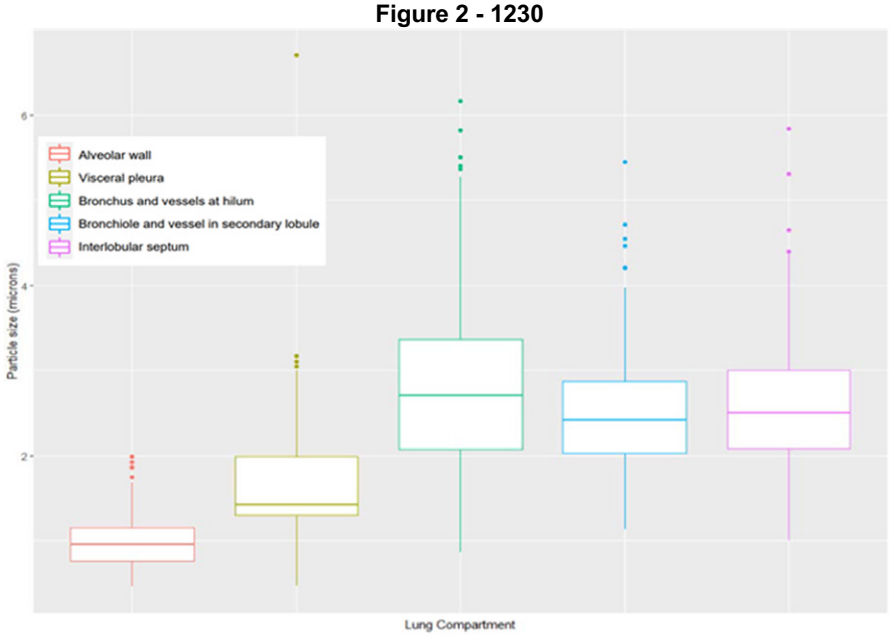

Conclusions: Staining of HA in human lung tissues shows that pulmonary IS are neither virtual nor artefactual and are continuous between all lung compartments. Also, via continuity with adventitia and perineurium, they link to a body-wide IS network. The size and distribution of APP support these interpretations. These findings have implications for pulmonary clearance of inhaled particles and organisms via the IS, as well as for understanding other lung pathologies such as tumor spread and interstitial lung diseases.

1231 Validation and Comprehensive Analysis of T790M mutation in Liquid Biopsy by Droplet Digital PCR

Trupti Pai[1], Omshree Shetty[2], Pradnya Joshi[2], Mamta Gurav[3], Dipika Dhanavade[2], Sangeeta Desai[3]
[1]Vashi, India, [2]Tata Memorial Hospital, Mumbai, India, [3]Tata Memorial Centre, Mumbai, India

Disclosures: Trupti Pai: None; Omshree Shetty: None; Pradnya Joshi: None; Mamta Gurav: None; Dipika Dhanavade: None; Sangeeta Desai: None

Background: Patients with non-small cell lung cancer (NSCLC) harboring epidermal growth factor receptor (EGFR) mutations often progress during treatment with EGFR-tyrosine kinase inhibitors (TKIs). TKI therapy requires a sensitive and accurate assay for the detection of drug-resistant mutations in patients undergoing TKI-based targeted therapy. The presence of T790M mutation in EGFR accounts for nearly 50% of the acquired resistance to EGFR-TKIs. Droplet digital polymerase chain reaction (ddPCR) and amplification refractory mutation system (ARMS)-PCR are routinely applied for detection of EGFR mutations, including T790M, which is associated with TKI sensitivity of which the former is a highly sensitive detection method with the capability of absolute quantification. We aimed to validate and compare the efficiency of ddPCR and ARMS-PCR in detecting T790M from the blood samples in NSCLC cases, which progressed on TKI to evaluate its applicability in diagnostic settings.

Design: For the initial validation of T790M mutation on blood samples, detection by ddPCR was performed using 2,3 and 5 ul template concentration, and satisfactory results were obtained with the 3ul template concentration. Subsequently, ctDNA was extracted in a total of 27 cases of NSCLC, which progressed on EGFR TKI. All the samples were subjected to ddPCR using Bio-Rad ddPCR™ Supermix for Probes and T790M Mutant and Wild Type Probes along with ctDNA template. The assay was performed using Bio-Rad QX200™ Droplet Generator and Bio-Rad C1000 Touch™ Thermal Cycler. The data was analyzed on Bio-Rad QuantaSoft™ Software. The results of the ddPCR were compared with the Real-Time PCR (RT-PCR) data for the concordance rates.

Results: Of 27 cases, T790M mutation was detected in 14 cases by ddPCR (51.8%). Concordant results for T790M mutation by both the platforms were obtained in 18 cases [66.7% (5 cases were positive and 13 cases were negative by both the platforms)]. In

all 9 discordant cases (Table), T790M mutation was detected by ddPCR, while were not detected by RT-PCR. The mutant copies ranged between 0.22-36.1/ul and the wild type copies were in the range of 21-303 copies/ul in these discordant cases.

Samples	ddPCR	Real time PCR	Concordance			
	Mutant (Copies/µl)	Wild Type (Copies/µl)	Result	Ct	Result	
Sample 5	5.2	32	Positive	-	Negative	No
Sample 8	14.1	40.9	Positive	-	Negative	No
Sample 9	8.1	303	Positive	-	Negative	No
Sample 12	4.7	21.2	Positive	-	Negative	No
Sample 14	0.49	32.4	Positive	-	Negative	No
Sample 17	23.8	146	Positive	-	Negative	No
Sample 20	36.1	138	Positive	-	Negative	No
Sample 21	20.8	224	Positive	-	Negative	No
Sample 27	0.48	No Call	Positive	-	Negative	No

Conclusions: DDPCR is a very sensitive assay and can satisfy the clinical need of detecting EGFR T790M mutations, even at extremely low allele frequency and can be used as diagnostic tool on liquid biopsy. It can be used as a monitoring strategy to evaluate the development of drug resistance, and therapeutic effects on disease progression.

1232 KRAS G12C – STK11 Co-Mutated Lung Adenocarcinomas. Are There New Hopes for Targeted Immunotherapy?

Radu Pirlog[1], Nicolas Piton[2], Florent Marguet[3], Aude Lamy[4], Jean-Christophe Sabourin[4]
[1]University of Medicine and Pharmacy, Cluj-Napoca, Romania, [2]Rouen University Hospital, [3]CHU de Rouen, Rouen, France, [4]Rouen University Hospital, Rouen, France

Disclosures: Radu Pirlog: None; Nicolas Piton: None; Florent Marguet: None; Aude Lamy: None; Jean-Christophe Sabourin: *Consultant*, AstraZeneca, Servier, BMS, MSD, AMGEN

Background: A new molecular target in lung adenocarcinomas (LUADs) is represented by the glycine-to-cysteine mutation at position 12, codon 34 (*KRAS G12C)* that is present in approximatively 13% of cases.

In 2021 two molecules were approved that target KRAS G12C mutated LUAD, Sotorasib, and Adagrasib, showing a partial response rate of 33,9% for Sotorasib and an overall response of 45% for Adagrasib. Results are promising, but there is still a large group of KRAS G12C LUAD that don't benefit from these molecules. Therefore, there is a need for a better characterization of the molecular landscape of these tumors in order to improve patient selection. A possible subgroup of responders is represented by the co-mutated KRAS G12C – STK11 LUADs that showed promising results in clinical trials.

Design: We aim to characterize a new molecular subtype of *KRAS G12C* LUADs that is also harboring a mutation in the *STK11* gene using classic histology, immunohistochemistry, and next-generation sequencing NGS). Samples from 51 patients diagnosed through NGS with a co-mutation KRAS G12C and STK11 were included in our study. Each case was individually assessed by two pathologists for morphological parameters: histology, tumor cellularity, nuclear atypia, presence of necrosis, and tumor-infiltrating lymphocytes (TIL). Routine diagnostic immunohistochemistry was performed on a BENCHMARK ULTRA Ventana-Roche.

NGS was performed on a MiSeq sequencer (Illumina©) and the gene library was prepared with the kit Tumor Hotspot MASTR Plus (Multiplicom®).

Results: The mean age was 62,2-year-old. The sex distribution included 33,33% males and 64% females. The main histology was acinar in 39,21% and no other specified (NOS) in 21,5% of samples. TILs were evaluated as high in 39,51% of cases and moderate in 27,45% of cases. Necrosis was present in 23,52% and nuclear atypia in 31,37% of samples. TTF1 immunohistochemistry was positive in 64,51% of samples and PD-L1 was positive in 19,6% of samples. NGS analysis identified additional mutations in multiple genes including *ALK, CDK2NA, CTNNB1, DDR2, FGFR3, MET, PIK3CA*.

Conclusions: We realized a complex characterization of a specific subgroup of KRAS G12C - STK11 co-mutated LAUDs that could have an improved response to KRAS G12C inhibitors. This result is of high interest as previously STK11 mutated LUADs were associated with a poor prognosis, reduced PD-L1 positivity, and resistance to anti-PD1 / anti-PD-L1 blockade.

1233 Tumor Microenvironment Characterization as a Source of Novel Molecular Biomarkers in Early-stage Lung Cancer

Radu Pirlog[1], Ioana Rus[1], Paul Chiroi[1], Ancuta Jurj[1], Liviuta Budisan[1], Ioana Neagoe[1], Doinita Crisan[1], Jean-Christophe Sabourin[2], Ioana Berindan-Neagoe[1]
[1]University of Medicine and Pharmacy, Cluj-Napoca, Romania, [2]Rouen University Hospital, Rouen, France

Disclosures: Radu Pirlog: None; Ioana Rus: None; Paul Chiroi: None; Ancuta Jurj: None; Liviuta Budisan: None; Ioana Neagoe: None; Doinita Crisan: None; Jean-Christophe Sabourin: *Consultant*, AstraZeneca, Servier, BMS, MSD, AMGEN; Ioana Berindan-Neagoe: None

Background: Recent advances in cancer biology and genomics research allowed in-depth characterization of lung cancers (LC) revealing a plethora of mutations like EGFR, ALK, KRAS that can be targeted with specific molecules. Of major importance but less investigated in the early stages is the role of the tumor microenvironment (TME) that could be used to identify new potential biomarkers for diagnostic and therapy. The discovery of small noncoding RNAs opens a new direction in the investigation of TME roles in tumor evolution. MicroRNAs are important regulators of oncogenic processes and can modulate each hallmark of cancer including the response to therapy.

Design: We investigated the TME in a subset of 51 early-stage LC patients in a quest of identifying novel LC-specific biomarkers. Patients were diagnosed between 2013-2016. Classic immunohistochemistry (IHC) for diagnosis was used, for the TME characterization, we investigated E-Cadherin, TP53 as markers for tumor cells and CD4, and CD8 for TME lymphocytes identification. CD4 and CD8 IHC were evaluated on a 5-level scale, separate for the intratumoral and peritumoral sectors. Based on these markers we performed a bioinformatics analysis (Figure 1) and 4 miRNAs (miR-29b, miR-205, miR-181a, and miR25) were selected for investigation.

Results: The mean age in our study group was 61 years. The morphological characteristics, TME particularities, and IHC distribution of the CD4 and CD8 tumor-infiltrating lymphocytes (TILs) in the stromal and intratumoral compartment are depicted in Table 1. The miRNAs expression analysis by qRT-PCR showed a down-regulation at the tumor level when comparing with adjacent normal tissue for tumor suppressor miRNAs miR-29b and miR-181a. The expression of tumor promoter miRNAs miR-205 and miR-25 was upregulated in the tumor (Figure 2).

Variable	Samples
Histology	22 Adenocarcinomas 21 Squamous cell carcinomas 8 Neuroendocrine tumors
Tumor Stage	T1a - 15 cases T1b - 9 cases T2a - 19 cases T2b - 8 cases
Intratumoral necrosis	Present - 39 cases Absent - 12 cases
Atypic nuclei	Present - 21 cases Absent - 30 cases
Peritumoral infiltrate	High – 18 cases Moderate – 23 cases Low – 10 cases
Intratumoral infiltrate	Moderate – 8 cases Low – 41 cases Absent – 2 cases
Tertiary lymphoid structures	Present - 38 cases Absent - 13 cases
Active germinative centers	Present - 25 cases Absent - 13 cases
E-cadherin IHC	Intense (3+) - 19 cases

	Moderate (2+) - 32 cases
P53 (IHC)	Positive - 23 cases Absent - 28 cases
Stromal CD4 TILs - IHC	Very high – 15 cases High – 29 cases Moderate - 4 cases Low – 3 cases
Intratumoral CD4 TILs - IHC	High – 3 cases Moderate – 1 case Low – 26 cases Absent – 21 cases
Stromal CD8 TILs - IHC	Very high – 1 case High – 14 cases Moderate - 17 cases Low – 17 cases Absent – 2 cases
Intratumoral CD8 TILs - IHC	Moderate – 8 cases Low – 28 cases Absent – 15 cases

Figure 1 - 1233

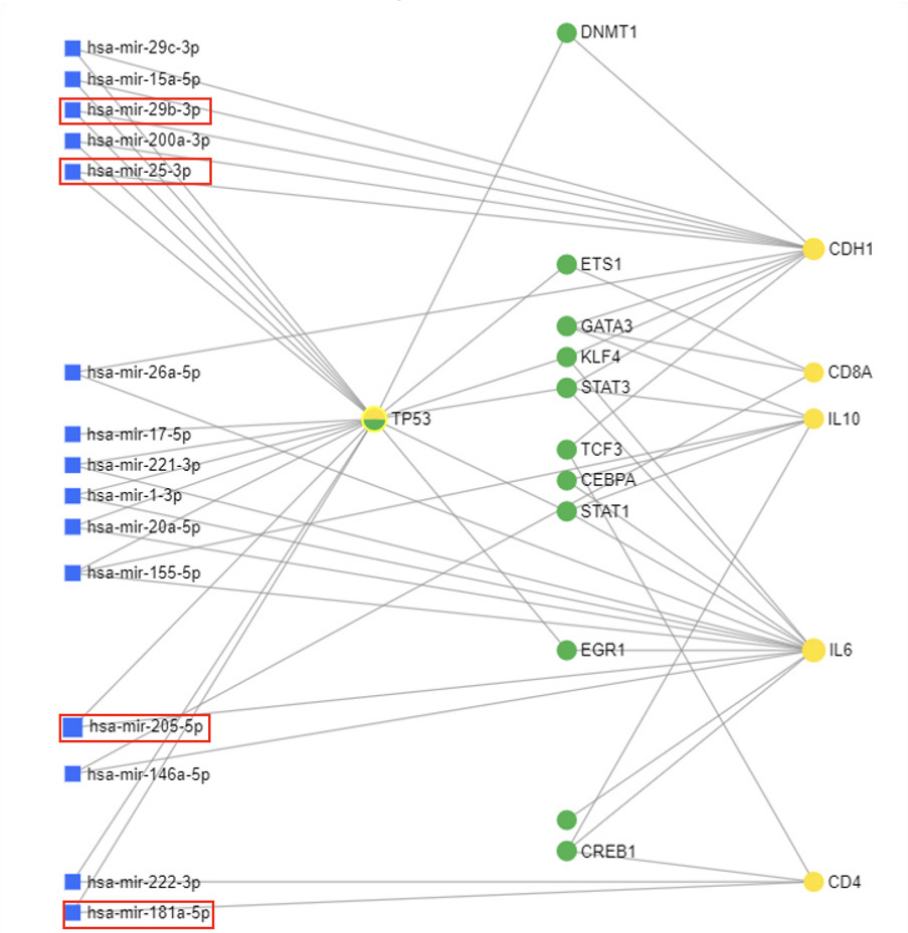

Figure 2 - 1233

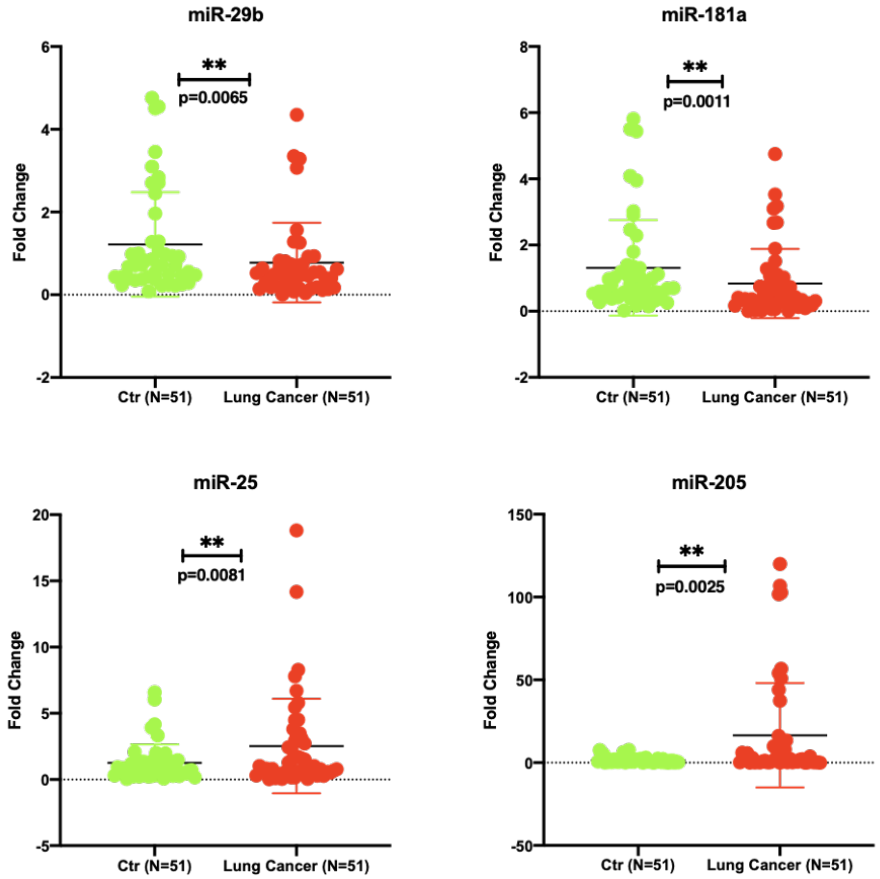

Conclusions: We present an in-depth characterization of the TME in a subset of early-stage LC. Our analysis pointed that these tumors are immunologic active with a moderate to high inflammatory TME in 80% of cases. The inflammatory infiltrate mainly is located in the stromal compartment where also the tertiary lymphoid structures were found in 74,5% of the cases. The main component of the TME is represented by CD4 lymphocytes. Moreover, based on the bioinformatics analysis we managed to validate 4 potential miRNAs that were dysregulated at the tumor level comparing with the adjacent normal tissue that can be further investigated as potential biomarkers for early-stage LC.

1234 Tumor Infiltrating CD8 Positive T Lymphocytes Estimation and Their Correlation with Progression Free Survival in Cancer Patients

Monika Roychowdhury[1], Maria Teresa Eyzaguirre Pellon[1], Lori Pai[1], David Yin[1]
[1]Tufts Medical Center, Boston, MA

Disclosures: Monika Roychowdhury: None; Maria Teresa Eyzaguirre Pellon: None; Lori Pai: None; David Yin: None

Background: PD-L1 expression is routinely used in non-small cell lung cancer as a biomarker to predict response for checkpoint inhibitors. However, there are cases where PD-L1 expression is discordant with response. It has been proposed that the percentage of CD8+ tumor infiltrating lymphocytes (TIL) could be used as a prognostic marker**.** This study aims to find the best practical way to measure tumor infiltrating lymphocytes to correlate with progression free survival (PFS).

Design: Metastatic/recurrent NSCLC cases treated with ICI between 2014-2019 at Tufts Medical Center were selected and reviewed for age, stage, chemotherapy use within 6 months, physician reported PFS, and PD-L1 expression. Slides were reviewed from 12 resections and 16 biopsies. TIL data was collected via estimation from hematoxylin and eosin (H&E) stains, CD8 immunohistochemically (IHC) stains, and artificial intelligence-calculated percentage of CD8 IHC stains provided by the neural

network trained by Tufts' pathologist using Cognex ViDi Suite 4.1. Estimates were scored accordingly: 0 =0%, 1=1-10%, 2=10-25%, 3=25-50%, 4=50-75%, 5=75-100%. Data was analyzed using a Pearson correlation coefficient and a multivariate Cox proportional hazards model.

Results: The correlation coefficient for AI estimate and PFS was 0.54727. The coefficient for H&E and PFS was -0.0307. The coefficient for estimated CD8 and PFS was 0.2329. The AI data and the estimated CD8 data had strong correlation with a coefficient of 0.9210. The Cox proportional hazards model for progression for all samples is shown in figure 1. The Cox proportional hazards model for progression for resection only is shown in figure 2. HR for AI assessed CD8 cells was 0.097 (>3% vs <3%) (p = 0.012) for all cases and 0.1 (>3% vs <3%) (p = 0.215) for resection only.

Figure 1 - 1234

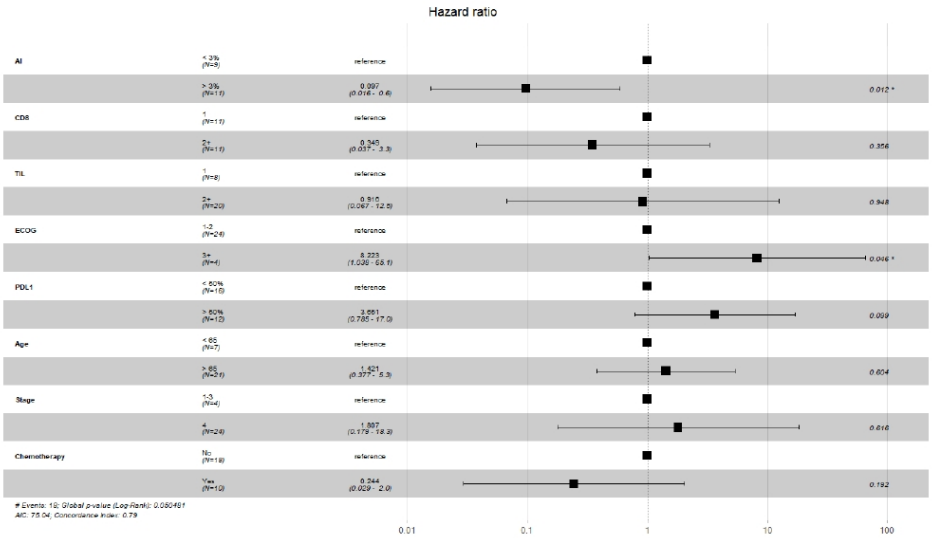

Fig 1. HR for all samples (biopsies and resections)

Figure 2 - 1234

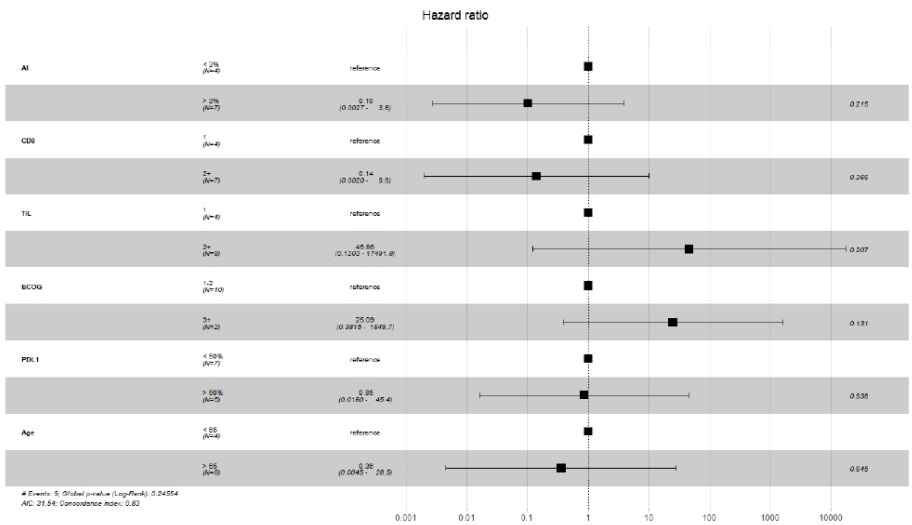

Fig 2. HR for resections only

Conclusions: The best correlate for PFS was the AI estimate. This was maintained when attributing for PD-L1 score, ECOG status, age, stage, and use of chemotherapy. The HR was consistent in both the resection and the biopsy cases. In contrast, the PD-L1 score showed a HR that differed between all cases and resections. This suggests that PD-L1 may not a reliable biomarker for response, especially in biopsies where there may be variability. The concentration of CD8+ T cells may be a better correlate

and marker of response for ICI than the current standard. Further prospective study is needed. This may provide another screening tool for the use of ICI in metastatic NSCLC.

Key words: Non-small cell lung cancer, Immune checkpoint inhibitor, Tumor infiltrating lymphocytes, PDL1, Artificial intelligence, Progression free survival, prognostic predictive factors

1235 RNA Expression Profiling of Paired Biopsy and Resection Specimens of Mesothelioma Reveals Potential Novel Treatment Strategies and Targets

Krasimira Rozenova[1], Beth Pitel[1], Carlos Sosa[1], Sydney Clausen[1], Matthew Petersen[1], Anja Roden[1], Kevin Halling[1], Ying-Chun Lo[1]
[1]Mayo Clinic, Rochester, MN

Disclosures: Krasimira Rozenova: None; Beth Pitel: None; Carlos Sosa: None; Sydney Clausen: None; Matthew Petersen: None; Anja Roden: None; Kevin Halling: None; Ying-Chun Lo: *Advisory Board Member*, Takeda Pharmaceutical Company Limited

Background: Mesothelioma (MM) is a highly lethal cancer partly due to difficulty in early detection and its poor response to treatments. BAP1 loss is frequently detected but not targetable yet. Current management is usually multi-disciplinary. We investigated the RNA expression profile of MM specimens at different phases of treatment, aiming to identify potential therapeutic options.

Design: Our cohort (N=57) consists of 17 paired MM specimens of diagnostic biopsy (Bx-Pre) and surgical resection (R-Post) from patients [age range 37-81, median 69; 88% male], 76% of which received neoadjuvant therapy (10 chemotherapy and 3 radiation), 17 biopsies (Bx-NonS) and 3 subsequent progression samples (Pro) from patients who were not surgical candidates [age range 55-91, median 80; 59% male], and 3 pleuritis cases (Benign). RNA was extracted from tumor enriched area from unstained FFPE slides. Expression profiling was performed by nCounter PanCancer Pathways Panel (NanoString, 770 genes). RNA expression was analyzed by nSolver software.

Results: Bx-Pre and Bx-NonS contained 82% and 59% epithelioid MM, respectively. Five genes were found to have >3 fold overexpression in R-Post compared to their paired Bx-Pre samples: NR4A1 (9.9X, p<0.001), FOS (8.2X, p<0.001), NR4A3 (4.5X, p<0.001), IL6 (3.7X, p<0.01) and IL8 (3.1X, p<0.01). This profile indicates pro-inflammation and proliferation after neoadjuvant therapy. The expression of SPP1 was significantly decreased (2.6X, p=0.009) in R-Post compared to Bx-Pre. Ten genes had >3 fold overexpression in both Bx-Pre vs Benign and Bx-NonS vs Benign, including MET (4.6X and 4.2X; combined Bx vs Benign p<0.001), FGF18 (8.4X and 3.8X; p<0.001), WNT2B (8.9X and 4.5X; p<0.001) and WNT10A (4.7X and 4.0X; p<0.001). This finding suggests a role for these genes in MM tumorigenesis. Only 1 gene, DKK1, had >3 fold overexpression in Bx-NonS versus Bx-Pre (3.3X, p=0.1). Comparing Pro to Bx-NonS, 10 genes had >3 fold overexpression, including DKK1 (3.6X, p=0.09) and WNT5A (3.2X, p=0.06). These results imply DKK1 and Wnt signaling pathways may be associated with aggressiveness and disease progression.

Conclusions: Our study revealed pro-inflammatory gene expression changes in MM after neoadjuvant therapy, which suggests a possible role for immunotherapy/immune modulation in the adjuvant setting. Overexpression of MET, FGF18, DKK1, and Wnt signaling pathways appear to be associated with tumorigenesis, aggressiveness, and disease progression. Targeting those genes are potential effective therapies for MM.

1236 Different Prevalence of Molecular Alterations for Non-Small Cell Lung Cancer in Mexican Cohort of 200 Patients

Sergio Sanchez Sosa[1], Tania Galindo Garcia[2], Arantxa Macias Martinez[2], Gabriela Cuauro Ruiz[2], Maricela Flores Cuautle[2], Amairani Ham Tirado[2], Iván González Espinoza[2]
[1]Labopat, Puebla, Mexico, [2]Puebla, Mexico

Disclosures: Sergio Sanchez Sosa: None; Tania Galindo Garcia: None; Arantxa Macias Martinez: None; Gabriela Cuauro Ruiz: None; Maricela Flores Cuautle: None; Amairani Ham Tirado: None; Iván González Espinoza: None

Background: Lung cancer is the most common cause of global cancer-related mortality. In the last 15 years, the use of new targeted therapies has improved survival and quality of life. This is due to the knowledge of oncogenome and the use of

biomarkers. Testing for EGFR, KRAS mutations; ALK, ROS1 fusions and PD-L1 expression are essential for treatment. Globocan 2020 Mexican lung cancer incidence is 3.9% and mortality 7.9%. Studies on the prevalence of biomarkers in Mexico have been published, however, they report a cohort of less than 100 patients. Otherwise less than 30% of the patients have access to biomarkers in the public health sector.

Design: Patients with advanced non-small cell lung cancer (NSCLC) included adenocarcinomas (AC), squamous cell carcinoma (SCC) and adenosquamous cells (ASC) in whom biomarkers were performed. Paraffin and cell blocks were used for QPCR detection of mutations in EGFR (Therascreen EGFR RGQ PCR Kit) and KRAS (Therascreen KRAS RGQ PCR Kit). ALK (Vysis LSI ALK Dual Color Abbott) and ROS1 (Dual color Abbott) by ISIS FISH system. PD-L1 (clone SP263) by IHC (Benchmark /Ventana) with a cut-off point of 25% positive expression.

Results: Of a total of 200 patients, 93 were women (46.5%) and 107 men (53.5%), with an average age of 64 years. 76% were diagnosed in the lung and 23.5% in metastasis; 165 patients (82.5%) were AC, 7 (4.2%) invasive mucinous AC and 158 (95.7%) to invasive non-mucinous AC. Of the latter, the predominant histological pattern and histological grade were acinar (56.9%) and grade 2 (53.8%), respectively. 14.5% were diagnosed as SCC where grade 2 predominated (65.5%). Finally, 3% of the cases were diagnosed as ASC, being moderately and poorly differentiated. Biomarkers results are summarized in table 1.

BIOMARKERS	RESULTS OF POSITIVE EXPRESSION			
	ADENOCARCINOMA		SQUAMOUS CELL CARCINOMA	
PD-L1 (IHC, clone SP263)	10.9%		20.7%	
ALK (FISH)	6.7%		0%	
ROS1 (FISH)	4.2%		0%	
EGFR (QPCR)	**32.7%**		**13.8%**	
	Exon 19 deletion	51.9%	Exon 19 deletion	50%
	L858R mutation	33.3%	L858R mutation	50%
	G719X mutation	1.9%		
	Exon insertion 20	3.7%		
	T790M mutation & exon -19 deletion	3.7%		
	L858R mutation & exon 19 - deletion	3.7%		
	G719X & S768I mutations	1.9%		
KRAS (QPCR)	**13.9%**		**6.9%**	
	GLY12ASP	30.4%	GLY12ASP	100%
	GLY12VAL	13.1%		
	GLY13ASP	8.7%		
	GLY12ARG	4.3%		
	GLY12CYS	21.7%		
	GLY12ALA & GLY12VAL	13.1%		
	GLY12ALA & GLY12SER	8.7%		

Conclusions: Three differences of prevalence are observed in our study for Mexican population with lung AC: EGFR 32.7%, 13.9% KRAS and ALK 6.7%. According to recent NGS studies in Mexico, EGFR has a prevalence of 36.7% and 20% for KRAS. In Mexico and Latin America (LA) the mutational frequency is inverse compared to Caucasian population, with KRAS (20-25%) being more frequent than EGFR (10-15%) and ALK (4.5-5%). The genetic diversity in LA people could generate different treatment responses (pharmaco-ethnicity). Other factors could be involved: socioeconomic (reduced access to healthcare for elderly patients), infections, occupational exposure to chemicals, lifestyle factors and diet. Further studies are required to clarify the genomic drivers.

1237 Non-small Cell Lung Carcinoma with Diffuse Co-expression of TTF-1 and p40: Clinicopathologic and Genomic Features of 13 Tumors

Omid Savari[1], Christopher Febres-Aldana[1], Jason Chang[1], Katia Ventura[1], Francis Bodd[1], Paul Paik[1], Frederic Askin[2], William Travis[1], Natasha Rekhtman[1]
[1]Memorial Sloan Kettering Cancer Center, New York, NY, [2]The University of North Carolina, Chapel Hill, NC

Disclosures: Omid Savari: None; Christopher Febres-Aldana: None; Jason Chang: None; Katia Ventura: None; Francis Bodd: None; Paul Paik: None; Frederic Askin: None; William Travis: None; Natasha Rekhtman: None

Background: TTF-1 and p40 are key markers for the diagnosis of lung adenocarcinoma (ADC) and squamous cell carcinoma (SqCC), respectively. Diffuse TTF-1/p40 co-expression has been described in only isolated case reports. Here we collected the largest series to date (n=13) of these unusual tumors with the goal to elucidate their clinicopathologic characteristics and genomic profiles.

Design: Cases were identified at Institution 1 (n=12) and Institution 2 (n=1); a subset (n=5) was submitted to Institution 1 as personals consultations. Immunohistochemistry (IHC) was performed using TTF-1 clone 8G7G3/1 and p40 clone SP1. Only cases with diffuse co-expression (each marker labeling >50% of tumor cells) were included. Detailed tumor and patient characteristics were collected, and 4 tumors were analyzed by targeted next-generation sequencing (NGS) of 410-505 cancer genes. The rates were compared to those in 9956 non-small cell lung carcinomas (NSCLC) analyzed by same methods.

Results: Patients with TTF-1/p40 co-expressing tumors had the following characteristics: 7/13 male, mean age 73, 92% smokers (mean 34 pack years). Morphologically, all tumors were NSCLCs, of which 43% had basaloid features. Focal keratinization was seen in 2 cases, whereas no SqCC or ADC morphology was seen in the other cases (85%). However, 5 cases (39%) showed focal labeling for Napsin A and/or mucicarmine, in one case concurrently with focal keratinization. All 4 tumors analyzed by NGS showed a high tumor-mutation burden (TMB) (median 10.6 mt/Mb) compared to median TMB of 5.3 mt/Mb for NSCLC overall (P =0.05). All tumors harbored *TP53* mutations and exhibited non-exclusive mix of alterations characteristic of ADC (2 *KRAS* G12C mutations, 1 *NKX2.1* amplification) or SqCC (3 *FGFR1* amplifications, 2 chromosome 3q gains). *FGFR1* amplifications rate (75%) was significantly higher than that in lung SqCC (11%, P=0.0057) and ADC (0.65%, P<0.00001).

Conclusions: Lung carcinomas with diffuse TTF-1/p40 co-expression represent primarily undifferentiated NSCLCs with frequent basaloid features, but some show morphologic or marker-based evidence of squamous, glandular or dual differentiation. Genomic analysis also supports hybrid features and suggests a distinctly high rate of *FGFR1* amplifications. The presence of *KRAS* G12C mutation is particularly notable given the recent development of targeted therapies for tumors harboring such alterations, which highlights the importance of molecular testing in these tumors.

1238 Mast Cells in COVID-19-Associated Lung Damage

Tina Schaller[1], Bruno Märkl[1], Rainer Claus[1], Jason Hornick[2], Lynette Sholl[3], Matthew Giannetti[2], Mariana Castells[2]
[1]Augsburg University, Augsburg, Germany, [2]Brigham and Women's Hospital, Harvard Medical School, Boston, MA, [3]Harvard Medical School, Boston, MA

Disclosures: Tina Schaller: None; Bruno Märkl: None; Rainer Claus: *Speaker*, AbbVie, Novartis, Janssen-Cilag; *Grant or Research Support*, Novartis, AstraZeneca; *Advisory Board Member*, Roche, Janssen-Cilag, AbbVie, BMS/Celgene; Jason Hornick: *Consultant*, Aadi Biosciences, TRACON Pharmaceuticals; Lynette Sholl: *Consultant*, Genentech, Lilly; *Grant or Research Support*, Genentech; Matthew Giannetti: *Consultant*, Blueprint Medicines; Mariana Castells: None

Background: SARS-CoV-2 infection results in acute respiratory distress and multiple organ failure, but the pathogenesis of the disease is poorly understood. Recent data suggest that viral RNA may be found in mast cells, but patients with asthma who have hyperplasia of mucosal mast cells do not experience asthma exacerbations during infection and do not suffer from increased mortality due to COVID-19-associated lung damage. Mast cells from bone marrow do not express the ACE2 receptor used for SARS-CoV-2 entry into human cells, and patients with mast cell activation disorders such as systemic mastocytosis do not show mast cell activation during infection. Because activated mast cells can release potent inflammatory mediators including IL-6 and have been implicated in fibrotic lung damage, the purpose of this study was to investigate the role of mast cells in COVID-19 fatal lung disease.

Design: We evaluated 19 autopsies and post-mortem biopsies performed on patients who died of COVID-19 in April and May 2020. Representative sections of lung tissue with typical histological changes of diffuse alveolar damage (DAD; both acute and organizing) were selected. Mast cells were identified by immunohistochemistry for KIT (CD117), tryptase, and chymase. Mean

values for mast cells were obtained by counting 3 different areas each with the highest and lowest density of CD117/tryptase-positive cells with 40x magnification.

Results: Patients in this cohort were mostly obese with systemic hypertension or diabetes and had elevated CRP and IL-6. All mast cells in COVID-19 lung autopsies were positive for tryptase and chymase, indicating a connective tissue phenotype (Figure 1). While both acute and organizing forms of non-COVID-19-related lung injury showed a 3-5-fold increase in mast cell numbers between low and high-density areas, acute COVID-19 showed a <2-fold increase. In contrast, organizing DAD in COVID-19 showed a 3-fold increase in mast cells between low and high-density areas (Figure 2). Few mast cells were co-localized with SARS-CoV-2 mRNA.

Figure 1 - 1238

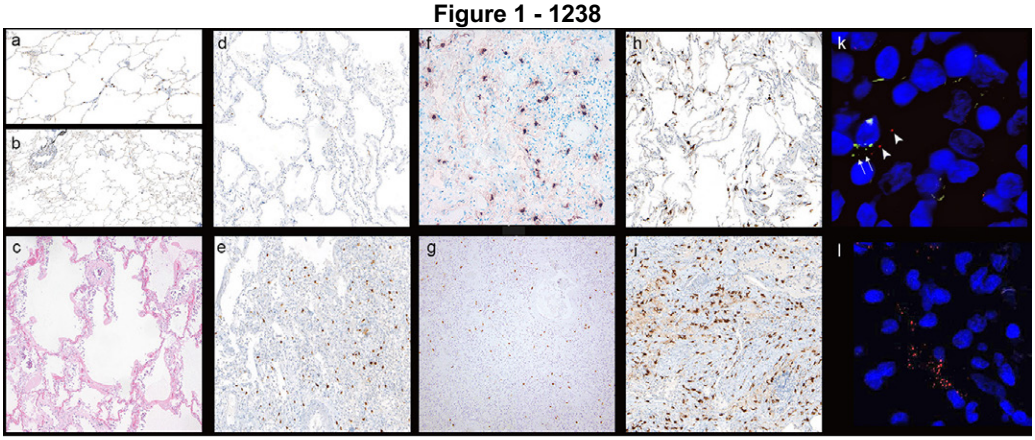

Figure 1: Density of mast cells in lung tissues from patients with COVID19 and other conditions. Normal lung tissue (A, CD117, 100x); higher numbers of mast cells in perivascular and peribronchiolar areas (B, CD117, 40x). In very early DAD with only hyaline membranes but lack of an inflammatory infiltrate (C, 40x), the numbers of mast cells decrease to only a few cells (D, CD117, 100x), whereas they increase in the organizing phase of DAD (E, CD117, 100x). Tryptase (F, 100x) and chymase (G, 100x) showing similar numbers of mast cells as CD117 with slight background staining in organizing DAD. The numbers of mast cells in COVID19 infection was compared to other conditions that change the structure of lung tissue, e.g., influenza as another viral disease (H, CD117, 100x) and UIP as a chronic inflammatory process (I, CD117, 100x). RNAscope with positive signals in SARS-CoV-2 in a case with a moderate mast cells density (K, 100x); RNAscope with questionable co-localization of SARS-CoV-2 and CD117 (L, 200x).

Figure 2 - 1238

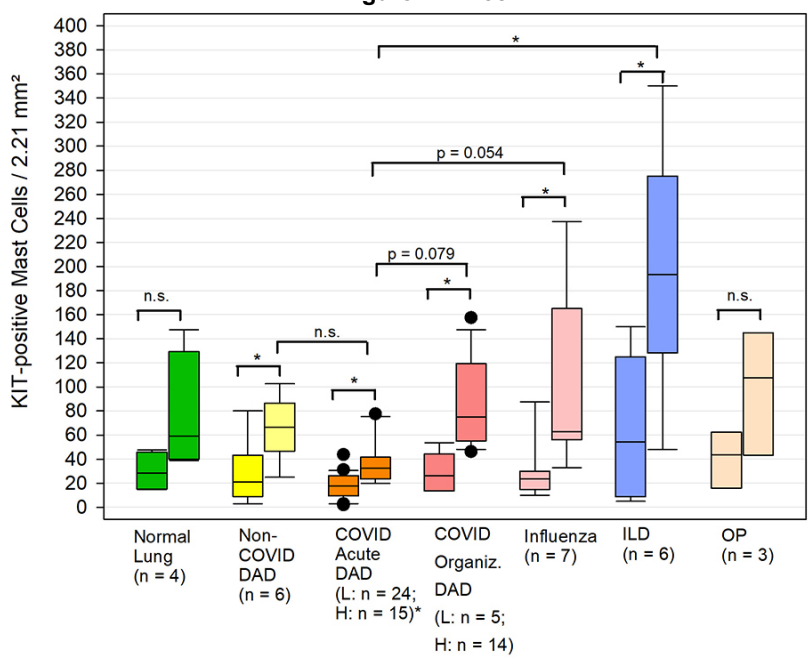

Conclusions: During the early phase of DAD in SARS-CoV-2 infection, mast cells are suppressed, potentially due to an interferon surge, which is reversed during the organizing DAD phase of infection. Viral RNA is rarely present in mast cells, consistent with the reported lack of ACE2 receptors in bone marrow mast cells.

1239 Pan-Lung Cancer: Integrative Genomic and Transcriptomic Analysis Suggest Novel Therapeutic Approach

Michele Simbolo[1], Giovanni Centonze[2], Luca Giudice[1], Federica Grillo[3], Patrick Maisonneuve[4], Giovanna Sabella[2], Paola Bossi[5], Paola Spaggiari[6], Alessandro Del Gobbo[7], Natalie Prinzi[8], Sara Pusceddu[9], Alessandra Fabbri[2], Luisa Bercich[10], Alessandro Mangogna[11], Luigi Rolli[12], Stefano Ferrero[13], Marco Volante[14], Carlo Capella[15], Aldo Scarpa[1], Massimo Milione[2]

[1]University of Verona, Verona, Italy, [2]Fondazione IRCCS Istituto Nazionale Tumori Milano, Milan, Italy, [3]University of Genova, Genova, Italy, [4]IEO, Milan, Italy, [5]Humanitas Cancer Center, Milan, Italy, [6]Istituti Clinic Humanitas, Rozzano, Italy, [7]Fondazione IRCCS Ca' Granda Ospedale Maggiore Policlinico, University of Milan, Milan, Italy, [8]IRCCS Foundation, Istituto Nazionale dei Tumori, Milan, Italy, [9]Fondazione IRCCS Istituto Nazionale Tumori Milano, [10]University of Brescia at ASST-Spedali Civili, Brescia, Italy, [11]University of Trieste, Trieste, Italy, [12]IRCCS Foundation National Cancer Institute, Milan, Italy, [13]Fondazione IRCCS Ca' Granda Ospedale Maggiore Policlinico, University of Milan, Milano, Italy, [14]University of Turin, Orbassano, Italy, [15]Uni-Insubria, Varse, Italy

Disclosures: Michele Simbolo: None; Giovanni Centonze: None; Luca Giudice: None; Federica Grillo: None; Patrick Maisonneuve: None; Giovanna Sabella: None; Paola Bossi: None; Paola Spaggiari: None; Alessandro Del Gobbo: None; Natalie Prinzi: None; Sara Pusceddu: *Grant or Research Support*, IPSEN, PFIZER, Merck; *Speaker*, AAA, Novartis; Alessandra Fabbri: None; Luisa Bercich: None; Alessandro Mangogna: None; Luigi Rolli: None; Stefano Ferrero: None; Marco Volante: None; Carlo Capella: None; Aldo Scarpa: None; Massimo Milione: None

Background: The World Health Organization (WHO) identifies six major histotypes of Lung Neoplasms dividing them according to two main, pure or combined, lineages: neuroendocrine – typical carcinoid (TC), atypical carcinoid (AC), large cell neuroendocrine carcinoma (LCNEC), small cell lung cancer (SCLC), and non-neuroendocrine – adenocarcinoma (ADC), squamous cell carcinoma (SQC). High-throughput molecular analysis, on a histologically re-evaluated large multicenter series of lung cancers, may be able to provide a more personalized characterization beyond histopathology and develop patient-tailored therapeutic approaches.

Design: Six-hundred patients with primary neuroendocrine lung neoplasms were retrieved from 5 Italian Centers, creating a retrospective cohort spanning 40 years (1978-2019), with follow up information. Pathological central revision on surgical specimens, both in terms of morphology and immunohistochemical features, enabled reclassification according to WHO 2021 criteria. Specific WHO categories were deeply characterized by means of wide genomic (409 genes) and transcriptomic (20.815 genes) analyses.

Results: Overall, 100 non-neuroendocrine lung neoplasms (40 ADC, 60 SQC), 114 lung neuroendocrine tumors (23 TC, 25 AC, 43 LCNEC, 23 SCLC) and 54 combined-lung tumors (41 co-LCNECs and 13 co-SCLCs) were identified as suitable for genomic and expression NGS analysis. Genomic screening of pure tumours (n=214) showed highly specific genomic alterations for each histotype. Transcriptomic analysis identified two molecular subgroups in each pure histotype, except for SQCs. In more details: two molecular clusters of ADCs were identified, linked both to different outcomes and to the association with the PD-1 blockade pathway, while an SCLC ATR positive and SCLC ATR negative were detected, highlighting new therapeutic possibilities. Deconvolution analysis also divided lung cancers in two major groups: “cold” and “hot” showing LCNECs as potential candidates for immunotherapy. Molecular characterization of combined-lung tumours identified potentially targetable alterations while transcriptomic analysis showed at least 3 distinct and standalone profiles compared to pure histotypes.

Conclusions: Our study detailed the molecular landscape of major histotypes of lung neoplasms, highlighting differences and links between various histotypes, and providing indications for a better molecular stratification for the purpose of an increasingly personalized therapeutic management

1240 Vascular Invasion Predicts Outcome in Early Stage Lung Adenocarcinoma but not Squamous Cell Carcinoma

Lubna Suaiti[1], Travis Sullivan[2], Kei Suzuki[3], Kimberly Rieger-Christ[2], Eric Burks[4]
[1]Boston Medical Center, Boston, MA, [2]Lahey Hospital & Medical Center, Burlington, VT, [3]Boston University, Boston Medical Center, Boston, MA, [4]Boston University Mallory Pathology Associates, Boston, MA

Disclosures: Lubna Suaiti: None; Travis Sullivan: None; Kei Suzuki: None; Kimberly Rieger-Christ: None; Eric Burks: None

Background: Adjuvant chemotherapy (AC) is an option for resected stage I non-small cell lung cancer (NSCLC) with vascular invasion (VI). Many studies have confirmed the prognostic significance of VI in NSCLC but often reporting overlapping definitions between vascular, lymphatic (LI), or angiolymphatic (AGL) invasion. Two studies have shown that VI and AGL are prognostic for stage I lung adenocarcinoma (LUAD) but not squamous cell carcinoma (LUSC), although fewer than 40 cases of stage I LUSC were included in each.

Design: Retrospective review of H&E-stained slides from surgically resected AJCC 8th ed. stage IA2-IB LUAD and LUSC from two institutions was performed. VI was defined as luminal invasion of a muscular artery or vein. LI was defined as invasion into non-muscular walled lymphatic spaces. AGL was defined by the presence of either LI or VI. Clinical findings and outcomes were assessed by chart review and 5-year Recurrence-free survival (RFS) was estimated using the Kaplan-Meier method. Stage IA1 tumors were excluded from this study as they are disproportionally more common among LUAD and rarely recur.

Results: Clinicopathologic features of the cohorts of LUAD (n=344) and LUSC (n=102) are summarized in the Table. The cohorts showed no significant differences regarding 5-year RFS (81% each), stage, age, or race; although patients with LUAD were more commonly female, having less smoke exposure, longer smoking cessation times, and smaller invasive tumor sizes. RFS for LUAD and LUSC stratified by VI and AGL are shown in Figure 1 and 2 respectively. The presence of either VI or AGL was predictive of recurrence for LUAD (VI- 90% vs. VI+ 64%, p<0.001 & AGL- 92% vs. AGL+ 71%, p<0.001) but not LUSC (VI- 80% vs. VI+ 83%, p=0.852 & AGL- 79% vs. AGL+ 84%, p=0.740). Among LUAD, VI was a stronger predictor of recurrence at 5-years than AGL (64% vs. 71% 5-year RFS; Figure 1A and 2A). Subset analysis of LI among LUAD stratified by VI showed a non-significant marginal trend favoring higher recurrence in cases with LI in both subgroups (VI-LI- 92% vs VI-LI+ 87%, p=0.347 & VI+LI- 66% vs. VI+LI+ 62%, p=0.422).

Clinicopathologic Findings	LUAD	LUSC	p value
N	*344*	*102*	
Age	69 (62-74)	69 (62-74)	0.770
Gender			
Female	207 (60)	50 (49)	**0.045**
Male	137 (40)	52 (51)	
Race			0.589
White	281 (82)	79 (77)	
Black	44 (13)	17 (17)	
Other	19 (5)	6 (6)	
Smoking Status			**0.011**
Current smoker	**133 (38)**	**52 (51)**	
Former smoker	171 (50)	47 (46)	
Never smoker	**34 (10)**	**1 (1)**	
Unknown	6 (2)	2 (2)	
Pack Years	40 (25-53)	50 (35-60)	**0.001**
Quit Years	14 (4-24)	7 (3-15)	**0.026**
Surgical Procedure			
Pneumonectomy	0	2 (2)	0.085
Lobectomy	240 (70)	70 (69)	
Sublobar	104 (30)	30 (29)	
pStage AJCC 8th ed.			0.122
IA1 (pT1mi/1a)	0	0	
IA2 (pT1b)	167 (49)	38 (37)	
IA3 (pT1c)	63 (18)	21 (21)	
IB (pT2a)	114 (33)	43 (42)	
Size			
Total Size, cm	2.0 (1.5-2.5)	2.1 (1.6-2.9)	**0.022**
Invasive Size, cm	1.7 (1.3-2.2)	2.1 (1.6-2.9)	**<0.001**
Invasive Feature			
Lymphatic Invasion	113 (33)	24 (24)	0.073
Vascular Invasion	125 (36)	46 (45)	0.110
Angiolymphatic Invasion	180 (52)	58 (57)	0.420
Visceral Pleural Invasion	96 (28)	25 (25)	0.498
STAS	179 (52)	52 (51)	0.852
Outcome			
5-year RFS (95% CI)	81 (76-85)	81 (70-89)	0.796

Note: The data are shown as the number (%) or median (Q1-Q3). Boldface indicates statistical significance.

*Pack years and quit years reported for ever-smokers and former-smokers respectively. The values in **bold** indicate which group(s) were noted as significantly different upon post-hoc comparison using a Bonferroni correction for multiple comparisons, where an adjusted p-value <0.05 was considered statistically significant.

Figure 1 - 1240

Figure 1: Stage IA2-IB NSCLC Stratified by Histologic Type and Vascular Invasion

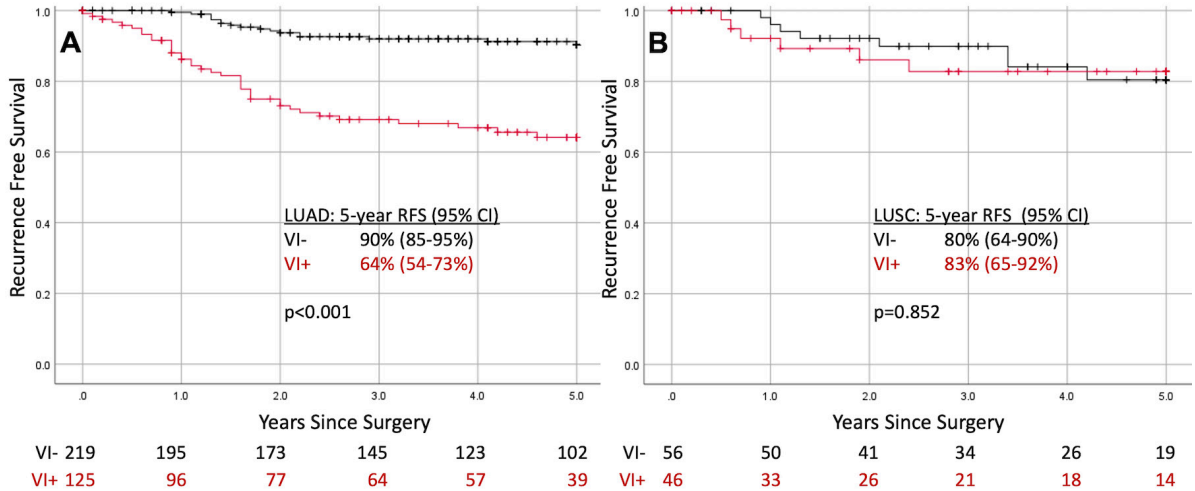

Figure 2 - 1240

Figure 2: Stage IA2-IB NSCLC Stratified by Histologic Type and Angiolymphatic Invasion

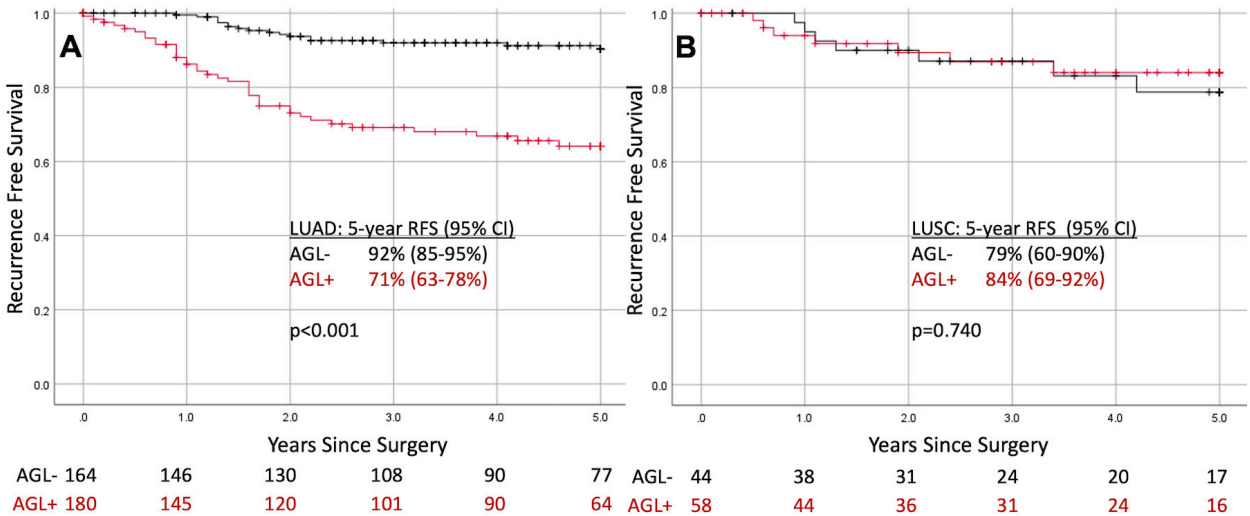

Conclusions: Vascular invasion is a strong predictor of recurrence in stage I LUAD but not LUSC. Treatment guidelines should be adjusted so that early stage LUSC are not over-treated with AC for a finding predictive only for LUAD. Moreover, VI and LI should be evaluated and reported separately, rather than AGL, as LI appears to be less predictive of recurrence in this context.

1241 Comparison of the Immune Response in Mild Versus Fatal Infection by SARS-CoV-2

David Suster[1], Esmerina Tili[2], Gerard Nuovo[3]
[1]Rutgers New Jersey Medical School/Rutgers University, Newark, NJ, [2]The Ohio State University College of Medicine, Columbus, OH, [3]The Ohio State University Medical Center, Columbus, OH

Disclosures: David Suster: None; Esmerina Tili: None; Gerard Nuovo: None

Background: COVID19 and its etiological agent SARS-COV2 may cause a wide spectrum of clinical disease ranging from asymptomatic infection to severe disease and death. Clinical severity of disease has been linked to the variable immune responses to the virus. Identification of markers that distinguish clinically mild from severe disease may be of benefit in predicting disease severity.

Design: Analysis of T cells (CD3), three subsets of macrophages (CD11b, CD163, and CD206), PDL1 and viral load in nasopharyngeal swabs of 20 people that were reverse transcriptase polymerase chain reaction positive with mild disease and 20 reverse transcriptase polymerase chain reaction negative controls versus the same variables in 20 lungs from people who died with COVID-19 versus normal aged matched controls was performed. The fatal COVID-19 lung data were stratified into the lung sections with high viral load versus lung sections, often from the same person, where viral involvement was not evident by in situ hybridization.

Results: There was a 20X fold increase in the percentage of CD3+ cells in the viral positive nasopharyngeal swabs versus the controls whereas no change was noted in the CD3 count in the lungs of fatal COVID-19 with high viral load. The percentage of cells positive for the macrophage marker CD163 and for PDL1 were equivalent in the mild versus fatal disease samples. There was a significant increase in the number of cells expressing CD11b and CD206 in the fatal lungs with virus compared to the normal lungs; however, these increases were significantly higher in the nasopharyngeal swabs with mild infection. In the fatal COVID-19 lungs without detectable virus, the PDL1, CD11b and CD206 counts were very low, indicating that even in fatal disease the virus was inducing this immune response. Surprisingly, viral load was equivalent in mild versus fatal disease.

Conclusions: It is concluded that markedly increased counts of CD3 T cells as well as CD11b and CD206 macrophages can differentiate mild versus fatal COVID-19 which may provide a way to predict clinical outcome by analyzing viral nasopharyngeal swabs for the T cell and macrophage response.

1242 The Clinicopathological Features of Cytokeratin 5-positive Pulmonary Adenocarcinoma

Kazuhiro Terada[1], Akihiko Yoshizawa[1], Hironori Haga[1]
[1]Kyoto University Hospital, Kyoto, Japan

Disclosures: Kazuhiro Terada: None; Akihiko Yoshizawa: None; Hironori Haga: None

Background: Cytokeratin 5 (CK5) is a marker of pulmonary squamous cell carcinoma. On the other hand, CK5 is sometimes present in tumor cells of pulmonary adenocarcinoma (P-ADC); however, little is known about the clinicopathological characteristics of CK5-positive P-ADC. The aim of this study was to explore the clinicopathological characteristics of CK5-positive P-ADCs.

Design: We prepared tissue microarrays (TMAs) containing 339 P-ADC cores that were obtained from resected P-ADC in our hospital. We performed immunohistochemical staining of CK5 with the TMAs. In this study, we considered the core to be CK5-positive P-ADC if it was revealed to be CK5-positive in at least 10% of the tumor cells.

Results: Of 339 cores, 36 (10.6 %) were positive for CK5. Among those, 28 expressed either thyroid transcription factor-1 (TTF-1) or hepatocyte nuclear factor 4 alpha (HNF4alpha). However, the other eight cores did not express TTF-1 or HNF4alpha, instead showing glandular differentiation or mucin secretion. All of the TMA cores did not express p40. CK5-positive P-ADCs were predominant in males ($p=0.017$) and smokers ($p=0.003$). CK5-positive P-ADCs were related to larger invasion sizes ($p=0.014$) and vascular invasion ($p<0.001$). Tumors with solid and discohesive components correlated with higher H-scores (30 or over; $p<0.001$). CK5-positive P-ADCs were correlated with HNF4alpha ($p=0.009$) and MUC5B ($p=0.005$) expression; however, they were conversely correlated with the absence of TTF-1 ($p<0.001$). CK5-positive P-ADCs correlated with KRAS mutations ($p=0.012$), ALK rearrangement ($p=0.029$), and EGFR wild type ($p=0.009$). Regarding survival, CK5-positive P-ADCs were associated with shorter disease-free survival ($p<0.001$) and overall survival ($p<0.001$).

Figure 1 - 1242

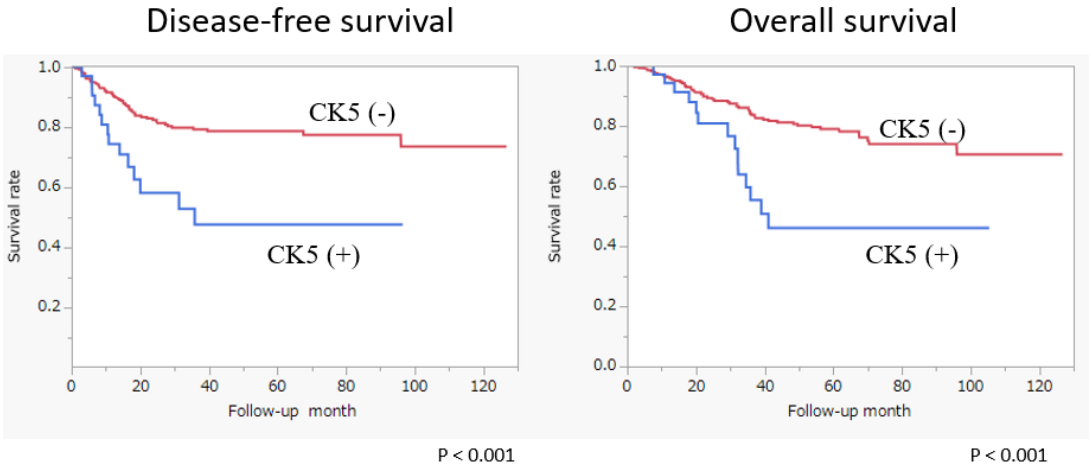

Conclusions: CK5-positive P-ADCs had more aggressive characteristics than CK5-negative P-ADCs.

1243 Primary Pulmonary Mucinous Carcinoma Versus Colorectal Metastasis: Heterogeneity of Immunohistochemical Stains

Alexander Wein[1], Chieh-Yu Lin[2], Jon Ritter[2]
[1]Barnes-Jewish Hospital/Washington University, St. Louis, MO, [2]Washington University School of Medicine, St. Louis, MO

Disclosures: Alexander Wein: None; Chieh-Yu Lin: *Consultant*, Natera; Jon Ritter: None

Background: Primary lung mucinous adenocarcinoma and pulmonary metastatic colorectal adenocarcinoma (CRC) can be morphologically similar, and have overlapping immunophenotypes and molecular signatures. Prior studies have evaluated SATB2 immunohistochemical staining (IHC) as a potential tool to distinguish these two entities. However, the heterogeneity of staining has not been fully described. With increased use of fine needle-aspiration and small biopsies to guide therapy, it is imperative to evaluate the staining heterogeneity of SATB2, along with other common IHC markers, in primary lung mucinous adenocarcinoma and metastatic CRC to the lung.

Design: With Institutional Review Board approval, we identified resection specimens of primary lung or metastatic colorectal mucinous adenocarcinomas in the past 5 years. All the archival slides were reviewed to confirm diagnosis and clinical data were collected. A panel of IHC stains (CK7, CK20, TTF1, NapsinA, CDX2 and SATB2) was performed in all cases, regardless the original workup. The stains were scored by a pathologist blinded to original diagnosis based on percentage of cells with moderate to strong staining (0: <10 %; 1: 10-75 %; 2: >75 %).

Results: In total, 59 cases (39 primary and 20 metastases) were identified, from 58 patients (age range 33 – 83; mean 61.5). SATB2 was positive in only 1 primary adenocarcinoma (2.6%, score 2). In contrast, all but one CRC metastasis was SATB2 positive (13 cases of score 2; 6 cases of score 1). For other nuclear markers, all the metastases showed score 2 CDX2 staining and score 0 TTF1 staining, while the primary cases were variable for both markers (CDX2: 79.4% score 0, 15.3% score 1, 5.1% score 2; TTF1: 30.8% score 0, 48.7% score 1; 20.5% score 2). Among cytoplasmic markers, CK20 and NapsinA stains were quite heterogenous in both primary and metastatic cases (see table). Most of the primary cases (92.3%) showed score 2 CK7 staining, and none of the metastatic cases showed score 2 CK7 staining (15% cases showed score 1).

	Primary			Metastasis		
	score 0	score 1	score 2	score 0	score 1	score 2
SATB2	97.4%	0.0%	2.6%	5.0%	65.0%	30.0%
CDX2	77.0%	18.0%	5.0%	0.0%	0.0%	100.0%
TTF1	30.8%	48.7%	20.5%	100.0%	0.0%	0.0%
CK7	5.1%	2.6%	92.3%	85.0%	15.0%	0.0%
CK20	76.9%	5.1%	18.0%	15.0%	40.0%	45.0%
NapsinA	38.5%	30.8%	30.8%	55.0%	20.0%	25.0%

Conclusions: IHC markers that are commonly used for distinguishing lung primary mucinous adenocarcinomas versus CRC metastases in the lung show variable, heterogeneous staining. Our data suggest that a combination of SATB2, CDX2, TTF1 and CK7 may be useful in small biopsies: any TTF1 positivity or lack of CDX2 staining is suggestive of a primary, while any SATB2 positivity or lack of CK7 is suggestive of metastatic CRC.

1244 Study of Molecularly Confirmed Pancreatic Adenocarcinoma (PDAC) Metastases to the Lung Can Define Morphologic Features that Distinguish Them from Primary Pulmonary Invasive Mucinous Adenocarcinoma (IMA)

Nicolas Wyvekens[1], Elizabeth Carstens[2], Mark Hammer[3], Lynette Sholl[4]
[1]Brigham and Women's Hospital, Harvard Medical School, Boston, MA, [2]Brigham and Women's Hospital, Dana-Farber Cancer Institute, Harvard Medical School, Boston, MA, [3]Brigham and Women's Hospital, Boston, MA, [4]Harvard Medical School, Boston, MA

Disclosures: Nicolas Wyvekens: None; Elizabeth Carstens: None; Mark Hammer: None; Lynette Sholl: *Consultant*, Genentech, Lilly; *Grant or Research Support*, Genentech

Background: Pulmonary IMA recapitulates the pathology of gastrointestinal-type mucinous tumors. The lung is also a common site of metastasis, including from PDAC. Distinguishing IMA from metastatic (met) PDAC can be challenging due to overlapping pathologic features. Using a "ground truth" cohort of molecularly-defined metPDAC to the lung, we aimed to identify an objective set of morphologic features distinguishing between IMA and metPDAC.

Design: Our cohort included 12 pairs of primary PDAC and metastatic lung site biopsies obtained between 2015-2020. 20 cases of resected IMA comprised the comparator cohort. All cases underwent panel next generation sequencing (NGS). Chest CT or PET images were reviewed by a thoracic radiologist blinded to the diagnoses. Chart review was performed to identify patient age, sex, smoking status, and sites of intra- and extrapulmonary disease. HE-stained sections of IMA and metPDAC were scored for a defined set of morphologic features.

Results: NGS showed shared oncogenic gene alterations in all 12 PDAC primary-metastatic pairs. *KRAS* mutations were detected in 95% and 92% of IMA and metPDAC, respectively, with no significant difference in the types of substitution. *NKX2.1* mutations were present in 45% of IMAs and absent in metPDAC ($p = 0.039$). *TP53* and *SMAD4* mutations were present in 58% and 25% of metPDAC, and absent in IMAs ($p = 0.003$ and $p = 0.07$, respectively). Radiology correctly classified metPDAC in only 53% of cases. No difference in age, sex or tobacco use was seen in patients with IMA versus metPDAC. The lung was the first metastatic site in all PDAC patients; the median interval from primary diagnosis to metastasis was 16 months (range 1-70). Morphologic features favoring a diagnosis of metPDAC included: invasion of interlobular septa ($p = 0.020$), intraluminal necrotic debris ($p = 0.009$), absence of basal nuclear polarity ($p = 0.037$), multinucleation ($p = 0.042$) and mitotic activity ($p = 0.012$).

Conclusions: Using a molecularly-defined cohort of metastatic PDAC to the lung, robust comparisons to IMA can be performed. On its own, *KRAS* mutational status is uninformative; detection of *TP53* or *NKX2-1* mutation favors metPDAC or IMA, respectively. Other than a prior history of PDAC, clinical and radiographic findings are not specific for either diagnosis. Importantly, morphologic clues can be used to favor a diagnosis of metPDAC in the differential with IMA. Validation of these morphologic features is needed.

1245 Reproducibility in Assessment of "Invasion" in Lung Adenocarcinoma with Lepidic Component: An Interobserver Concordance Study with Cytokeratin 7 Stain

Ellen Yang[1], Najd Alshamlan[2], Jessica Weiss[3], Michael Cabanero[4], Ming Tsao[5]
[1]University of Toronto, Toronto, Canada, [2]King Abdullah bin Abdulaziz University Hospital, Riyadh, Saudi Arabia, [3]Princess Margaret Hospital, Toronto, Canada, [4]Laboratory Medicine Program, Departments of Anatomical Pathology, University Health Network and University of Toronto, Toronto, Canada, [5]University Health Network, Toronto, Canada

Disclosures: Ellen Yang: None; Najd Alshamlan: None; Jessica Weiss: None; Michael Cabanero: None; Ming Tsao: None

Background: Lepidic growth is considered a non-invasive histological pattern in lung adenocarcinoma, while others (acinar, papillary, micropapillary, cribriform and solid) are considered invasive. Studies reported considerable interobserver variability when assessing "invasive" vs. "non-invasive" patterns due to the overlapping features between lepidic and acinar/papillary patterns,

affecting accurate tumor staging. We set out to assess the use of cytokeratin 7 (CK7) stain to improve interobserver concordance in the assessment of invasive vs. non-invasive patterns among lepidic or acinar-predominant lung adenocarcinoma.

Design: pT1N0 lung adenocarcinoma with lepidic- (*n* = 53) and acinar-predominant (*n* = 53) diagnoses with hematoxylin and eosin (H&E) and CK7 stained slides were retrieved. Cases were randomized for the original diagnoses. Slides (*n* = 158) were reviewed by 2 thoracic pathologists, 1 fellow and 1 resident. The H&E and CK7 slides were independently scored for estimated percentage of non-invasive (NI), probable non-invasive (PNI), invasive (I) and probable invasive (PI) components. For H&E, lepidic and non-lepidic patterns represent NI and I patterns, respectively. For CK7, organized alveolar pattern represents putative NI pattern (Fig.1), vs. disorganized I pattern (Fig.2). "Training" was conducted prior to study commencement. Intraclass Correlation Coefficient (ICC) for the absolute agreement between the raters was measured using two-way random effect models for a single rater, for all cases and within each diagnosis.

Results: For all cases, the range of mean percentages for NI+PNI pattern between raters were 30.6-72.2% on H&E and 26.6-48.8% on CK7; the range of mean percentages for I+PI pattern were 26.5-72.4% on H&E and 51.2-73.3% on CK7. The ICCs for NI+PNI pattern were 0.35 (95% CI 0.16-0.51) on H&E and 0.54 (95% CI 0.42-0.63) on CK7; the ICCs for I+PI were 0.35 (0.16-0.52, 95% CI) on H&E and 0.53 (0.42-0.63, 95% CI) on CK7. For the lepidic-predominant cases, the ICCs for NI+PNI pattern were 0.23 (95% CI 0.05-0.42) on H&E and 0.42 (95% CI 0.26-0.58) on CK7. For the acinar-predominant group, the ICCs for I+PI pattern were 0.27 (95% CI 0.11-0.44) on H&E and 0.44 (95% CI 0.29-0.59) on CK7. Result of re-scoring after consensus review and criteria of "invasive" CK7 patterns will be presented.

Figure 1 - 1245

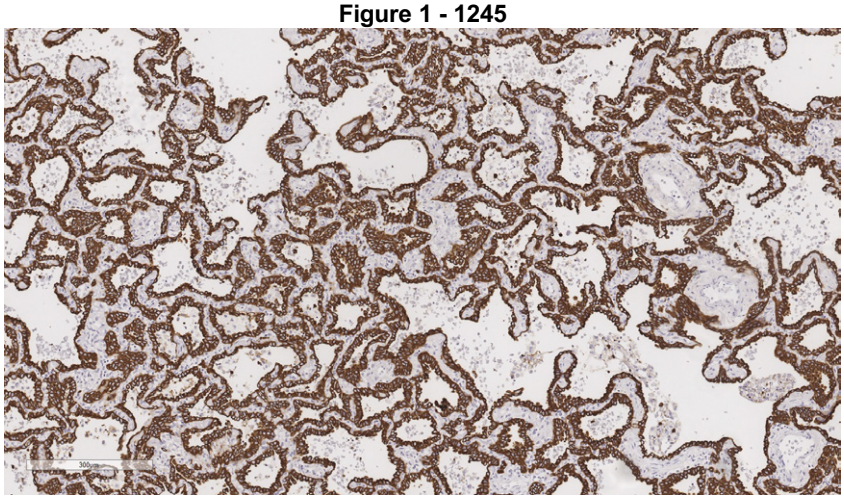

Figure 2 - 1245

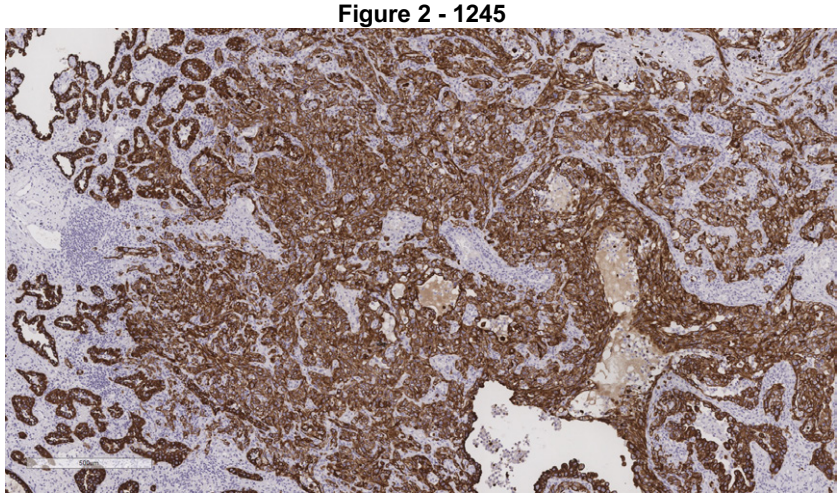

Conclusions: Preliminary results suggest that CK7 stain reveals "non-invasive" and "invasive" patterns that may be recognized with higher reproducibility than those recognized on H&E stain.

1246 Homologous Recombination Deficiency and Tumor Mutational Burden as Clinical Biomarkers for Non-Small Cell Lung Cancer

James Yip[1], Christopher Lum[1]
[1]*University of Hawaii, John A. Burns School of Medicine, Honolulu, HI*

Disclosures: James Yip: None; Christopher Lum: None

Background: Homologous recombination deficiency (HRD) cancers have high levels of genetic instability, potentially being targets for poly-ADP ribose polymerase inhibitors. Tumor mutational burden (TMB), which is used to guide immunotherapy, is thought to be associated with HRD. This study aimed to evaluate the frequency of HRD and its correlation with other genomic parameters in lung cancer.

Design: A total of 39 cases with the diagnosis of lung carcinoma were found in the genomic database between March 1 to July 30, 2021. Copy number variations and absence of heterozygosity detection were analyzed by the NxClinical software (BioDiscovery, El Segundo, CA).

HRD was scored by three DNA-based measures of genomic instability (loss of heterozygosity (LOH), telomeric allelic imbalance (TAI) and large-scale transitions (LST)). HRD-LOH is the number of LOH regions longer than 15 Mb but shorter than the whole chromosome and do not cross the centromere. HRD-TAI is the number of regions longer than 10 Mb with allelic imbalance that extend to one of the subtelomeres but do not cross the centromere. HRD-LST is the number of break points between regions longer than 10 Mb. A high HRD score and LOH percentage were defined as ≥ 42 and ≥ 16%, respectively.

Results: Of the 39 cases, 16 had a high TMB (41.0%). A high HRD score was found in 4 cases (10.3%); high LOH percentage was found in 7 cases (17.9%). PD-L1 expression was present in 22 of the 30 cases tested. A high HRD score correlated with high LOH percentage by Pearson's chi-squared test (p<0.01). No significant association was found between TMB and HRD score, LOH percentage or PD-L1 expression. Common alterations among cases with high TMB included mutations in KRAS (6/16; 37.5%), EGFR (5/16; 31.3%), BRAF (2/16; 12.5%), TP53 (2/16; 12.5%), PIK3CA (3/16; 18.8%), RB1 (1/16; 6.3%), CDKN2A (1/16; 6.3%), STK11 (1/16; 6.3%), AKT1 (1/16; 6.3%), APC (1/16; 6.3%) and ATM (1/16; 6.3%). Amplifications were found in EGFR (1/16; 6.3%), ERBB2 (1/16; 6.3%), PIK3CA (1/16; 6.3%), BRAF (1/16; 6.3%), CDK4 (2/16; 12.5%), CDK6 (1/16; 6.3%) and MDM2 (1/16; 6.3%). Fusions in NOTCH3-BRD4 (1/16; 6.3%) and RPS6KB1-VMP1 (1/16; 6.3%) were detected. Two cases with high TMB had no mutations detected.

Table 1. Genomic alterations in lung cancer. A high HRD score (≥ 42%) was significantly associated with a high LOH percentage (≥ 16%). No significant association was found between TMB and HRD score, LOH percentage or PD-L1 expression.

Case	TMB	HRD Score	HRD CALL	LOH (%)	LOH CALL	PD-L1	PD-L1 Expression (>0%)	PD-L1 Expression (>50%)
1	LOW	2	LOW	1.0	LOW	35	PRESENT	ABSENT
2	HIGH	11	LOW	2.5	LOW	0	ABSENT	ABSENT
3	HIGH	42	HIGH	26.8	HIGH	NONE		
4	HIGH	0	LOW	0.0	LOW	0	ABSENT	ABSENT
5	HIGH	22	LOW	12.5	LOW	35	PRESENT	ABSENT
6	HIGH	32	LOW	11.1	LOW	40	PRESENT	ABSENT
7	HIGH	0	LOW	1.1	LOW	70	PRESENT	PRESENT
8	LOW	14	LOW	5.1	LOW	0	ABSENT	ABSENT
9	LOW	10	LOW	1.6	LOW	0	ABSENT	ABSENT
10	HIGH	79	HIGH	39.1	HIGH	3	PRESENT	ABSENT
11	LOW	9	LOW	0.3	LOW	30	PRESENT	ABSENT
12	LOW	12	LOW	2.3	LOW	60	PRESENT	PRESENT
13	HIGH	2	LOW	0.0	LOW	NONE		
14	HIGH	2	LOW	0.3	LOW	98	PRESENT	PRESENT
15	LOW	0	LOW	1.0	LOW	1	PRESENT	ABSENT
16	LOW	22	LOW	4.6	LOW	15	PRESENT	ABSENT
17	LOW	0	LOW	0.0	LOW	70	PRESENT	PRESENT
18	HIGH	20	LOW	7.9	LOW	0	ABSENT	ABSENT
19	LOW	15	LOW	2.5	LOW	NONE		
20	LOW	47	HIGH	24.7	HIGH	0	ABSENT	ABSENT
21	LOW	4	LOW	0.9	LOW	65	PRESENT	PRESENT
22	LOW	0	LOW	0.5	LOW	1	PRESENT	ABSENT

23	HIGH	38	LOW	34.4	HIGH	5	PRESENT	ABSENT
24	LOW	25	LOW	5.0	LOW	1	PRESENT	ABSENT
25	HIGH	25	LOW	10.2	LOW	99	PRESENT	PRESENT
26	LOW	10	LOW	2.0	LOW	0	ABSENT	ABSENT
27	LOW	0	LOW	0.2	LOW	NONE		
28	HIGH	2	LOW	0.4	LOW	1	PRESENT	ABSENT
29	HIGH	3	LOW	1.3	LOW	NONE		
30	LOW	2	LOW	0.8	LOW	NONE		
31	LOW	2	LOW	1.2	LOW	100	PRESENT	PRESENT
32	LOW	13	LOW	1.9	LOW	100	PRESENT	PRESENT
33	LOW	3	LOW	0.8	LOW	0	ABSENT	ABSENT
34	LOW	50	HIGH	17.8	HIGH	15	PRESENT	ABSENT
35	HIGH	12	LOW	0.9	LOW	80	PRESENT	PRESENT
36	LOW	19	LOW	27.7	HIGH	0	ABSENT	ABSENT
37	LOW	33	LOW	21.3	HIGH	NONE		
38	HIGH	10	LOW	12.2	LOW	NONE		
39	LOW	17	LOW	5.7	LOW	60	PRESENT	PRESENT

Conclusions: In our study, HRD score is not associated with TMB status. There is a strong correlation between HRD score and LOH percentage, suggesting that LOH is a major component in the genomic scarring seen in HRD. HRD may be an independent biomarker of immunogenicity to guide immunotherapy.

1247 Difference Between EBV-related and EBV-unrelated Poorly Differentiated Nonkeratinizing Squamous Cell Carcinoma of the Thymus

Yijun Zhang[1], Siping Xiong[1], Yuanzhong Yang[1], Sha Fu[2], Yuefeng Wang[3], Guiyang Jiang[4], Yun Cao[1], Yuhua Huang[1], Jingping Yun[5], En Hua Wang[6], Jiang-bo Zhang[1]

[1]Sun Yat-sen University Cancer Center, Guangzhou, China, [2]Guangzhou, China, [3]The First Affiliated Hospital of Sun Yat-sen University, Guangzhou, China, [4]China Medical University, Shenyang, China, [5]Sun Yat-sen University Cancer Center, [6]The First Hospital of China Medical University, Shenyang, China

Disclosures: Yijun Zhang: None; Siping Xiong: None; Yuanzhong Yang: None; Sha Fu: None; Yuefeng Wang: None; Guiyang Jiang: None; Yun Cao: None; Yuhua Huang: None; Jingping Yun: None; En Hua Wang: None; Jiang-bo Zhang: None

Background: The knowledge of thymic EBV-related poorly differentiated nonkeratinizing squamous cell carcinoma (EBV-related PDNKSCC) was extremely poor due to its rarity. We conducted a multi-institutional study of 85 patients with thymic PDNKSCC and established the clinicopathologic features, tumor immune microenvironmental composition and genomic landscape of this rare disease.

Design: DNA in situ hybridization was performed to evaluate the EBV status of all 85 thymic PDNKSCC. Immunohistochemistry and whole exome sequencing were used to compare the differences of clinicopathological, tumor-infiltrating lymphocytes (TILs) and molecular features between EBV-related and EVB-unrelated PDNKSCC.

Results: All 85 cases were classified into 27 EBV-related PDNKSCCs (31.8%) and 58 EBV-unrelated PDNKSCCs (68.2%) according to the EBV status. Compared to the EBV-unrelated PDNKSCC, EBV-related PDNKSCC showed younger patient predominance, more common of lymphoepithelioma-like pattern (LLP) and lower CD5 and CD117 expression. EBV-related PDNKSCC had a significantly higher portion of PD-L1+ tumour cells (TCs) and PD-L1+ and CD8+ immune cells (ICs) than EBV-unrelated PDNKSCC. The tumour microenvironment immune type (TMIT) I (PDL1-Tumor+/CD8-High) was more common in EBV-related PDNKSCC than in EBV-unrelated PDNKSCC. The four Groups based on the EBV status and growth patterns showed a significantly association with patients' OS and PFS, and more than 90% of Group 1 cases were classified to TMIT I. For the genomic features, EBV-related PDNKSCC has a significantly higher mutation burden than that of EBV-unrelated cases. We discovered that there were 30 genes mutated in at least 3 EBV-related cases while only 6 genes in EBV-unrelated cases. Furthermore, arm level copy number alterations were only detected in EBV-related cases (15q26.1 and 6q16.1).

Figure 1 - 1247

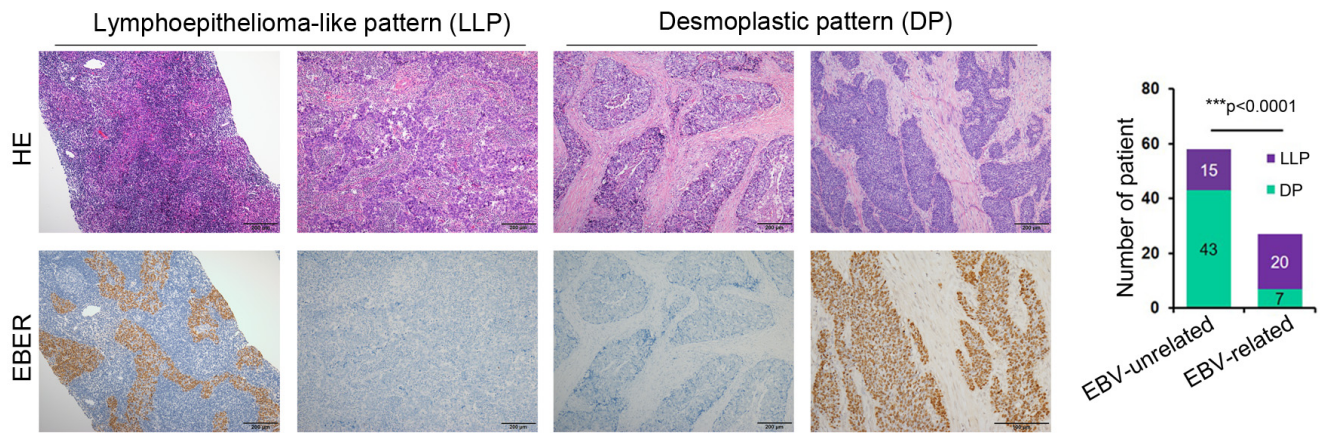

Conclusions: This study uncovered the multidimensional features of PDNKSCC of the thymus for the first time. The results indicated that EBV-related PDNKSCCs could be candidates for immune checkpoint therapy, especially for the Group 1, and the higher rate of mutation and copy number alteration of EBV-related cases may provide an indicator for the selection of targeted therapy.

1248 Pathology of Double Lung Transplantation of 12 Cases Following COVID-19

Haijun (Steve) Zhou[1], Mary Schwartz[1], Roberto Barrios[1]
[1]Houston Methodist Hospital, Houston, TX

Disclosures: Haijun (Steve) Zhou: None; Mary Schwartz: None; Roberto Barrios: None

Background: Pulmonary failure is one of the major causes of death in COVID-19 (SARS-CoV-2) patients. Lung transplantation has been evolving to rescue those patients' lives with promising success. Explanted native lungs post COVID-19 are valuable to understand the long-term pulmonary pathology of this deadly disease, as currently available data is very limited.

Design: Lung transplantation cases post COVID-19 were collected through the pathology database in our institution from January 2020 through September 2021. Patient clinical courses, CT imaging data prior to transplantation and pathological findings are evaluated.

Results: The cohort consisted of 12 male patients with a median age of 46.5 years (range 24 - 67). Co-morbidities were present in 6 patients including obesity, diabetes mellitus and hypertension. No prior known pulmonary specific disease was present in any of the patients. Extracorporeal membrane oxygenation (ECMO) was used in 10 of 12 patients for 54 - 130 days. CT imaging pre-transplantation showed extensive bilateral consolidation (5 cases), extensive bilateral ground-glass (3 cases) or extensive infiltration/air space disease (4 cases). All patients survived post double lung transplantation (including one patient with concurrent heart transplantation) and no significant pathologic alteration was identified on most recent surveillance biopsies (26 - 183 days post transplantation). The most prominent pathological finding in the explanted lungs is nonspecific interstitial pneumonia (NSIP)-like interstitial fibrosis (100%, 12 cases). Other findings include collections of numerous hemosiderin-laden macrophages (8 cases), patchy diffuse alveolar damage (DAD) (hyaline membrane formation and/or organizing DAD) (5 cases), intrapulmonary small vessel thrombosis (5 cases), organizing pneumonia (5 cases), necrosis (2 cases), calcifications (5 cases), acute pneumonia (3 cases), peribronchiolar metaplasia (8 cases), and microscopic honeycombing (8 cases). No viral cytopathic changes were seen. The pathologic findings of the two patients who did not receive ECMO are similar to those in patients with variable length of ECMO treatment.

Conclusions: Lung transplantation is a successful treatment option for eligible candidates with pulmonary fibrosis and failure post COVID-19. NSIP-like interstitial fibrosis is a universal finding, consistent with a sequala of DAD. A spectrum of acute, subacute, vascular and airway-related changes are also prominent findings in respiratory failure post COVID-19.